AFCRL 923 FINAL REPORT

STUDIES IN IONOSPHERIC PROPAGATION

Research
Initiated and Sponsored by

PROPAGATION SCIENCES LABORATORY
ELECTRONICS RESEARCH DIRECTORATE
AIR FORCE CAMBRIDGE RESEARCH LABORATORIES
OFFICE OF AEROSPACE RESEARCH
UNITED STATES AIR FORCE
BEDFORD, MASSACHUSETTS

CONTRACT AF19(604)-5230

Issued: 30 June 1961

RAYTHEON COMPANY
Waltham, Massachusetts

RAYTHEON

AFCRL 923 Final Report

STUDIES IN IONOSPHERIC PROPAGATION

ISSUED: 30 June 1961

RAYTHEON COMPANY
WALTHAM, MASSACHUSETTS

CONTRACT AF19(604)-5230

Research
Initiated and Sponsored by

Propagation Sciences Laboratory
Electronics Research Directorate
Air Force Cambridge Research Laboratories
Office of Aerospace Research
United States Air Force
Bedford, Massachusetts

Submitted by Harry Hoogasian
Harry Hoogasian

Reviewed by Leonard C. Edwards
Leonard C. Edwards

Donald A. Hedlund
Donald A. Hedlund
Propagations Systems
and Research Dept.

Period Covered

1 February 1960 to
31 May 1961

Requests for additional copies by agencies of the Department of Defense, their contractors, and other Government agencies should be directed to the:

ARMED SERVICES TECHNICAL INFORMATION AGENCY
ARLINGTON HALL STATION
ARLINGTON 12, VIRGINIA

All other persons and organizations should apply to:

U. S. DEPARTMENT OF COMMERCE
OFFICE OF TECHNICAL SERVICES
WASHINGTON 25, D. C.

CONTENTS

ILLUSTRATIONS

1. ABSTRACT

This report describes experimental studies and a development program relating to the reception of high-frequency radio waves after reflection from the ionosphere. The report covers work accomplished from 1 February 1960 to 1 June 1961, under the sponsorship of the Propagation Sciences Laboratory, AFCRL. Four separate subjects were investigated in the overall program. These were:

a. The spectrum of HF backscatter, and a related study of the phase stability on forward propagated paths.

b. Observations of signals circulating around the world.

c. Application of PPI and interferometer techniques on ground backscatter to study sporadic E.

d. Development of a punched paper tape system to collect propagation data for later analysis by digital computers.

A spectrum analysis was made of backscattered returns resulting from 22-mc pulse transmissions originating from South Dartmouth, Massachusetts. The spectrum center under normal conditions was observed to correlate well with the rate of change of the skip distance from early morning to late afternoon. Disturbed conditions evidenced by SID's, (sudden ionospheric disturbances), spread F, and other phenomena result in unusual spectrum changes with recognizable characteristics. Tests made to compare the effect of land and sea areas on the spectrum of backscatter had inconclusive results. In the study of phase stability on forward paths, the phase path for the South Dartmouth - Grand Bahama Island circuit was computed and compared with

experimental observations.

Around-the-world echoes were observed on three occasions in January 1961. Tests were held to measure the horizontal and vertical angles of arrival. Multifrequency transmissions showed the mode open over the 14- to 27-mc band of frequencies. These transmissions also showed that the time of one transit was essentially independent of the frequency.

A series of experiments were made to study sporadic E by receiving ground backscatter on a radio interferometer and a rotating antenna. Useful results from the interferometer were compromised by a small number of observations and the lack of an adequate signal-to-noise ratio. On the basis of PPI experiments, occurrences were noted most frequently when scanning south. A secondary maximum was observed scanning north from South Dartmouth. Estimates of the size of the reflecting region from 22-mc backscatter measurements ranged from 110 to 220 km.

A punched paper tape system was developed for the sampling and storage of receiver outputs. A coding system was developed in order to permit the processing of a tape by either a Royal McBee LGP-30 or an IBM 650 digital computer. Stability and accuracy tests showed the entire system to operate satisfactorily within its design limitations.

2. INTRODUCTION

This report describes and summarizes the results of studying several problems arising from the transmission of HF radio waves through the ionosphere. The primary objective in the several topics pursued was to design and perform conventional pulse propagation experiments for the purpose of studying transmission characteristics, some of which have hitherto received insufficient attention. The specific areas covered are a spectrum analysis of backscatter and one-way transmissions, with special attention devoted to the phase stability of the signals under normal and disturbed conditions; experiments to investigate properties of signals circulating around the world; and an investigation of sporadic E backscatter, employing a radio interferometer and a

rotating antenna. A final item concerns the development of a punched paper tape system intended to record propagation data in a form adaptable to processing by digital computers.

In order to isolate a wanted signal characteristic for closer study, some of the experiments have made use of processing techniques which in some respects are rather novel to HF experiments. Notable examples of this were in the use of coherent detection for the signal phase studies and in the operation of a radio interferometer during the sporadic E studies. Since coherent detection, especially, was basic to the spectrum analysis studies, the problem of instrumenting this technique is taken up in considerable detail.

3. PHASE-COHERENT DETECTION OF IONOSPHERICALLY REFLECTED SIGNALS

3.1 General Background

Normally, studies of ground-returned backscatter at HF concentrate on the amplitude-range time characteristics of the envelope of the backscattered signal. A fairly comprehensive literature has been built up in this area; the points of chief interest have been the variation of minimum transmission times and peak amplitude with operating frequency. In contrast to this wealth of research activity, relatively few thorough studies of the waveform spectrum are known to the literature; most of those existing deal with signals reflected only from the ionosphere, with the ground effects not included. The spectrum characteristics of ground-returned backscatter is virtually an unexplored area whose potential, in terms of describing or predicting the quality of communication between links, is as yet undetermined.

The study into the spectral details of backscatter was pursued along two parallel lines. The first attack was an experimental program which was planned to determine if there were regular patterns which might characterize the gross behavior of the backscatter spectrum. Therefore, the experiments were aimed at studying effects on the spectral composition, with respect to the

principal factors involved: time of day, the rate of change of the skip distance, operating frequency, terrain features in the region returning signal energy back to the receiver, the sampling point in the backscatter, major structural features within the ionosphere, and unusual disturbance conditions (SID's, storms, and anomalous perturbations). Experiments to measure phase path changes in one-way transmissions from a remote sender were scheduled during about one-third of the backscatter soundings in order to provide a comparison between the one-way and the two-way effects.

The underlying purpose of this phenomenological approach was to establish the basic factual background against which one might hope to correlate a measured effect with the cause producing it and, thereby, predict or identify major structural features or changes taking place in the ionosphere. To help guide the interpretation of the basic experimental data towards this objective, a series of computations were made on the basis of simple ray theory applied to a highly simplified geometry and ionospheric model. The computations determined the optical path corresponding to a specified layer height and a critical frequency. From these were derived optical path changes and, hence, the frequency shifts caused by changes in height and critical frequency. For application to transmissions among SDFS (South Dartmouth Field Station), GBI (Grand Bahama Island), and the Canal Zone, the optical path was computed for fixed ground ranges of 1780 and 3670 km. The corresponding problem for backscatter was treated by computing optical paths for a fixed two-way range time of 24 ms, corresponding to the nominal propagation time of signals between SDFS and the Canal Zone. This choice was made with the intention of comparing the Doppler shifts in the forward Canal Zone signal with measurements of backscatter from the same range.

3.2 The Experimental System

3.2.1 Antenna and Pulse Transmission System

The transmitting and receiving sites for these experiments are shown in Figure 1. All backscatter measurements were made on

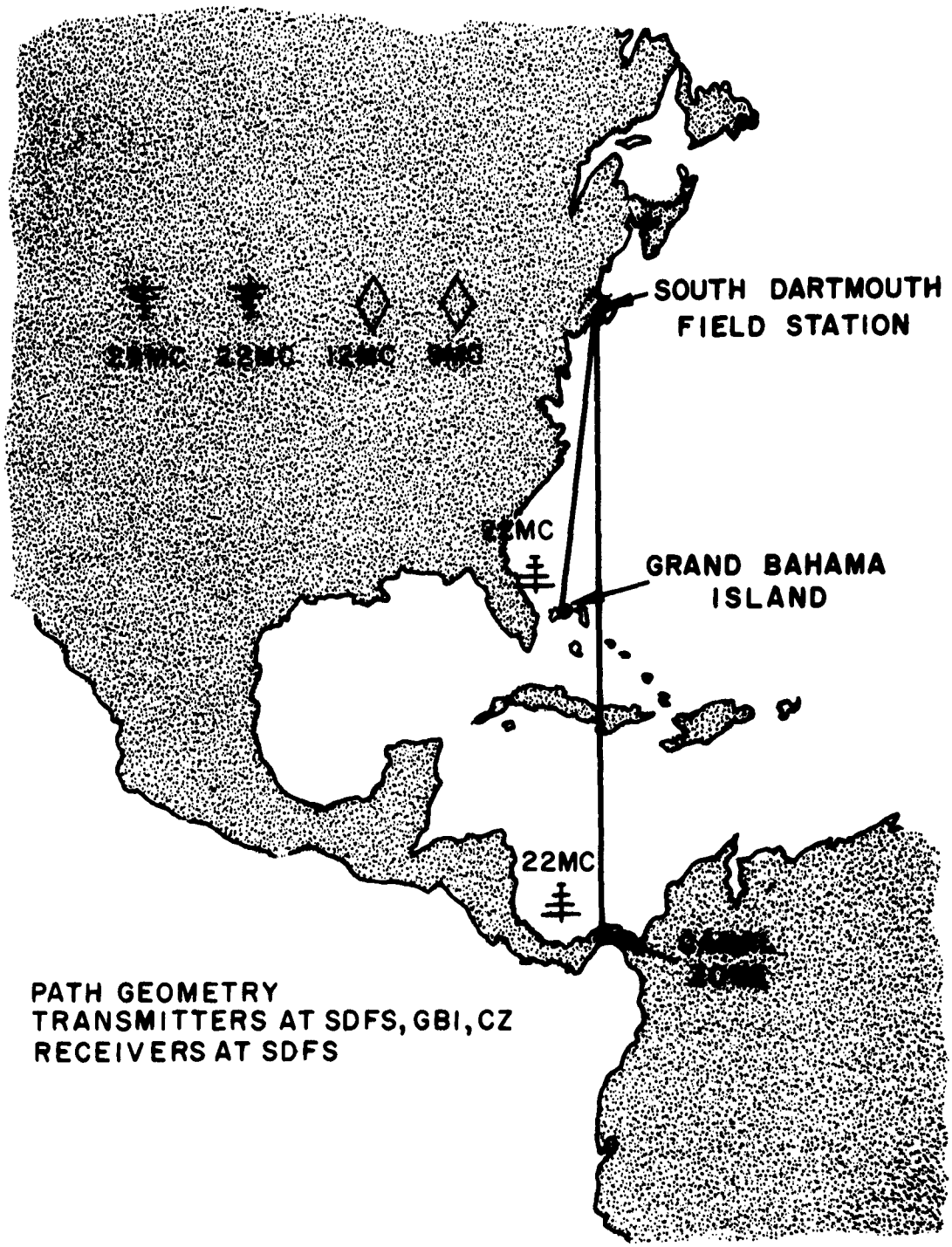

Figure 1. Location of South Dartmouth, Grand Bahama Island, and Canal Zone Facilities

transmissions from SDFS. One-way phase measurements were also made at SDFS on signals received from the GBI and Canal Zone transmitters. As Figure 1 shows, backscatter soundings required the use of four antennas on those occasions when four operating frequencies were simultaneously in use. Duplexing of all four antennas permitted their use for receiving as well. The pulsed transmissions from SDFS radiated 100 kw (peak), used 200-μs to 400-μs pulsewidths, and 20-cps repetition rates. GBI transmitters were a nominal 10 kw (peak), and Canal Zone transmitters radiated 1 kw (peak) during the experiments of this period. Operating frequencies at all these sites were derived from stable 1-mc standard oscillators with a long-term stability of better than 1 part in 10^8 per day. At an operating frequency of 10 mc, the maximum difference between standards is less than .1 cps, an amount which has been found to be adequate for observing phase path changes on forward propagated signals over long distances.

3.2.2 Receiving System

A receiving system was used which allowed extraction of either phase or amplitude information, or both. Receivers were dual conversion, with the first IF at 1600 kc. The second IF was 15 kc, and is the output frequency recorded. Frequency integrity was maintained by deriving the conversion mixing frequencies from the primary standard supplying the transmitter. Receiver RF bandwidths were approximately 5 kc.

3.2.3 Recording and Data Processing System

The receiver output at the 15-kc level was continuously recorded on magnetic tape with an Ampex Model FR1100 Tape Recorder. Seven channels were available, of which four were reserved for data when sounding simultaneuosly on four frequencies, leaving three channels to carry timing and reference carrier information. The recorded reference carrier was a 15-kc signal derived from the primary standard, which was later injected into a balanced demodulator to beat the receiver IF signal down to zero frequency. Figure 2 is a block diagram of the receiving-recording system.

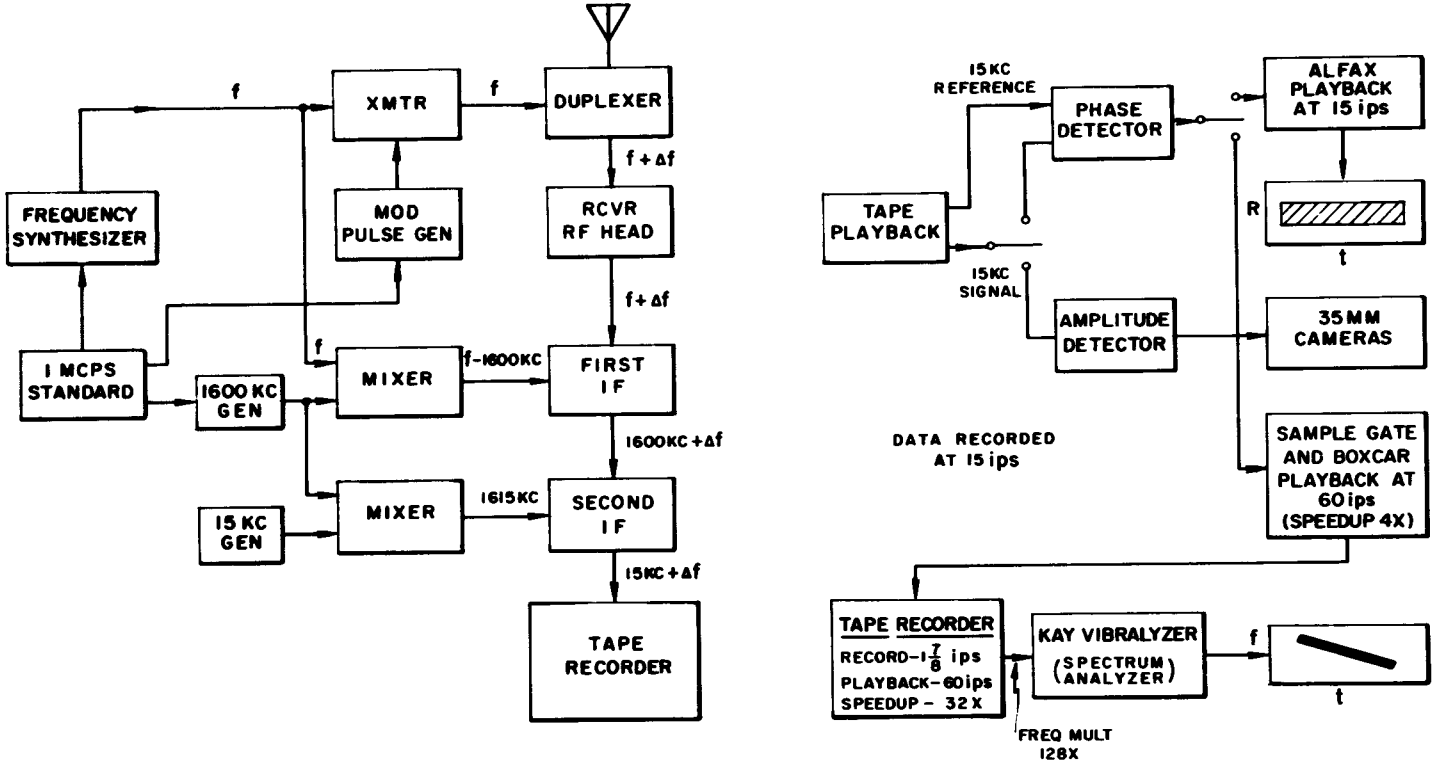

Transmitting, Receiving and Data Recording System

Data Processing System

Figure 2. Transmitting, Receiving, Recording, and Data Processing Systems, Block Diagrams

The recorded data was processed during playback of the tape. Received signal and reference carrier were injected into the balanced demodulator or phase detector to give an output video waveform equal to the product of the envelope of the received signal and cos ϕ, where ϕ was the phase difference between the received and reference signals. As Figure 2 illustrates, the output video is then boxcarred at the desired sampling delay time, generating a waveform varying in accordance with cos ϕ, and the envelope amplitude at the sampling point. This waveform is symmetrically bipolar, and still preserves both phase and amplitude information. Phase variations alone can be displayed directly on an Alden Alfax Facsimile reproducing device, yielding a range-time record. This device reproduces positive and negative amplitudes as dark and white marks on sensitized paper, with low-amplitude voltages registering as a grey tone. Thus, if the envelope itself contains no zeros, the time separation between successive dark or white bands corresponds to a change in phase of one cycle. When analyzing well-defined one-way transmissions, the range-time records were well-adapted to counting the number of complete cycles in a given time interval, thus determining the frequency shift in the received signal. When analyzing backscatter, the irregularities of the records, in most cases, prevented an accurate qualitative description. Nevertheless, such displays proved useful in revealing the presence of major disturbing structures in the ionosphere, and so were extensively used.

In addition, a harmonic analysis of range-gated portions of the backscatter records were produced. To this end, a Kay Vibralyzer spectrum analyzer was used. The heart of the Vibralyzer is a filter whose bandwidth is about 2 cps. By heterodyning, this filter scans any input record of 20-second duration containing frequencies between 5 and 500 cps. The output is a record indicating the amplitude of each frequency present in a short interval of time (at least 1/2 second). Thus, a progressive record of the frequency content of the input waveform is left on paper as a dark trace. However, since the frequency range of interest in these experiments is much lower than the range accepted by the scanning filter, the technique requires a frequency multiplication of the input. This was accomplished by playing back the original data tape at high tape speed and re-recording into another recording

at low speed, continuing the process until a speedup of 128 times was reached. Thus, an original frequency component of 1 cps was multiplied upwards to 128 cps and a real-time record of approximately 3/4 hour was compressed to an input of 20 seconds. A sample record is shown in Figure 3.

Since it became apparent that sense information was important in certain cases, a technique was developed which upon playback changed the reference 15-kc frequency in steps of 1 cps up to ± 5 cps. Thus, in cases where the actual frequency excursions were less than the offset frequency, both magnitude and sense could be deduced from the records. Some of the illustrations in this report are of data reduced by offset and are labeled accordingly.

3.3 The Spectrum of Backscatter

3.3.1 Temporal Variations

This section will discuss the results of the experimental portion of the study of the spectral composition of backscatter. The purpose of these experiments was to determine the principal characteristics of the spectrum and to establish a correspondence between the spectrum and the state of the ionosphere producing it. To this end, a spectrum analysis was made from backscatter records at several sampling points. The center and bandspread of the resulting spectrum were scaled off and compared with the time rate of change of the leading edge and other variables.

The great portion of the routine data collected and analyzed in this report was taken during the period from December 1960 to March 1961. Backscatter soundings were made simultaneously on as many as four separate frequencies in a total of 19 days over this time. A full analysis has been completed for 22-mc transmissions, the lengthy time for data processing preventing any but occasional examinations of other frequencies. In a few cases of special interest, the records of other frequencies were processed and analyzed; a description of the main features is given in sections to follow.

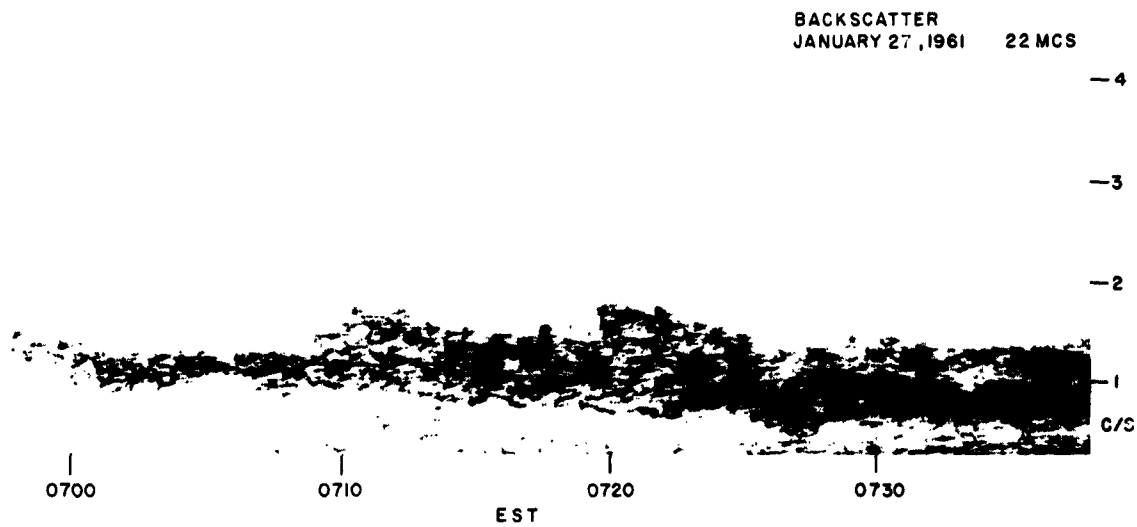

Figure 3. Sample Spectrum Record of Backscatter

We turn now to an example which will illustrate the method of analysis used. Figure 3 gives a spectrogram of backscatter samples taken on January 27, 1961. The times shown are Eastern Standard, and spectrum frequencies are indicated by calibration marks along the vertical axis. At any given time, the spectral distribution of the backscatter sampled at the range time is given by the band of frequencies occupied. In analyzing the data, the center and width of the occupied band of frequencies were scaled off at 5-minute intervals to test for any correlation between these quantities and such things as time of day and rate of change of delay to leading edge of backscatter. In Figure 4, the range-delay to the leading edge of backscatter is shown for the same period. The plot shows an apparent roughness which is, at least, partly caused by amplitude fluctuations of little or no relevance to the problem being studied. The roughness was, therefore, removed by threading a smooth "best fit" curve through the points. At the 5-minute intervals of the smoothed curve, the slope was scaled off to give the skip-distance rate of change at that point. Using this procedure for data collected over a long period results in Figure 5, which shows a plot of the average delay to the leading edge of 22-mc backscatter. At the top of the plot, there is an indication of the number of days

involved in obtaining the averages. The shape of the delay time plot is in the form of the letter U, showing the normal decrease in skip distance between 0600-0900 EST and an increase between 1600-1930 EST, with substantially no changes between 0900 and 1600 EST. The question being studied is whether or not these regular ionospheric variations result in consistent frequency shifts in returned backscatter.

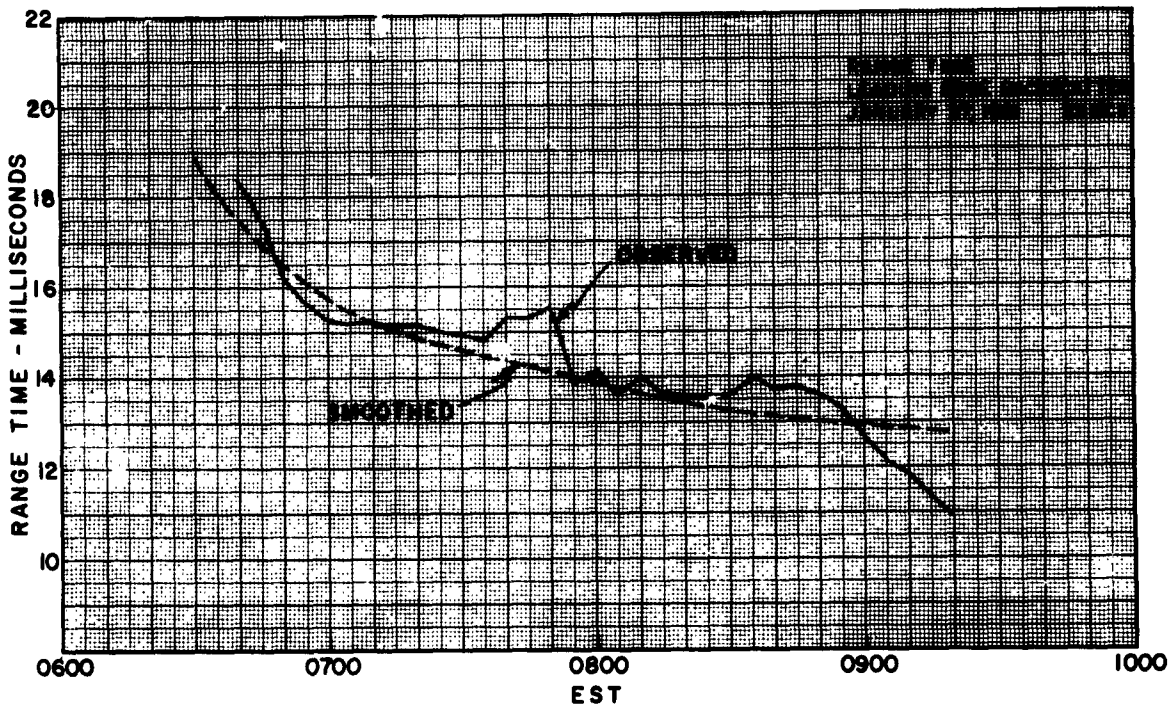

Figure 4. Smoothing Range-Time Record

The average center frequency of the spectral distribution is plotted against Eastern Standard Time in Figures 6 and 7. Figure 6 is the result of sampling the first-hop backscatter in up to three ranges, beginning at least 1 ms beyond the leading edge. Figure 7 involves a single sample at a range which is less than 1 ms from the leading edge. The division, which is somewhat artificial, was made to determine whether the single mode of propagation more likely to be present near the leading edge would lead to important differences on the spectrum. This will be made clearer in the theoretical section which follows. Actually, some rather irregular differences are observed,

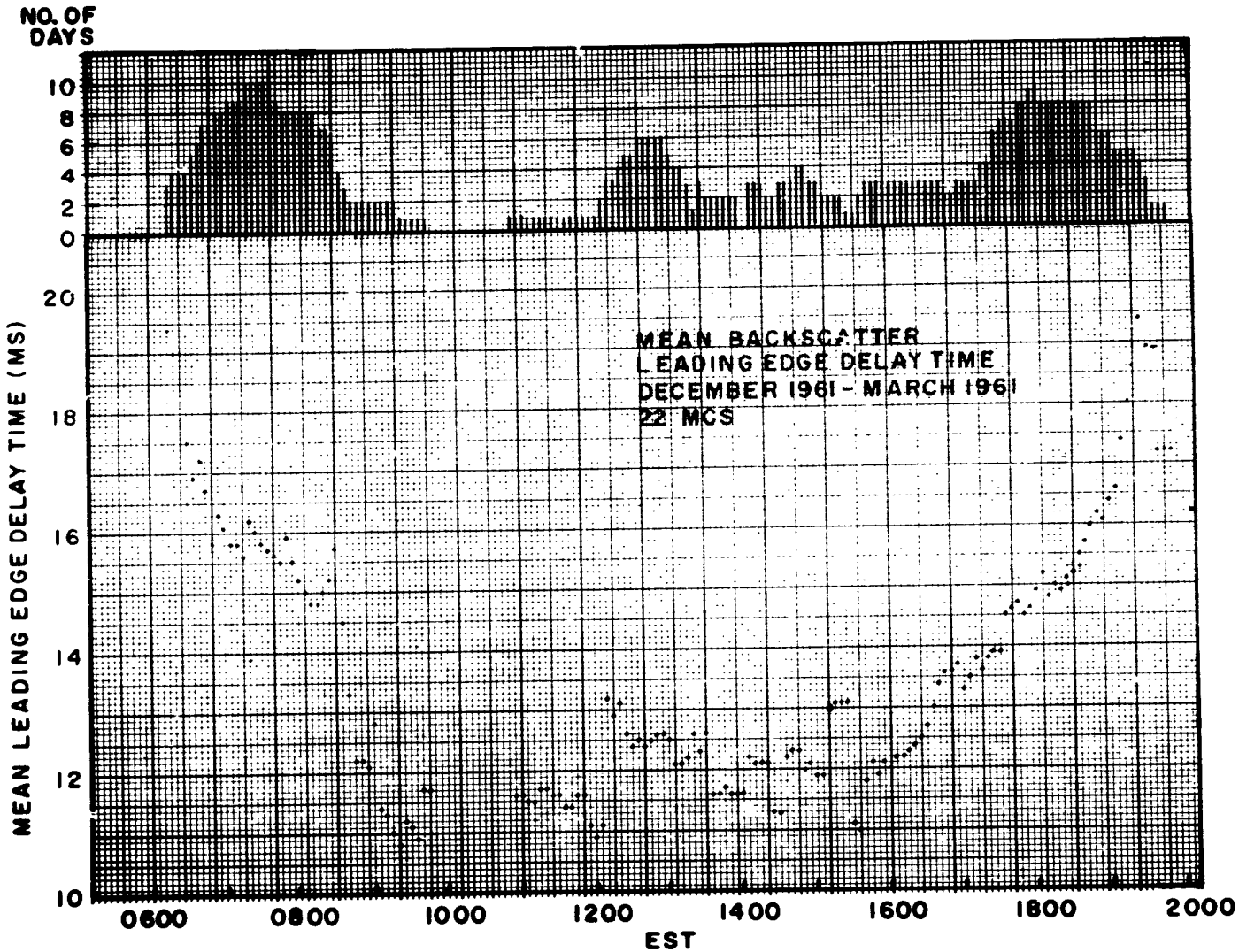

Figure 5. Plot of Average Backscatter Leading Edge Range Time

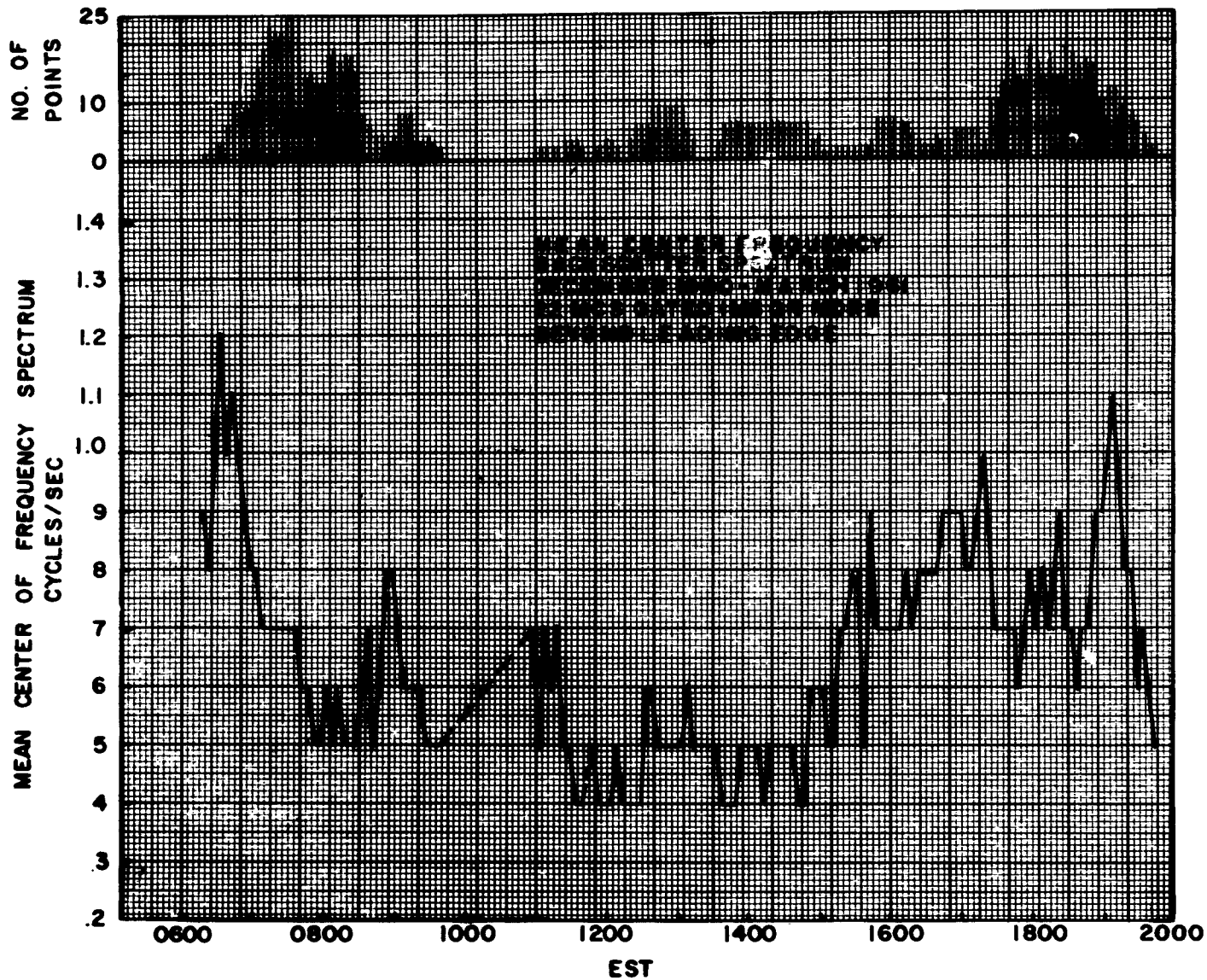

Figure 6. Average Spectrum Band Center, Sampled beyond Leading Edge

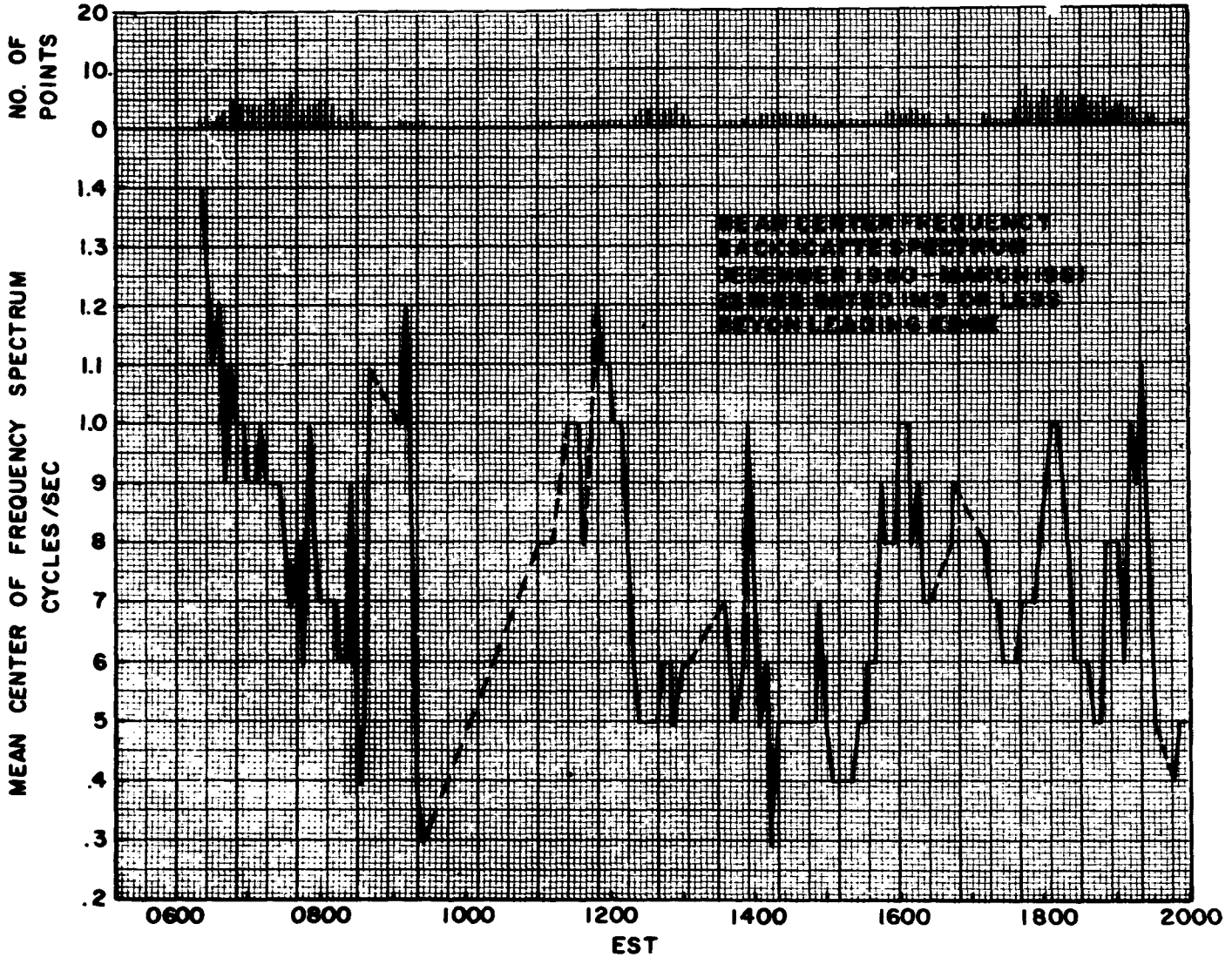

Figure 7. Average Spectrum Band Center, Sampled near Leading Edge

but are probably the result of fewer samples being included near the leading edge. Both plots are somewhat-compressed replicas of the previous U-shaped figure, indicating some correlation between skip distance changes and spectral content. An exception is noted around 1700 when the curve slopes downward, even though the skip is increasing. An examination of the spectrograms at this time offers a possible explanation for the unexpected decrease. It may be due to an amplitude loss to a point below equipment writing level in the higher of two frequency components often present at that time.

The average bandwidth of the occupied spectrum is shown in Figures 8 and 9. The spectrum bandwidth evidently has less of a diurnal variability than the frequency shift. The anomaly at 1700 is also less evident, although still observable.

To show the degree of correlation between the center frequency and the rate of change or delay time, the correlograms of Figures 10 to 12 were prepared. Frequency values plotted in these diagrams were extracted from a smooth "best fit" curve, through the actual spectrum data, in the same fashion as the rate of change values were derived. This was done to remove "noise" in the scaling of frequency values and to place both parameters on the same basis before comparing them. A division into one morning and two evening periods has also been made. Referring to Figures 10 to 12, both morning and early evening data indicate that a fairly close direct correlation exists. Late evening data tends to show that a negative correlation holds, reflecting again the effect of amplitude loss in the higher frequency components at this time. A more significant aspect, probably, is the evidence that the correlation on a given day seems much closer than the correlation when all days are included. It may be concluded from this that at least one parameter besides the rate of change of the minimum delay time is effective in determining the spectrum center frequency, such parameter or parameters varying considerably from day to day.

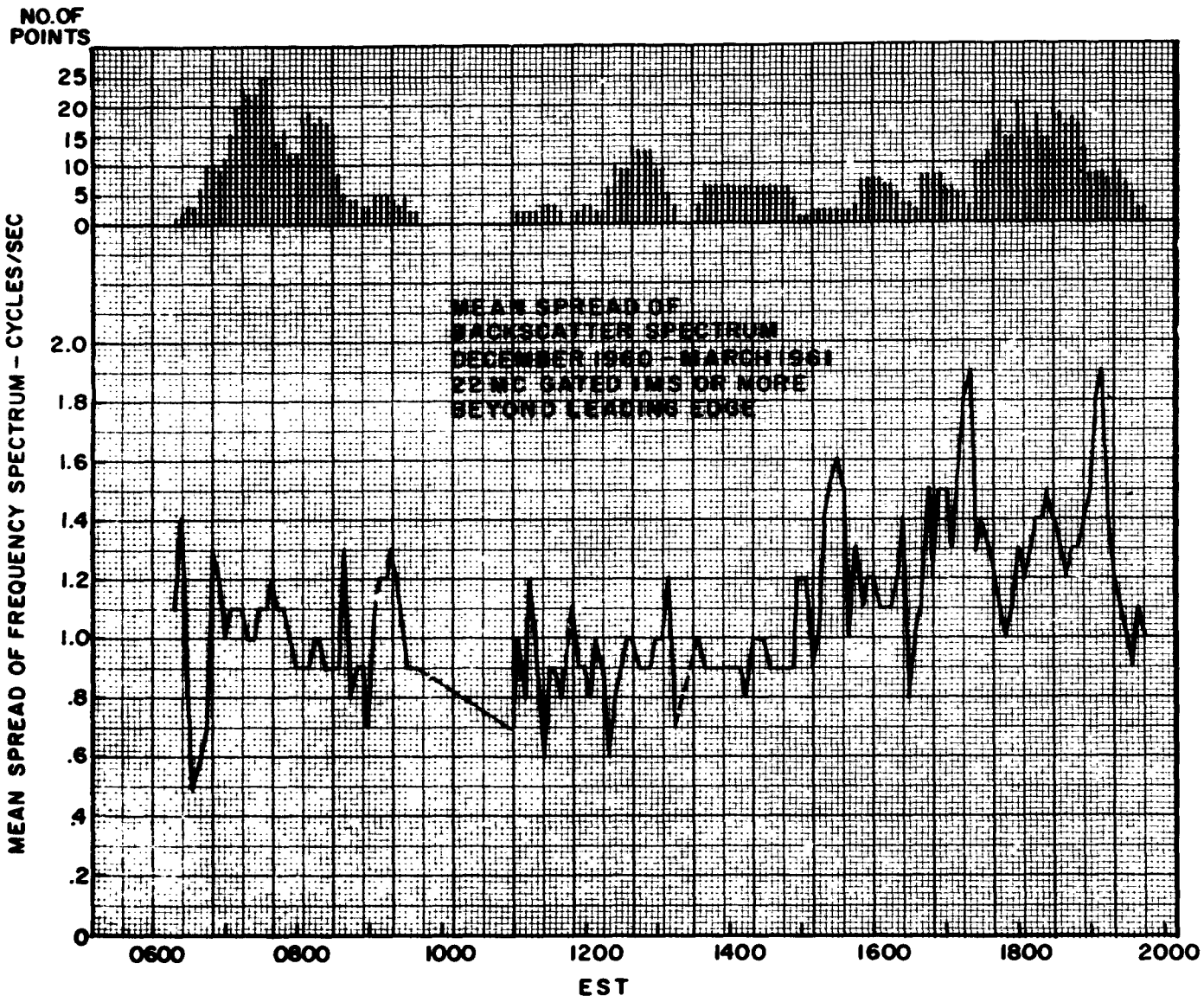

Figure 8. Average Spectrum Spread, Sampled beyond Leading Edge

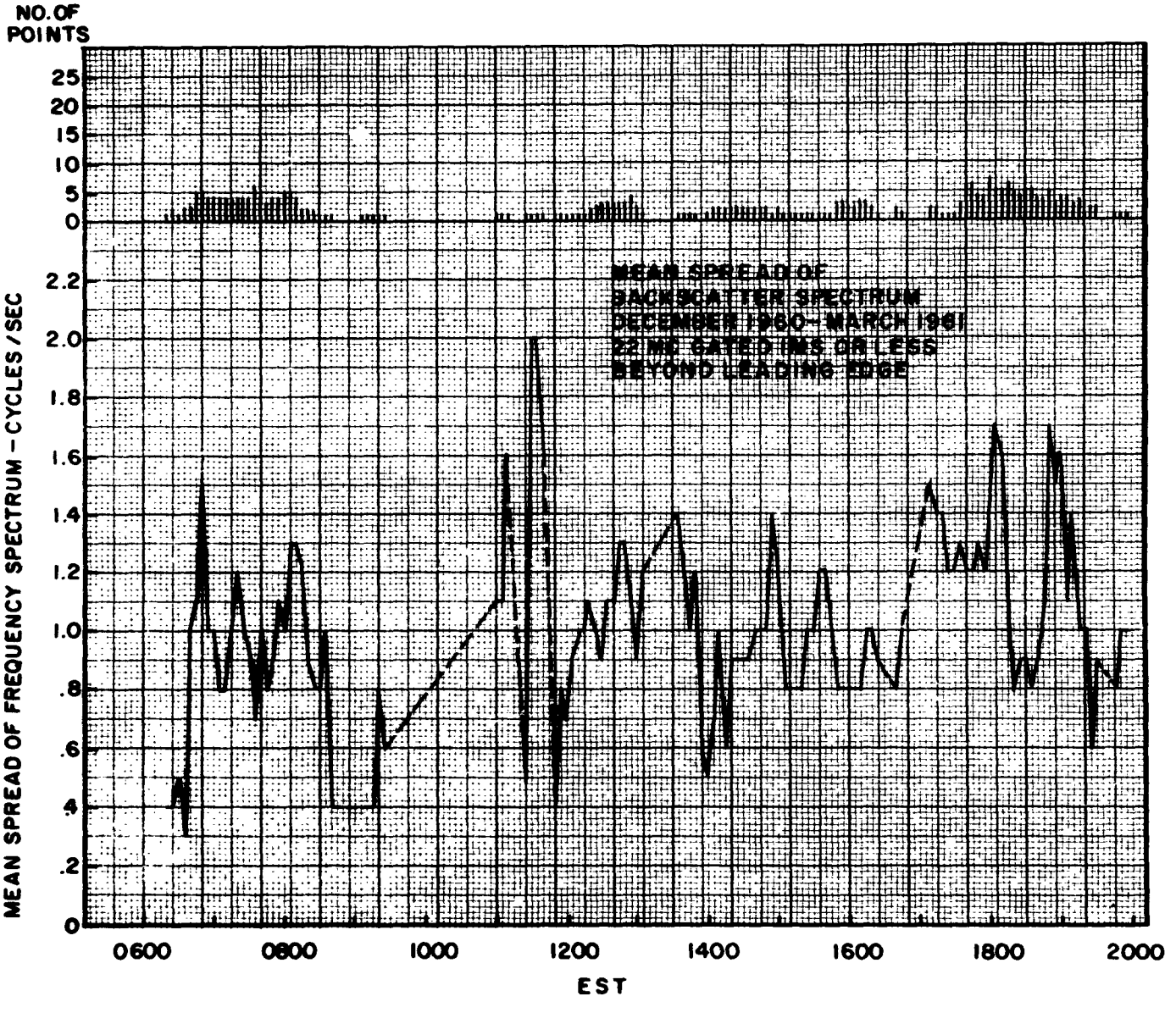

Figure 9. Average Spectrum Spread, Sampled near Leading Edge

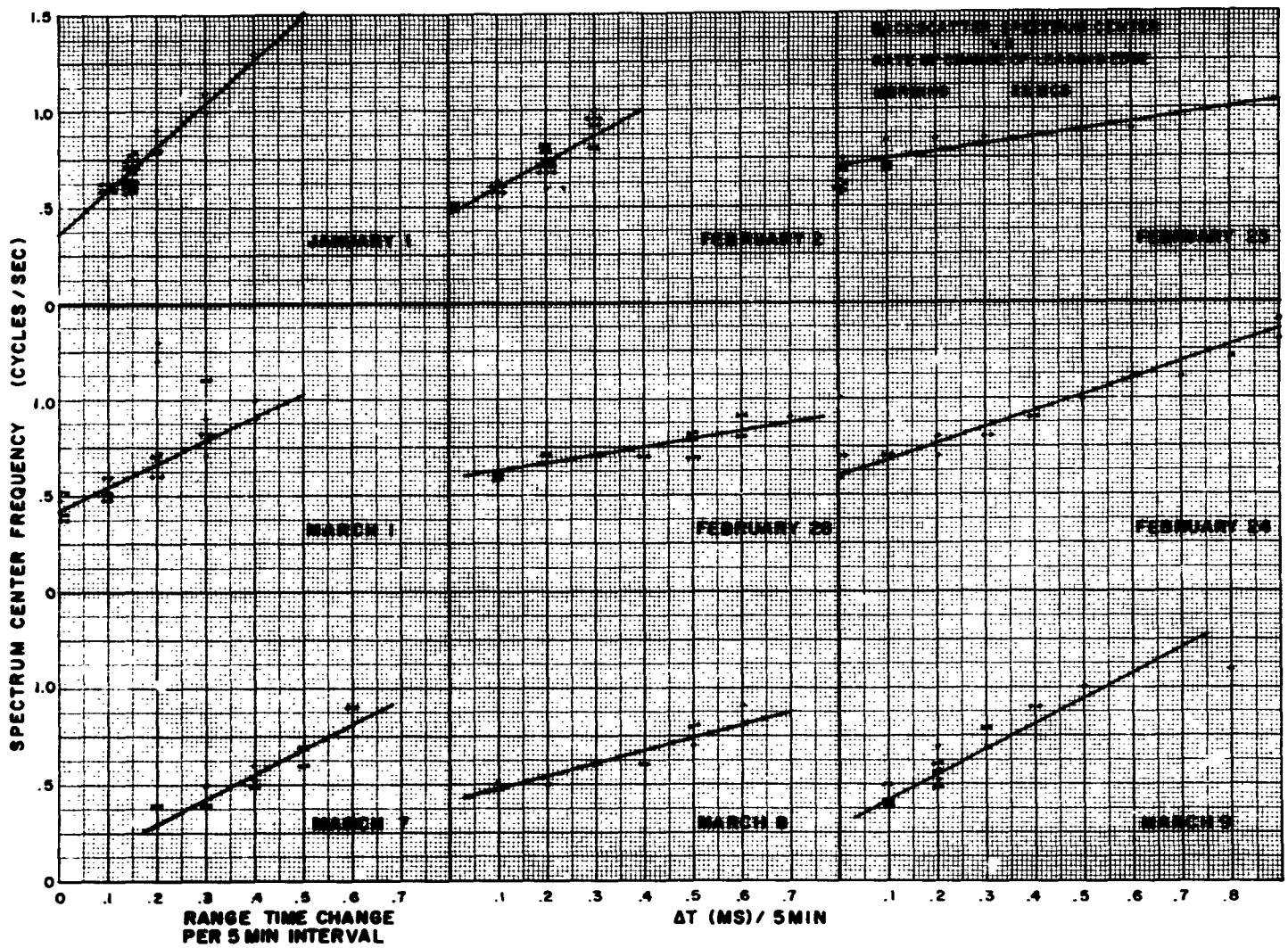

Figure 10. Correlogram of Spectrum Center and Rate of Skip-Distance Motion, Morning Hours

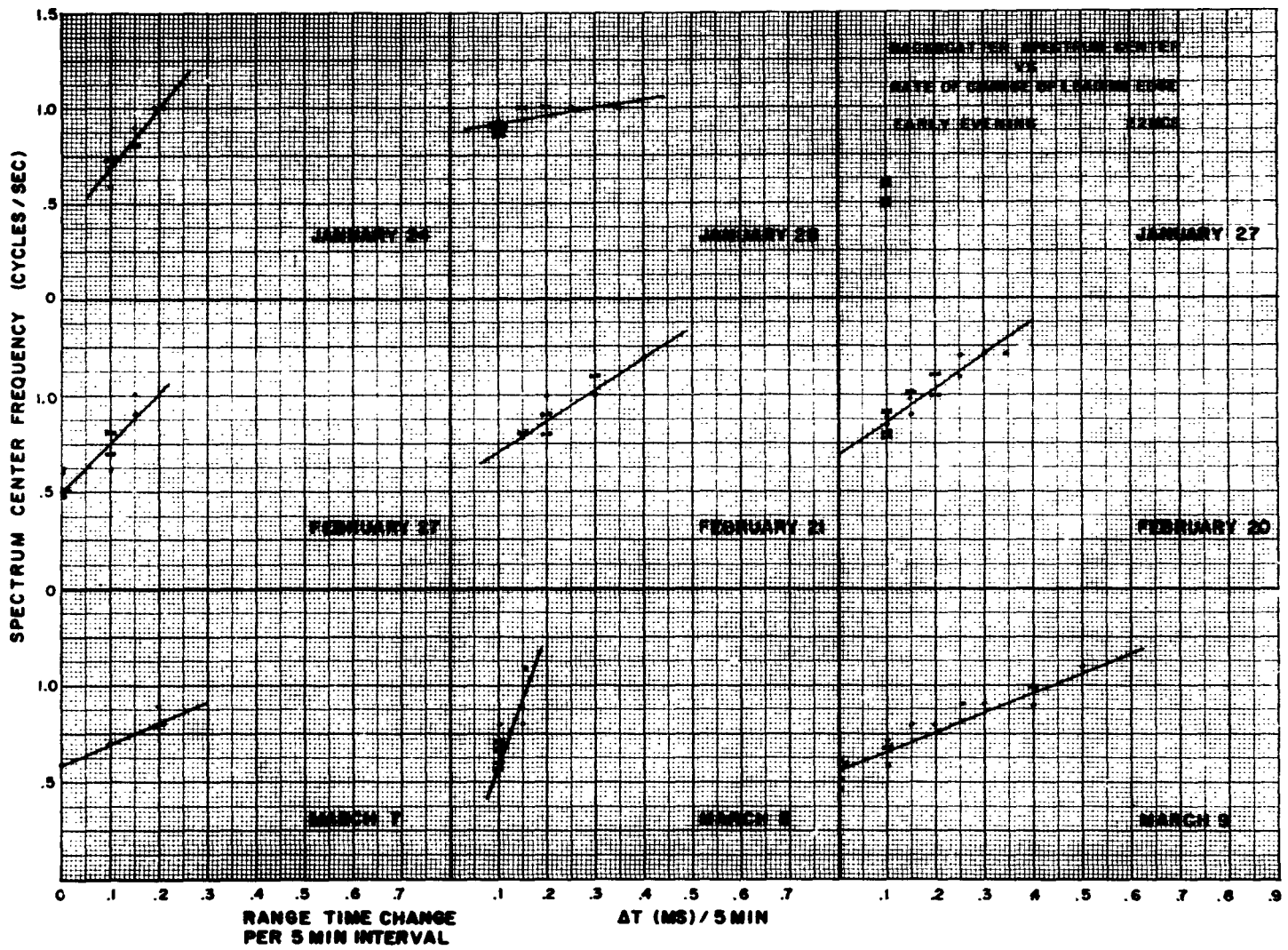

Figure 11. Correlogram of Spectrum Center and Rate of Skip-Distance Motion, Early Evening Hours

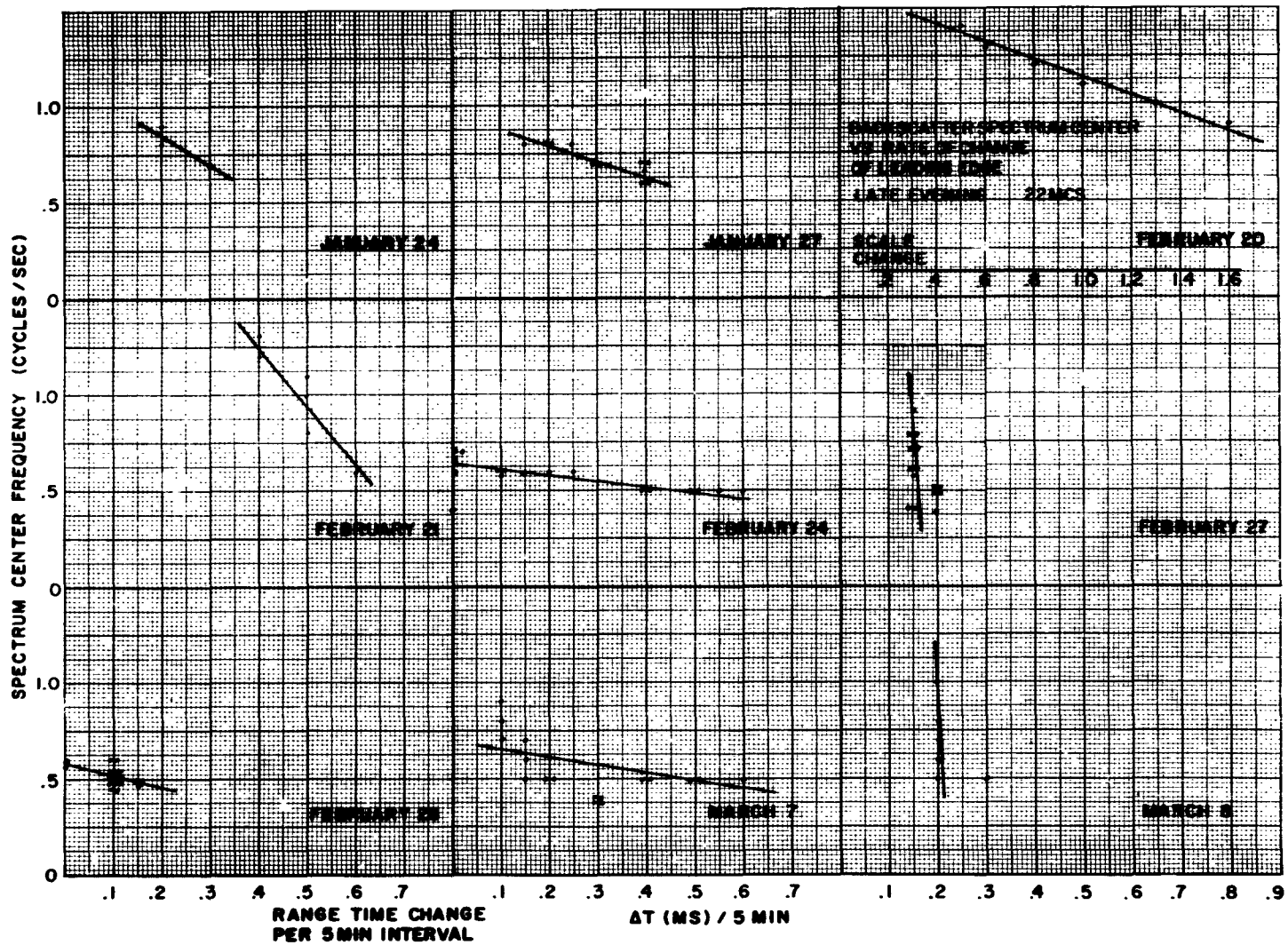

Figure 12. Correlogram of Spectrum Center and Rate of Skip-Distance Motion, Late Evening Hours

The interpretation of noontime data is somewhat more difficult. In all cases observed, the time rate of change was essentially zero, and one might be tempted to expect the spectrum would also be centered at or near zero. It is not clear from the data whether or not this condition actually occurs because of the foldover at zero referred to earlier. Typical spectrograms of this period show the spectra to appear as an intense band with sharply defined edges extending upward from zero cycles. In any one experiment, there was remarkably little variation noticed in the spectrum. The apparent width of the spectrum varied from .4 cps to .7 cps on different days. However, because of the finite width of the spectrum and the possibility of foldover, it was not possible to observe a center frequency at or near zero and, therefore, no conclusions were actually drawn about the position of the spectrum center or its width. The possibility, therefore, remains that during stable periods the center frequency actually approaches zero, and that the spectrograms should be interpreted as having a finite width, which could be due to random variations either in the ionosphere or on the ground.

3.3.2 Terrain Variations

In the discussion of the relation between the backscatter spectral center frequency and the rate of change of skip distance, the possibility was raised that terrain effects might contribute to the spectrum of the backscatter. If the mechanism producing the effect is similar to that in ground or sea clutter, one might anticipate that different kinds of terrain would result in different additive components. If the differences are reasonably large, their effects could be observed by simply rotating an antenna so that the beam illuminated selected earth areas in turn.

A few attempts to observe terrain effects were made at South Dartmouth, with interesting (but so far inconclusive) results. The Atlantic coastline furnished an excellent line of demarcation for these tests. The coastline extending southwest from SDFS does not deviate too far from a straight line at a heading of approximately 225°. Tests were conducted on April 13 and 18 and on May 10, 1960. In the April tests, the antenna positions

were switched alternately between headings of 160° and 260° so that the surface illuminated was entirely land or entirely sea. During the May test, the antenna position was changed in small angular increments over the same range. A broadband log-periodic antenna (beamwidth 70°) was duplexed for use in both transmitting and receiving for the tests of April 18 and May 10. Tests on April 13 were made with a five-element 60° beam.

The results of these few tests were not consistent and, therefore, inconclusive. They were, nonetheless, of considerable interest. Although the test of April 18 showed little change in the spectrum of the backscatter as the antenna direction was changed from land to sea, the test of April 13 offered very prominent differences. Spectrograms illustrating these results are shown in Figure 13a, b, c. The three spectrograms shown represent three sampled range points within the backscatter. The spectral differences are quite obvious—in this case, the frequency translation being somewhat higher when the antennas were beamed over the sea.

The inconclusive results of the first two tests prompted a third test, on May 10, 1961, to determine whether the additive component contributed by the impact area might be obscured by larger differences in the ionospheric component from widely divergent azimuths. This test differed from the preceding ones in that more antenna rest positions were scheduled, so that any systematic large changes in the ionospheric component, with changing azimuth, could be taken into account.

The vibrogram in Figure 13d shows the spectral distribution in each of the antenna rest positions. (The reference 15-kc signal during the processing of this record was decreased by 2 cps, so that zero reference frequency is marked at approximately the mid-position of the vibrogram.) The beam position in the first time period (1155-1200) was directed seawards and moved closer to the coastline in the next time period. At 1205, the azimuth was abruptly changed 70° so that the illuminated area was entirely over land. There is little discernible difference in the spectrum of the two sea positions, but a rather pronounced change can be noted when the direction was

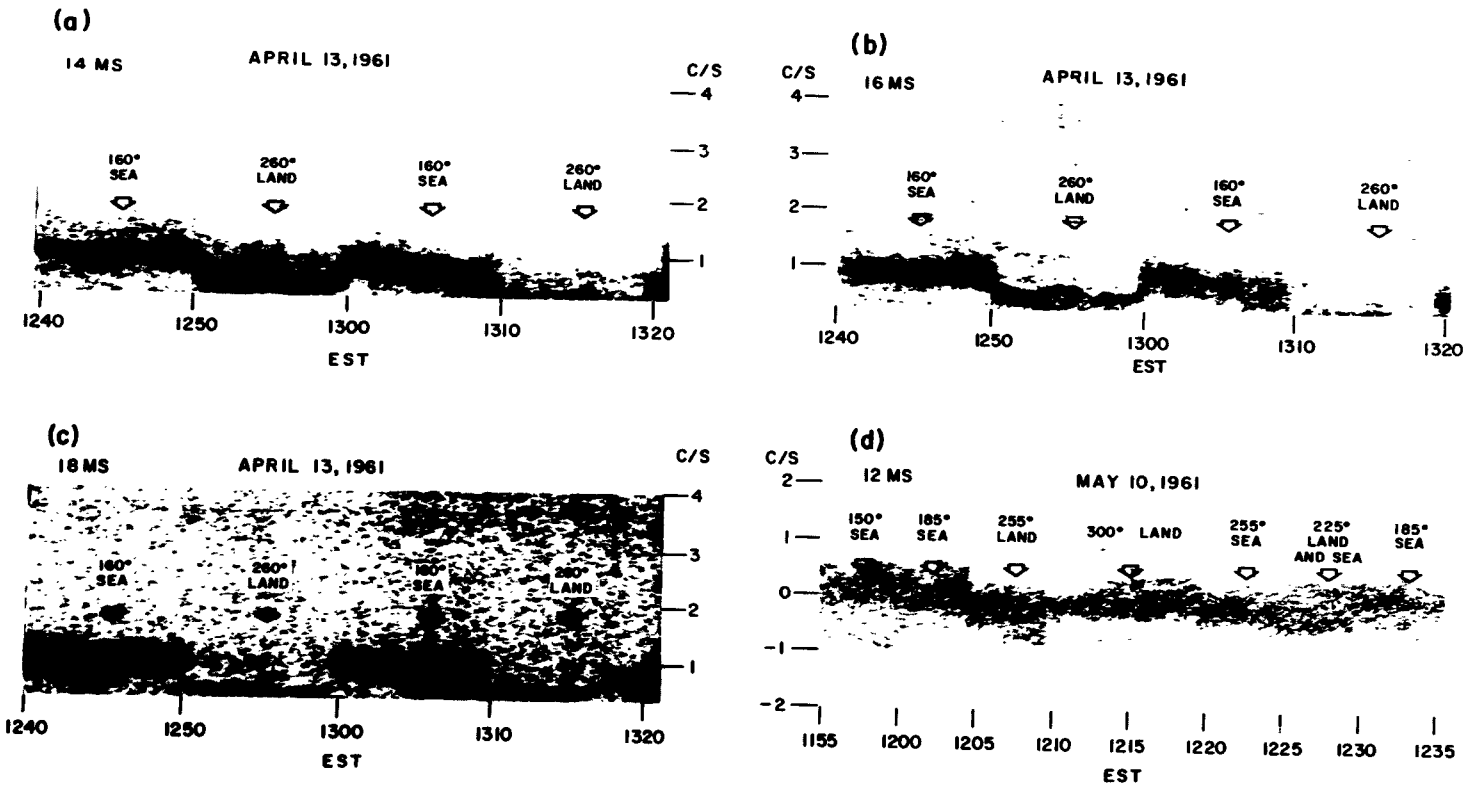

Figure 13. Spectrograms of Land-Sea Tests, April 13, and May 10, 1961

changed landward. At 1210, the beam was directed towards its maximum landward azimuth and began retracing its steps to the original sea position at 1225. An abrupt transition in the spectrum was not observed at 1230 when the land-to-sea transition was made the second time, and examination of the vibrogram shows that most of the drop at 1205 was regained during the 1210 to 1220 period, when the antenna was positioned at 300°. It must, therefore, be concluded that the test failed to distinguish between ground and ionospheric contributions, possibly because azimuthal and temporal variations masked a smaller component from the ground.

Although these preliminary tests failed in their purpose of establishing a definite contribution to the spectrum of ground origin, the importance of establishing whether such effects do occur merits deeper study and the planning of more careful experiments in the future. The tests were useful in that they point up the necessity of using at least two narrow-beam antennas in simultaneous operation, so that "noise" in the form of natural spatial and temporal fluctuations in the spectrum will have minimum effect. Future plans for continued experiments are being built around the use of narrow-beam interferometers to achieve the azimuthal restriction necessary.

3.4 Comparison of Observed and Theoretically Derived Phase Path Variations

3.4.1 General

In the preceding sections, the phase variations and frequency spectra measurements discussed are undoubtedly influenced by the temporal changes in the portion of the ionosphere through which the propagation is taking place. In this section of the report, an attempt is made to explain these observed results by development of a simplified model to approximate the actual ionosphere and its variations. For simplicity, the model chosen is that of a parabolic layer taken over a plane earth. Geometric relationships among the distance, group, and phase paths are then developed. The section concludes with a discussion of the comparison between observed and theoretically derived results.

3.4.2 Summary of Relevant Theory

3.4.2.1 Theoretical Expressions

With the assumption that ray theory is applicable, the integrals of distance, group, and phase paths can be shown to be:

$$h' = \int_0^{h_T} \frac{dh}{\mu} \tag{1}$$

$$P' = 2\int_0^{h_T} \frac{dh}{\mu \sin\beta} \tag{2}$$

$$D = 2\int_0^{h_T} \frac{dh}{\tan\beta} \tag{3}$$

$$P = 2\int_0^{h_T} \frac{\mu dh}{\sin\beta} \tag{4}$$

h = height in km

h_T = maximum ray penetration

μ = index of refraction

β = angle made with horizontal

h' = virtual height (vertical incidence)

P' = equivalent group path

D = distance

P = equivalent phase path

Assuming that the effects of collisional friction and magnetic field can be neglected in the region of HF propagation, the refractive index can be represented in the following form:

$$\mu = \sqrt{1 - \frac{N/N_o}{f_o^2/f_c^2}} = \sqrt{1 - \frac{n}{f^2}} \tag{5}$$

N = electron density (electrons / cm^3)

N_o = maximum value of electron density in layer

f_o = operating frequency (mc)

f_c = critical frequency (mc)

n = normalized electron density = N/N_o

F = relative frequency = f_o/f_c

It is assumed that the differences in the properties of the ordinary (O) and extraordinary (X) rays, arising from the effects of the earth's field, can be represented to a first order by an appropriate shift in the relative frequency.

The application of a parabolic profile (Figure 14) to the ionization gradient results in the following relationships:

$$n = 1 - \frac{(h - h_m)^2}{H^2} \tag{6}$$

$$N = -\frac{1.24 \times 10^4 f_c^2}{H^2} \left[(h - h_m)^2 - H^2\right] \tag{7}$$

h = height (km)

h_m = maximum height of the layer (km)

H = semi-thickness of the layer (km) = $h_m - h_o$

h_o = bottom of the layer (km)

Making use of a plane-stratified-parabolic ionosphere, ray theory results in a series of useful analytical relationships:

$\mu \cos \beta = \mu_T = \cos \beta_o$

$$D = 2\int_0^{h_T} \frac{dh}{\tan \beta} = 2 h_o \cot \beta_o - HF \cos \beta_o \log e \frac{1-F \sin \beta_o}{1+F \sin \beta_o} \tag{8}$$

$$P' = 2\int_0^{h_T} \frac{dh}{\mu \sin \beta} = 2 \frac{h_o}{\sin \beta_o} - HF \log e \frac{1-F \sin \beta_o}{1+F \sin \beta_o} \tag{9}$$

$$P = 2\int_0^{h_T} \frac{\mu\, dh}{\sin\beta} = \frac{2\, h_o}{\sin\beta_o} + H \sin\beta_o - \frac{FH}{2}\left(1 - \frac{1}{F^2} + \cos^2\beta_o\right) \log e \frac{1 - F \sin\beta_o}{1 + F \sin\beta_o} \quad (10)$$

β_o = angle of departure at the transmitter
β = angle made with horizontal
μ_T = refractive index at top of ray path
D = ground distance (km)
P' = equivalent group path (km)
P = equivalent phase path (km)

The nomenclature is illustrated in Figure 15.

A special case of HF propagation that is often used in the determination of the relationship of ion density to true height is that of vertical incidence soundings. For the case of vertical incidence, the relationships involving distance and equivalent group and phase path are greatly simplified:

$$\sin\beta_o = 1 \quad (11)$$

$$D = 0 \quad (12)$$

$$P' = 2\, h' = 2\left(h_o - \frac{H}{2} F \log e \frac{1 - F}{1 + F}\right) \quad (13)$$

$$P = 2\left(h_o + \frac{H}{2} - \frac{H}{4}\left[\frac{F^2 - 1}{F} \log_e \frac{1 - F}{1 + F}\right]\right) \quad (14)$$

where D is the ground distance, P' is the equivalent group path, h' is the equivalent virtual height and P is the equivalent phase path. It should be noted that when F = 1, the equivalent phase path is equal to $(2h_o + H)$.

The conversion of the equivalent group and phase paths from km to seconds and wavelengths, repectively, is shown in the following relationships:

$$T = \frac{2}{c} P' \tag{15}$$

$$P_\phi = \frac{P}{\lambda_o} \tag{16}$$

T = two-way delay time (sec)

c = speed of light $\frac{(km)}{(sec)}$

P_ϕ = number of wavelengths in one-way path

λ_o = free space wavelength at the operating frequency

3.4.2.2 Numerical Results

Numerical solutions for the distance and equivalent group and phase paths were obtained by making use of the computer facilities available at Raytheon. Values of h_o (bottom of the F_2 layer) were chosen from 100 km to 350 km. A value of H was assumed to remain constant at 100 km.* The results of these computations are presented and discussed on page 30.

---

* This value was the median semi-thickness of 50 "best fit" parabolas, covering profiles taken at GBI and selected at random for all times of the day over the period from Jan '60 to Jan '61. Over two-thirds of these curves fell in the range of 90 km to 110 km.

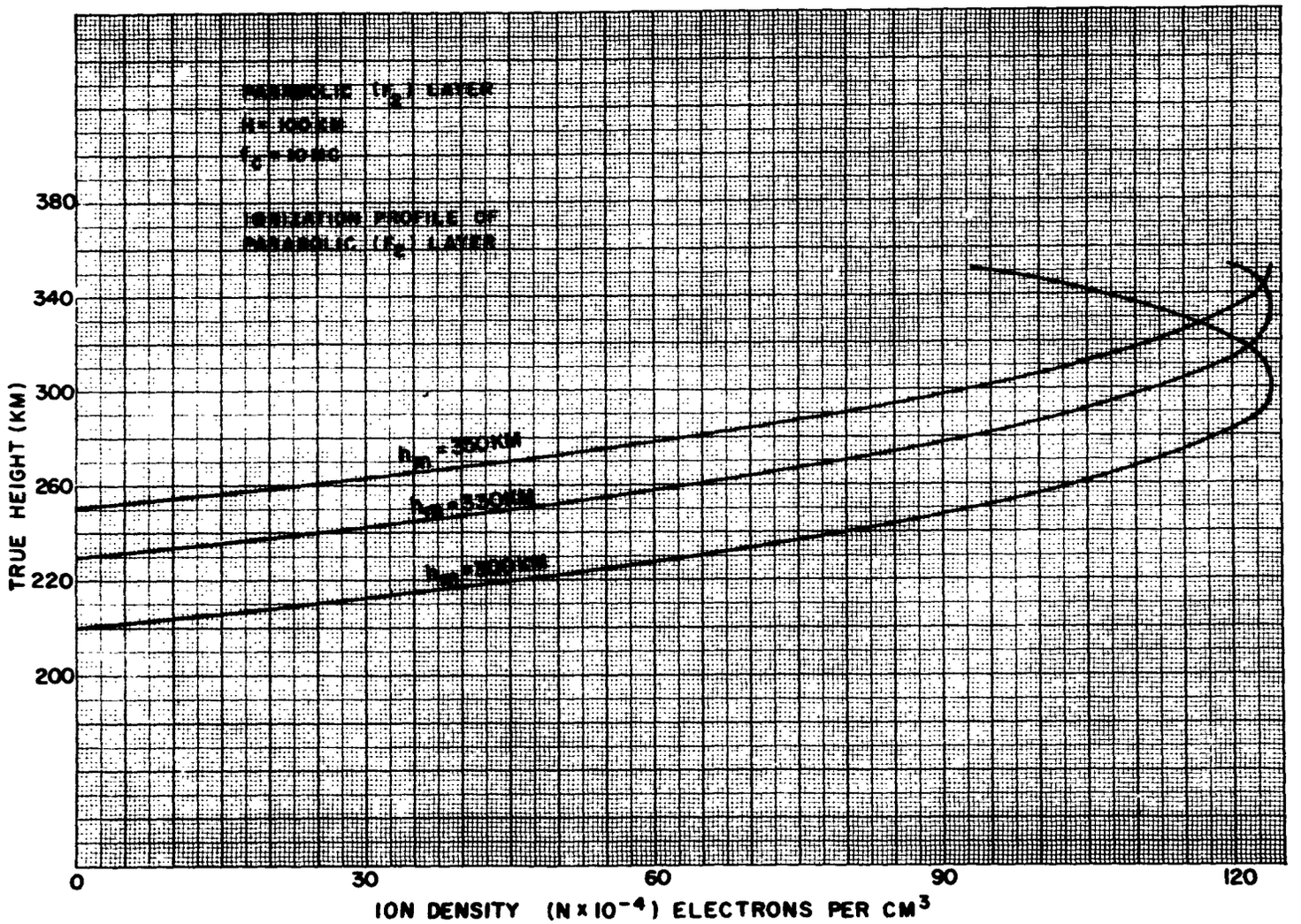

Figure 14. Ionization Profile of Parabolic (F_2) Layer

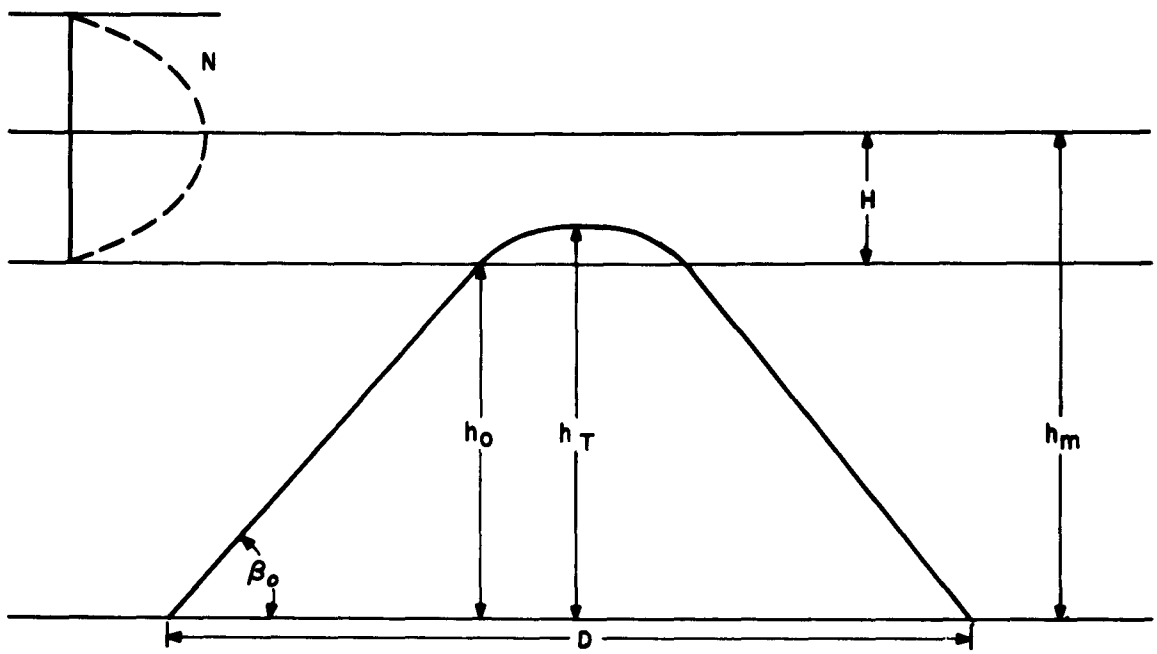

Figure 15. Ray Path through Plane Layer

The general relationship between distance and equivalent phase path, both measured in km, is illustrated in Figures 16 and 17. A similar relationship between the equivalent group and phase path is shown in Figures 18 and 19.

In order to facilitate the comparisons between calculated results and observed results, a group of specific functional dependencies were derived from the general relationships as exemplified in Figures 16 — 19. Figure 20 indicates the variation of the equivalent phase path with the relative frequency for a fixed ground distance. The relationship shows that the equivalent phase path is the greatest at the skip, decreasing slowly on the low-angle branch and falling rapidly on the high-angle branch, with a decreasing relative frequency.

A similar relationship between the equivalent phase path and the relative frequency for a constant equivalent path length is shown in Figure 21. In contrast to that of a constant ground distance, the phase

path is greatest for the lowest angle ray possible. The equivalent phase path increases slowly along the upper branch as the relative frequency decreases from its value at T_{MIN} (the minimum time ray), while falling more rapidly on the lower branch. In this example, the equivalent phase becomes greater on the upper branch and falls rapidly on the lower branch. This is contrasted with the example involving a constant distance where the phase path on both branches decreases.

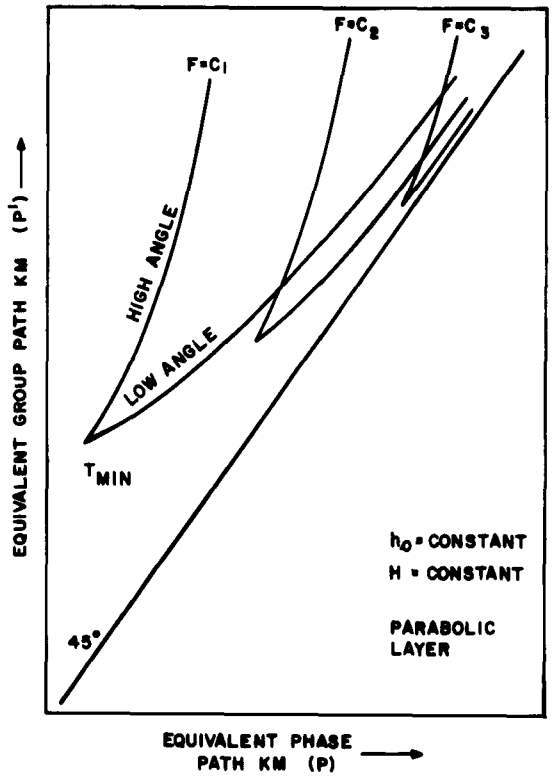

Figure 16. Representation of Distance vs Equivalent Phase Path for Constant Height

A final relationship, found useful in evaluating the observed backscatter records, is the relationship between T_{MIN} and the equivalent phase path for a fixed position in the backscatter (Figures 22 and 23). It should be noted that the equivalent phase path is strongly dependent upon T_{MIN}, with substantial changes in the height of the layer only slightly influencing the value of the equivalent phase path.

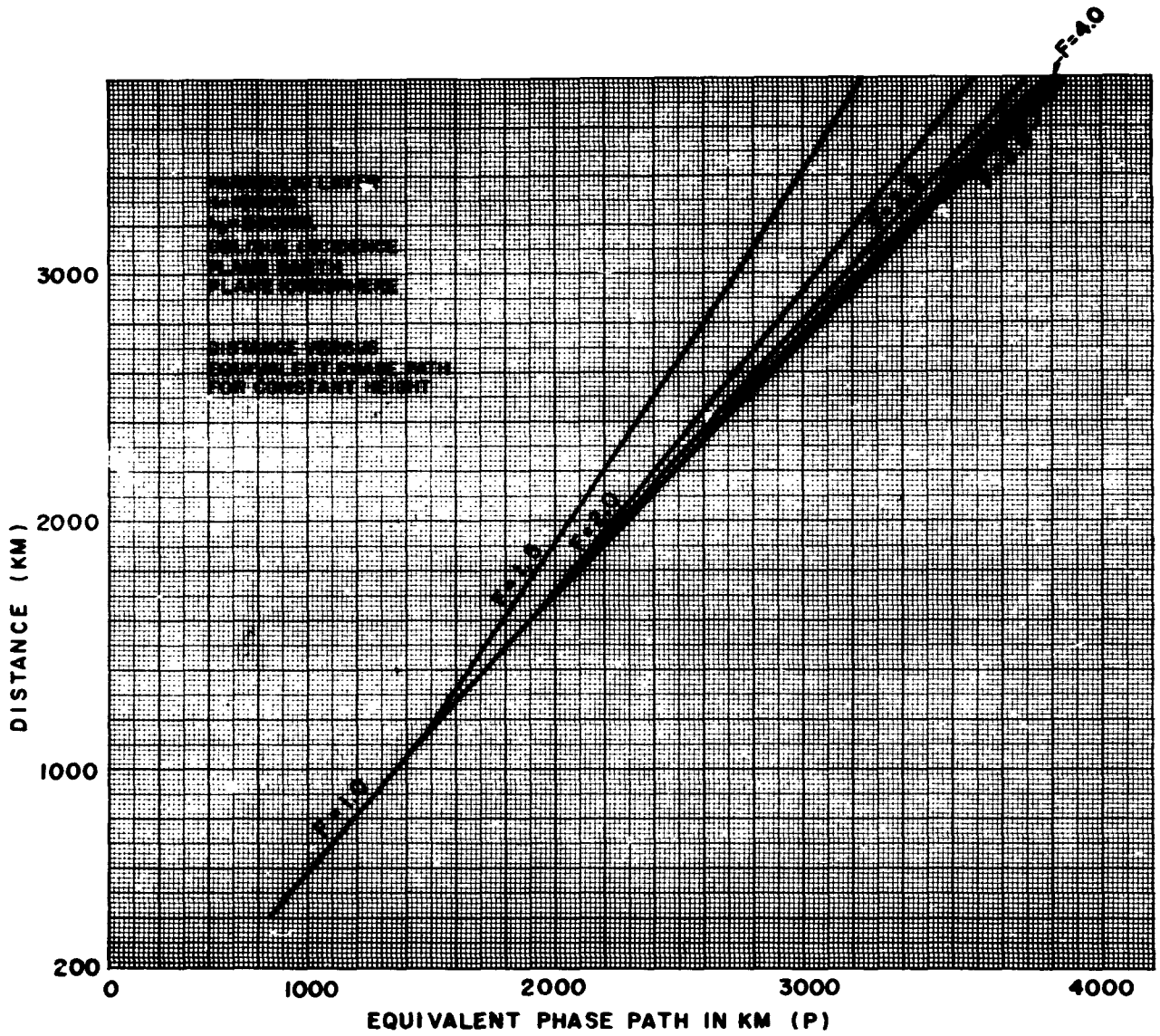

Figure 17. Distance vs Equivalent Phase Path for Constant Height

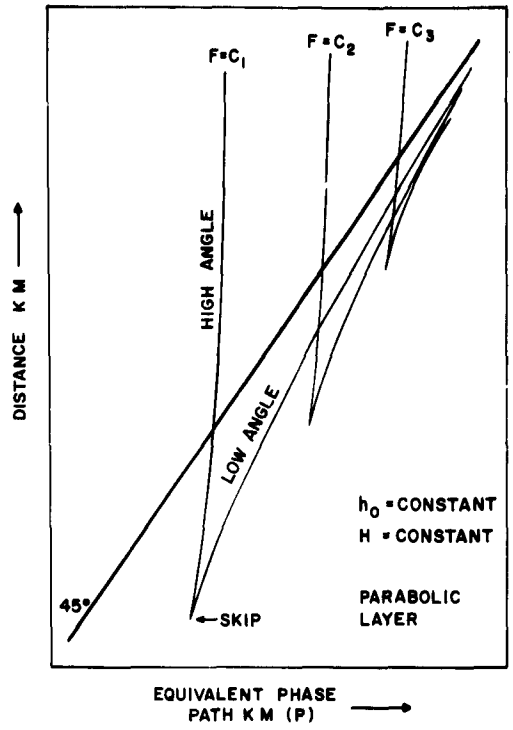

Figure 18. Representation of Equivalent Group Path vs Equivalent Phase Path for Constant Height

3.4.2.3 Effect of Time Variations

With the relationships among the ground distance and equivalent group and phase paths defined, it is possible to demonstrate the type of changes in the phase path for given changes in the ionospheric parameters. The changes in the phase path can best be defined as a frequency shift equal to the difference between the transmitted and received frequencies. The relationship between Δf and the phase path, as measured in wavelengths (P_ϕ), is the time derivative of the change in the phase path:

$$\Delta f = \frac{\Delta P_\phi}{\Delta t} \qquad (17)$$

Δf = frequency shift (cps)

Δt = $t_2 - t_1$ (sec)

ΔP_ϕ = change in the total number of wavelengths over the one-way path (cycle)

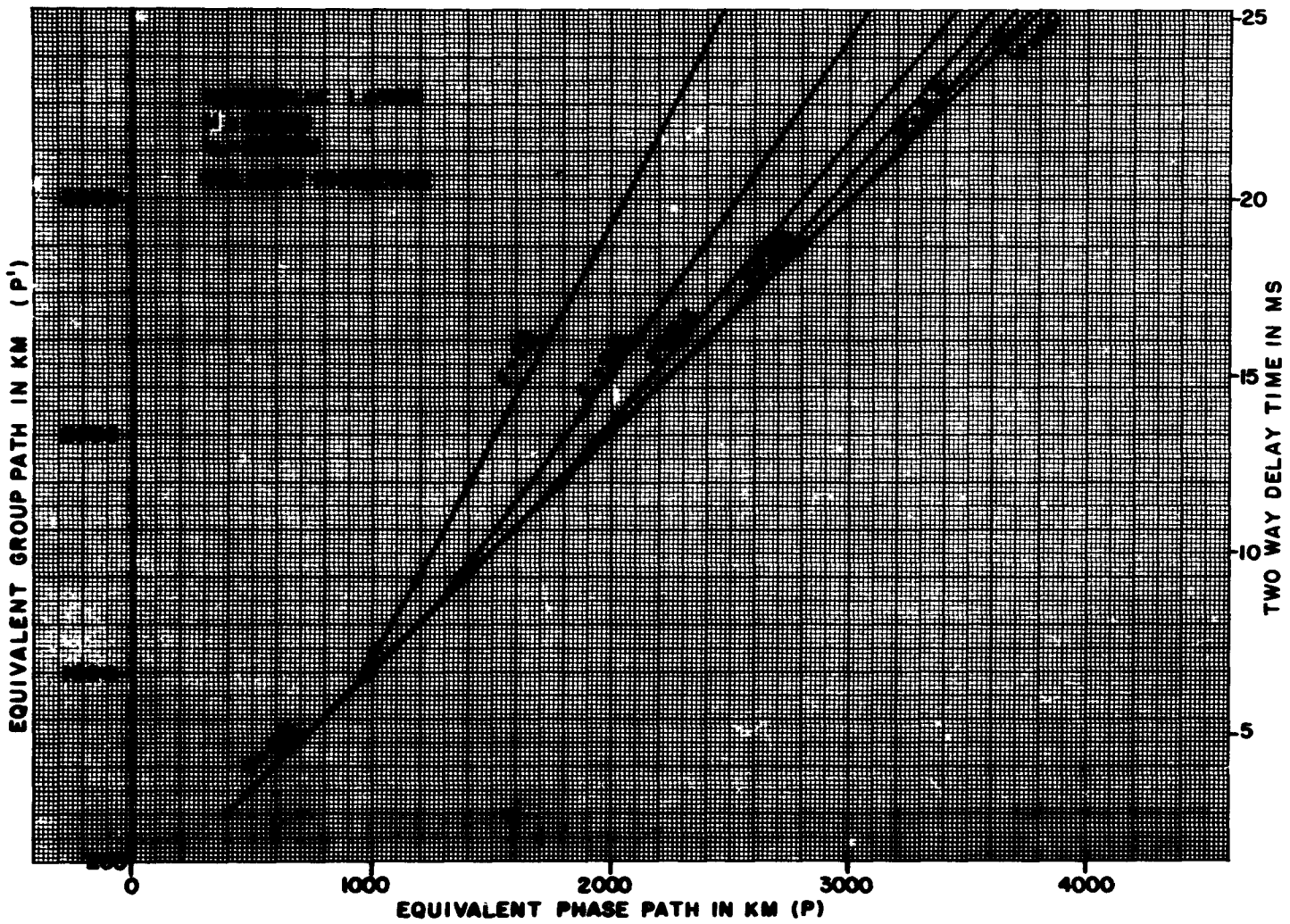

Figure 19. Equivalent Group Path vs Equivalent Phase Path for Constant Height

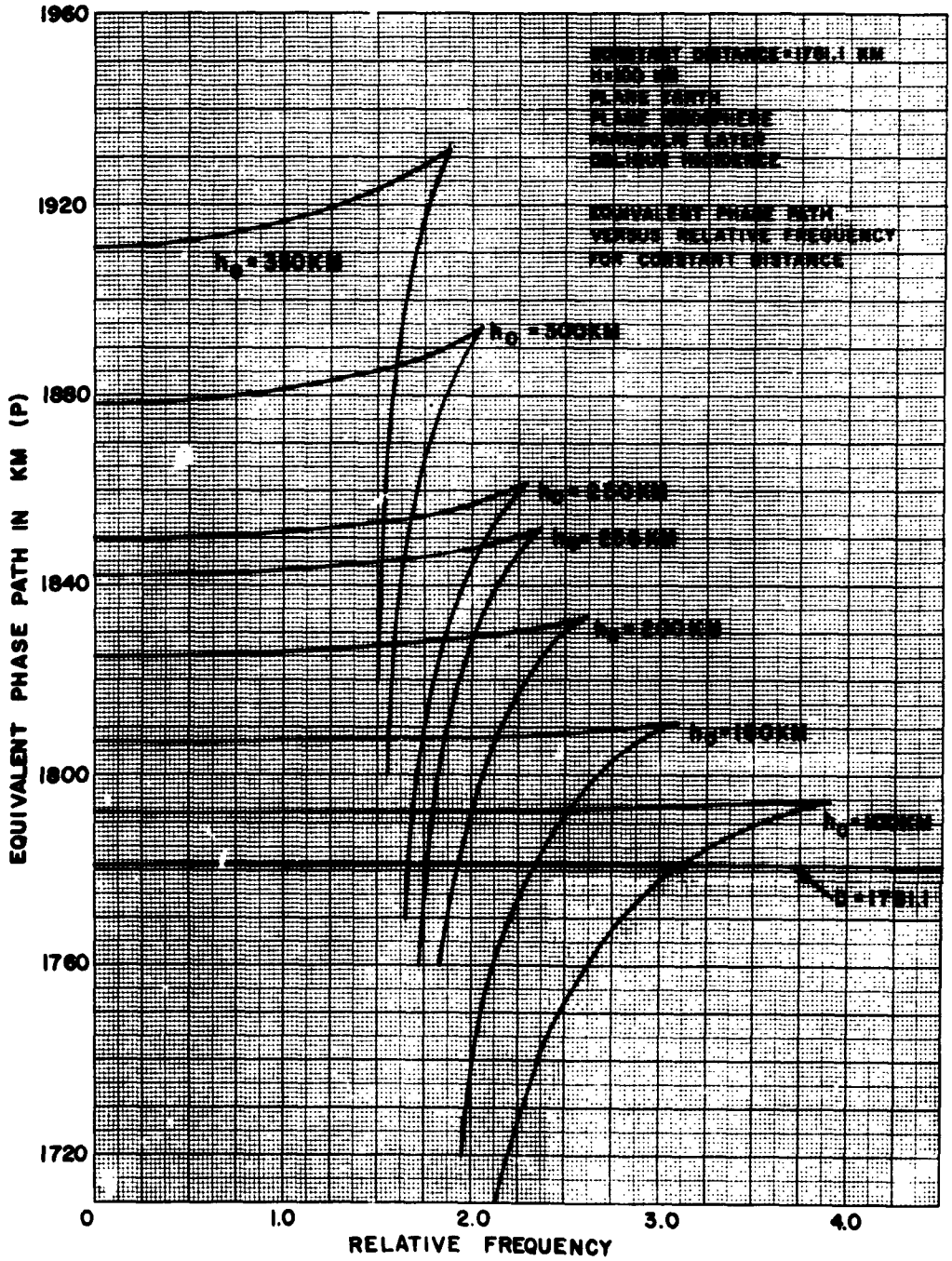

Figure 20. Equivalent Phase Path vs Relative Frequency for Constant Distance

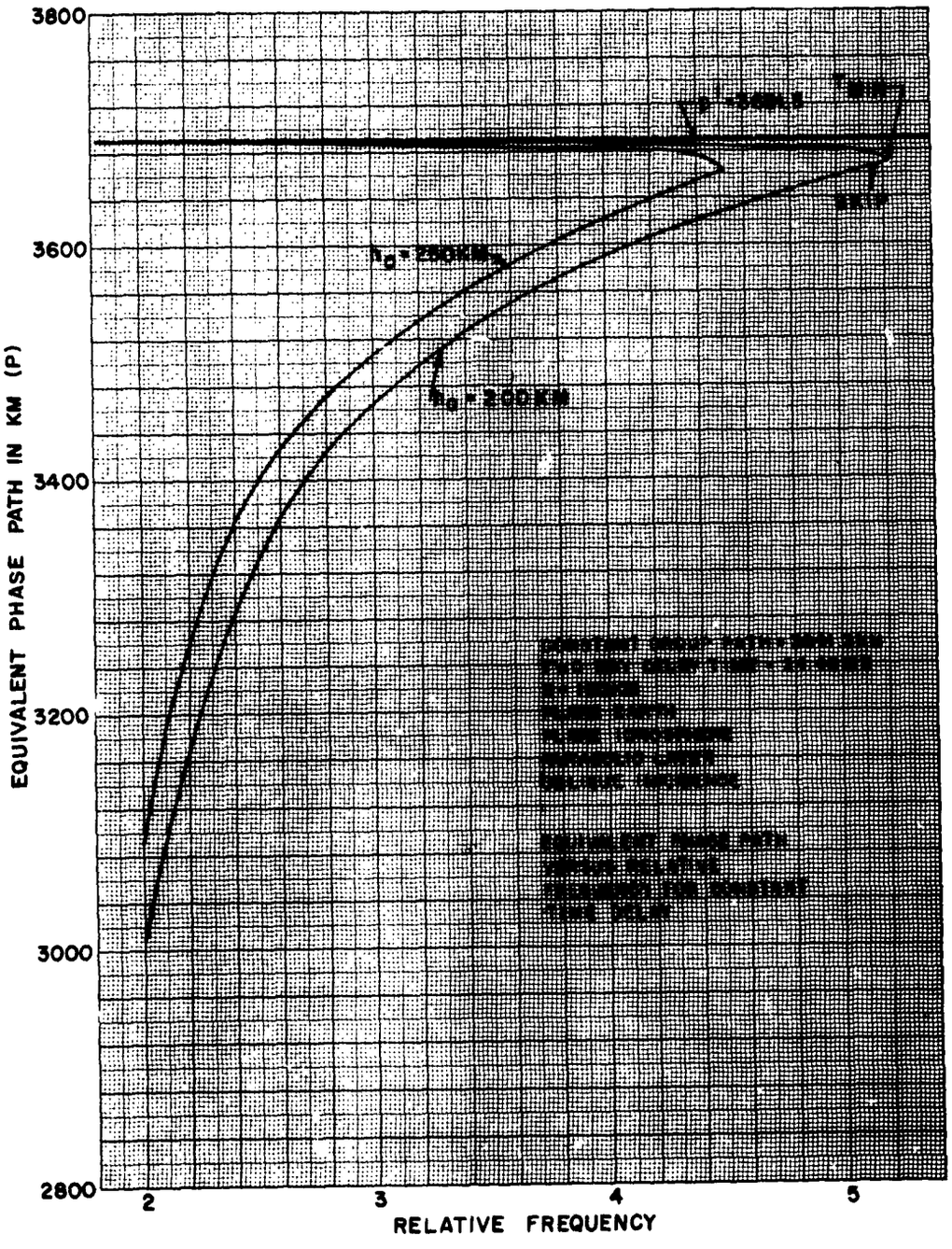

Figure 21. Equivalent Phase Path vs Relative Frequency for Constant Time Delay

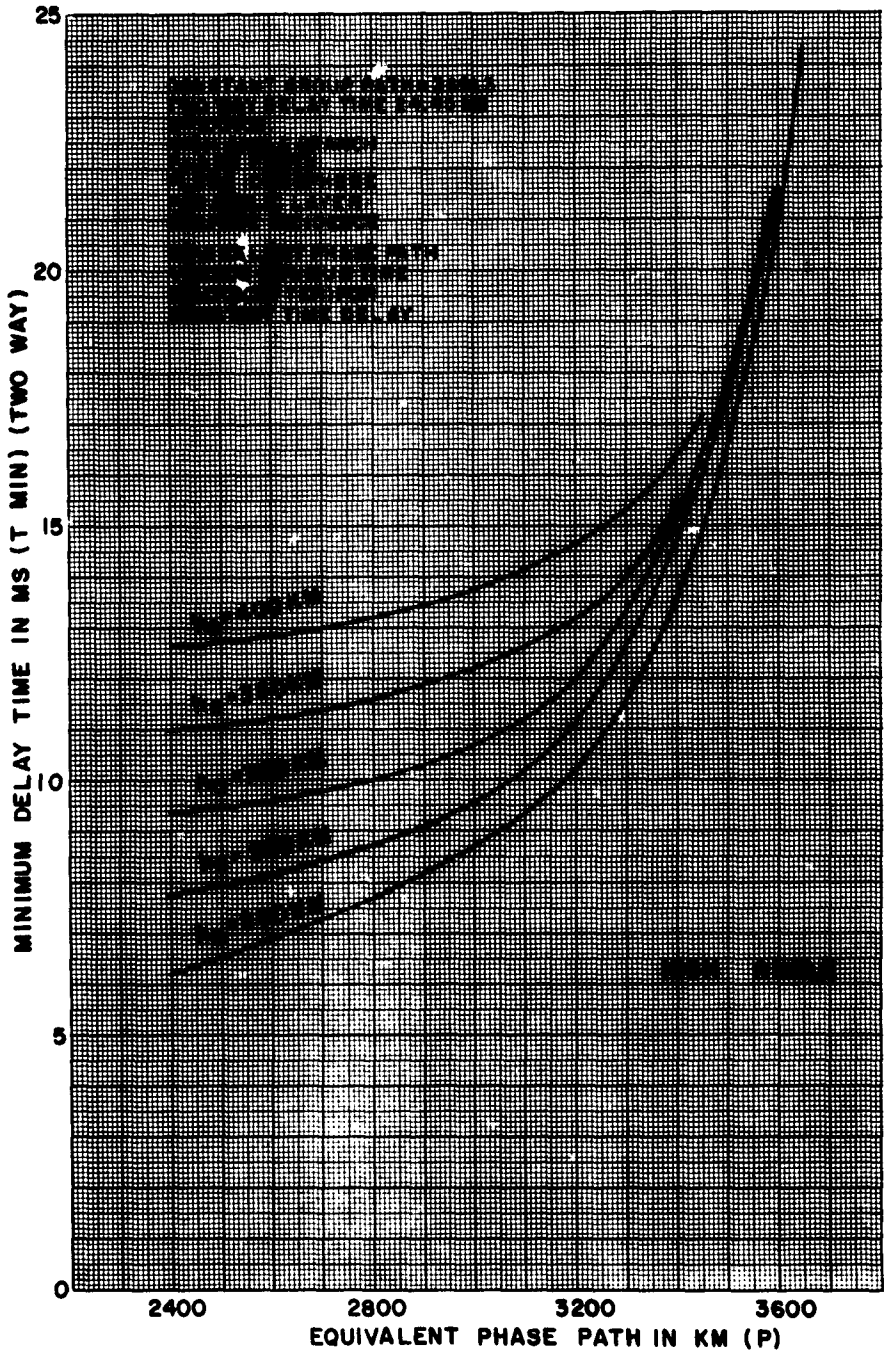

Figure 22. Equivalent Phase Path vs Minimum Time (Backscatter) for Constant Time Delay (High Angle)

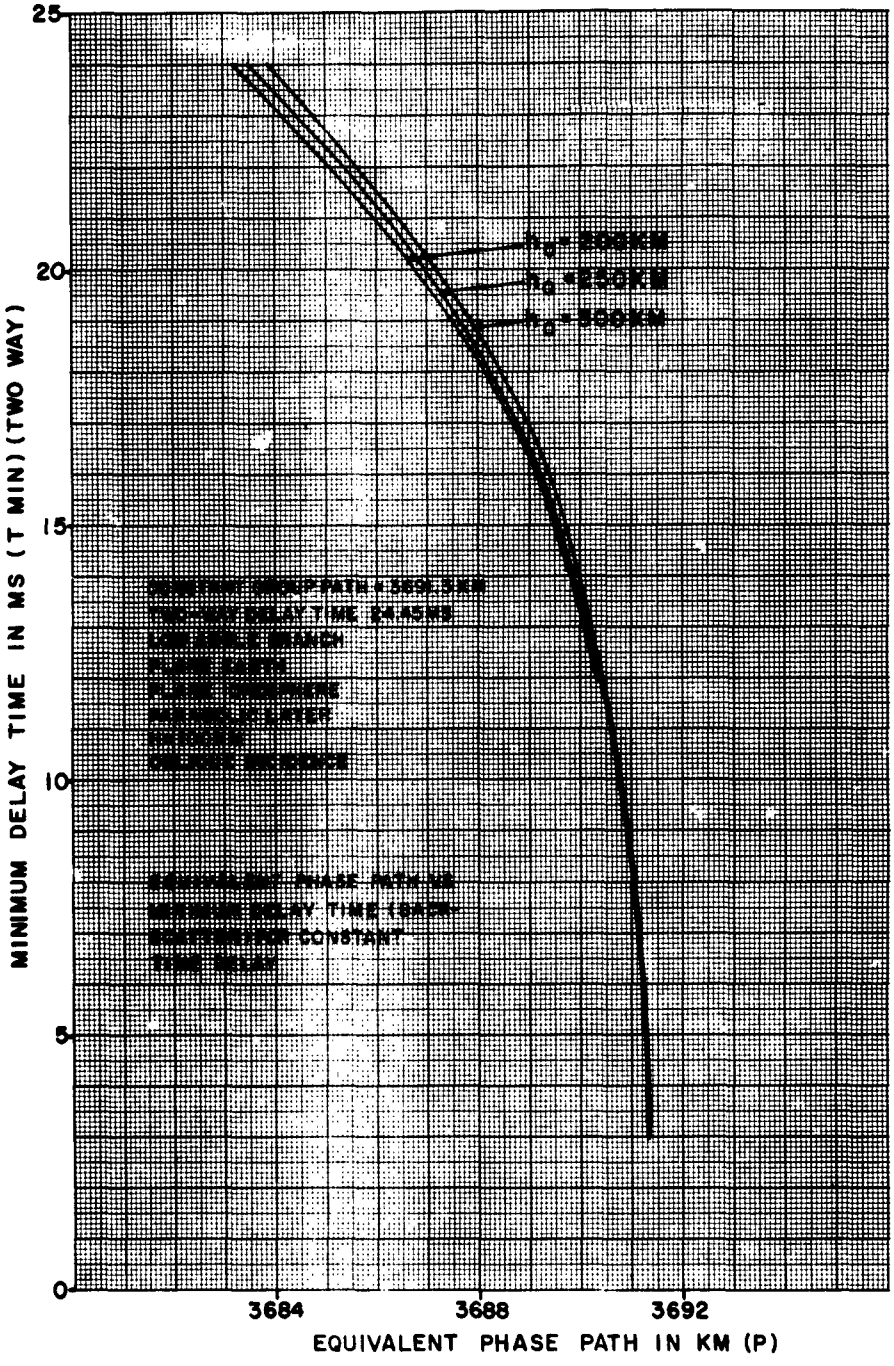

Figure 23. Equivalent Phase Path vs Minimum Delay Time (Backscatter) for Constant Time Delay (Low Angle)

A simple example of the range of values to be expected for Δf is shown for the vertical incidence case in Figure 24. This illustrates the frequency shift (Δf) to be expected for small percentage changes in the relative frequency. If the relative frequency is near unity, very small changes in the ionization of the layer can cause a substantial frequency shift.

Referring to Figures 20 — 23, showing the dependence of the equivalent phase path on the relative frequency and also T_{MIN}, the following summary has been made to illustrate the ranges to be expected in Δf over an oblique path:

Table 1

Parameter * Changed (All Other Const)	P vs F Const Dist		P vs F Const P'		P vs T_{MIN} Const P'	
	Low Angle	High Angle	Low Angle	High Angle	Low Angle	High Angle
Positive ΔF	Δf small and positive	Δf large and positive	Δf small and positive	Δf large and positive	———	———
Positive Δh_o	Δf large and positive	Δf large and positive	Δf small and negative	Δf large and positive	Δf very small and negative	Δf small and negative
Positive ΔT_{MIN}	———	———	———	———	Δf small and negative	Δf very large and positive

* Table 1 demonstrates the effect of positive changes in relative frequency (F), layer height (h_o) and T_{MIN}. Only one parameter is changed at a time, with all others remaining constant.

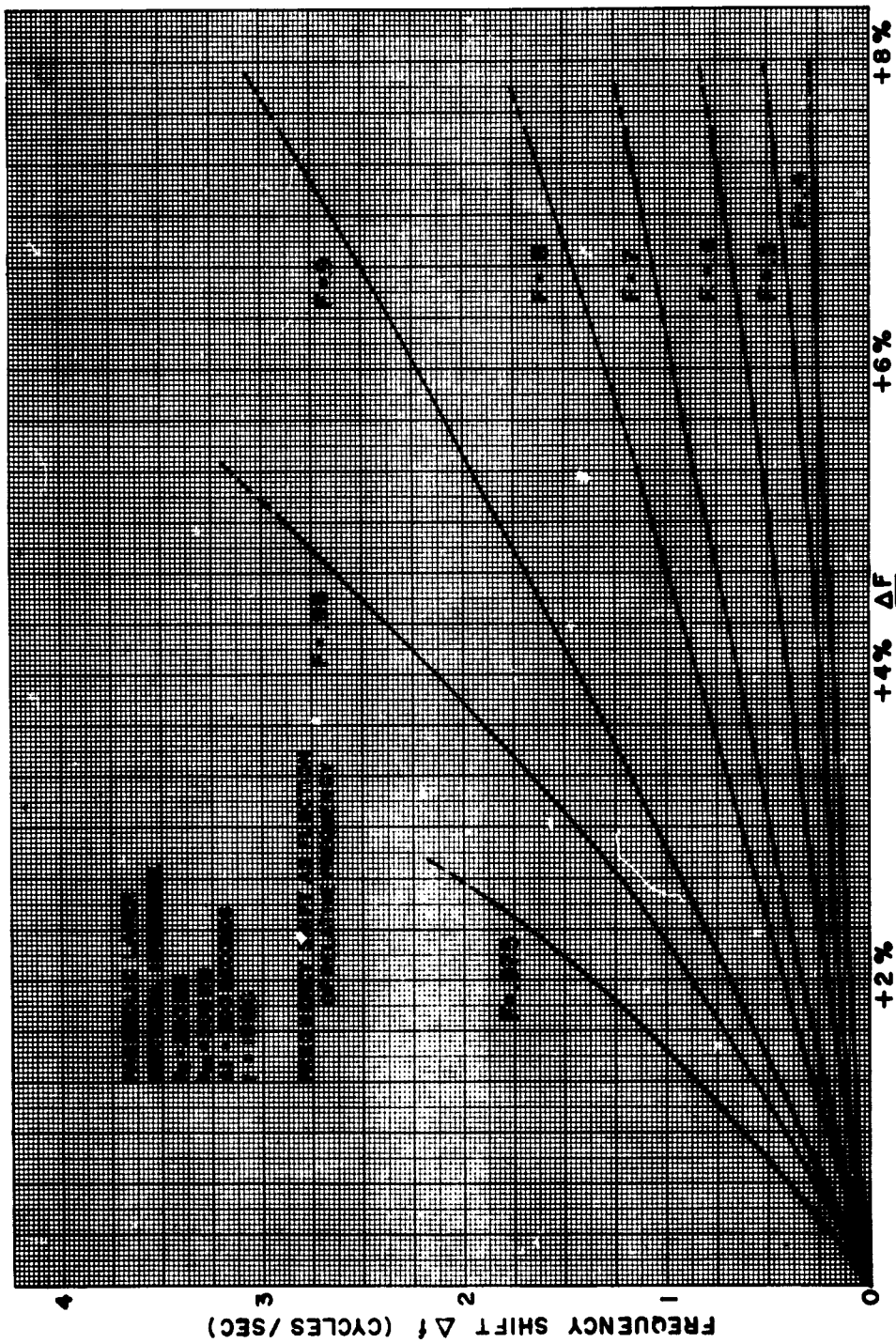

Figure 24. Frequency Shift as Function of Relative Frequency

3.4.3 Experimental Comparison

The purpose of this section has been to compare the results derived from the theoretical relationships involving the phase path with the observed changes in the phase path. The following is a discussion of the comparisons made for both vertical and oblique incidence cases.

3.4.3.1 Vertical Incidence

The first group of comparisons to be made involved coherent detection of vertical incidence transmissions at GBI. Since, for this case, the transmitter and receiver are located at the same point, it is very easy to compare transmitted with received frequency. A total of four cases were studied, one of which is illustrated in detail. In Figure 25a, the range-time recording is shown for the coherently detected vertical incidence signal between 1350 and 1405.5 on April 18, 1960.

Observing the frequency changes covering the ordinary ray path, 258 cycles are obtained over the 930-second interval, with interpolation necessary over the missing 45 seconds. The average frequency shift is:

$$\Delta f = .277 \text{ cps} \qquad (18)$$

By making use of the relationship shown in Equations (14) and (17), the analytical determination of the time derivative of the change in phase path, i.e., frequency shift, for the vertical incidence case can be shown to be:

$$\Delta f = \frac{\Delta P}{\lambda_o \Delta t} = \frac{2}{\lambda_o \Delta t} \left(\Delta h_o + \frac{1}{2} \Delta H + \Delta G\right) \qquad (19)$$

where

$$G = \frac{H (F^2 - 1)}{4 F^2} \log_e \frac{1 + F}{1 - F}$$

In order to obtain the parameters necessary for the analytical solution of the frequency shift, two ionograms are used:

one for the beginning of the selected interval, t_1 (1350 - Figure 25b), and one for the end of the interval, t_2 (1505.5 - Figure 25c). A best fit is made between the observed h' - f records and calculated h' - f profiles, assuming a parabolic ion-density distribution. The corresponding changes in the parameters of the h_o, H, and F are obtained from the two calculated h' - f profiles for the times t_1 and t_2. The resulting calculated value of Δf, using the analytical method is:

$$\Delta f = .329 \text{ cps} \qquad (20)$$

A second method of obtaining the value of Δf is shown by the relationship in Equation (4). This is the direct integration of the integral, $\int_o \mu dh$, $(\sin\beta_o = 1)$, by graphical means. Using the Schmerling 10-point system the two N-h profiles are obtained for the beginning and end of the test from the two ionograms shown. Making use of the relationship shown in Equation (5), the respective μ-h curves are obtained and are shown in Figure 26. By measuring the change in the area under the μ-h curve from t_1 to t_2, the value of the change in the integral is obtained. By substituting into Equations (16) and (17), the graphically calculated value of Δf is obtained.

$$\Delta f = .296 \text{ cps} \qquad (21)$$

The calculated and observed values of the remainder of the four cases are shown in the accompanying Table 2. Although the agreement is not as close as that in the case presented, the results show the same general trend.

Table 2

Case	Date Time	Observed	Calculated Graphical Integration	Calculated Best Fit
I	Apr 18, '60 1350 - 1405.5	.277 cps	.296 cps	.329 cps
II	Mar 25, '60 1644 - 1655	.088 cps	.184 cps	.104 cps
III	Mar 8, '60 0828 - 0830	1.17 cps	1.08 cps	1.47 cps
IV	Mar 8, '60 0838-0840.5	.36 cps	.44 cps	.59 cps

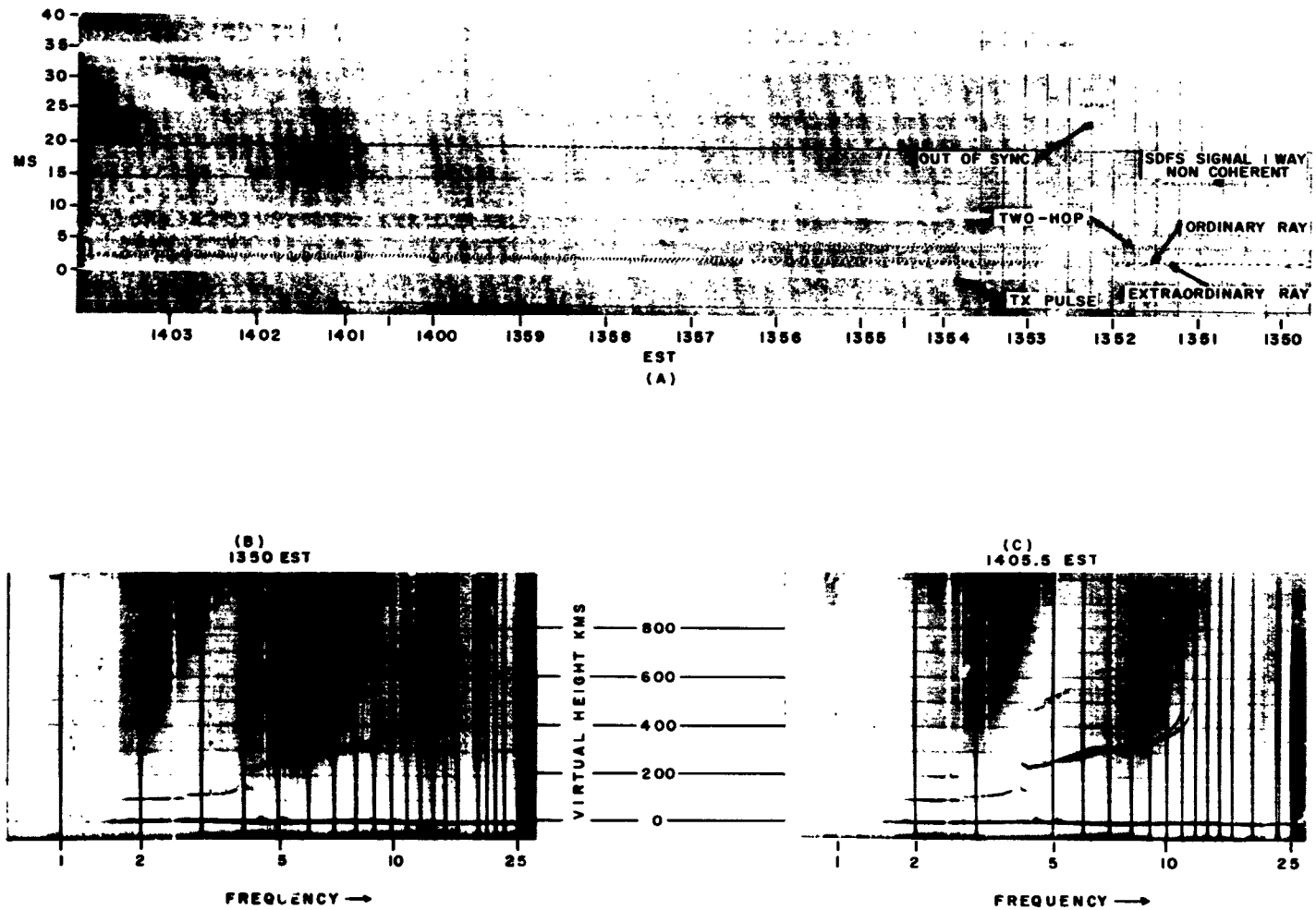

Figure 25. Ionograms and Range-Time Record for Vertical Incidence Test, April 18, 1961, 1350-1405.5, GBI

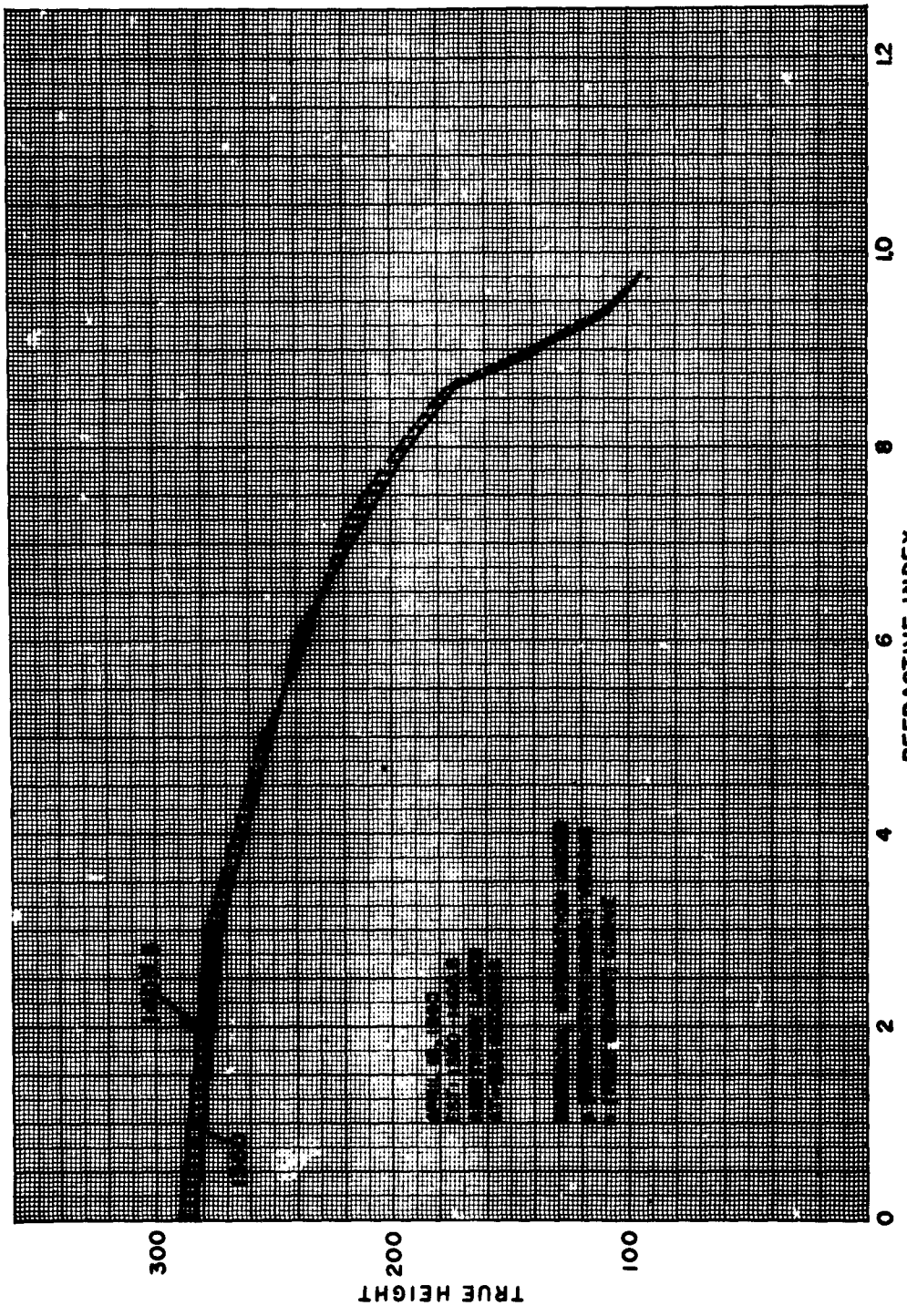

Figure 26. Graphical Integration under μ (Refractive Index) vs h (True Height) Curve

3.4.3.2 Oblique Incidence

The second group of comparisons to be made involved phase-coherent transmissions over the 1781-km oblique path between GBI and SDFS (Figure 27). In the operation over this path, a 150- μs pulse was transmitted from GBI on both 9 and 12 mc. Since the transmitter and receiver were separated, it was necessary that highly stable frequency sources be employed to permit accurate frequency comparisons. For this purpose, frequency standards, stable to at least one part in 10^8 per day, were used in both transmitter and receiver.

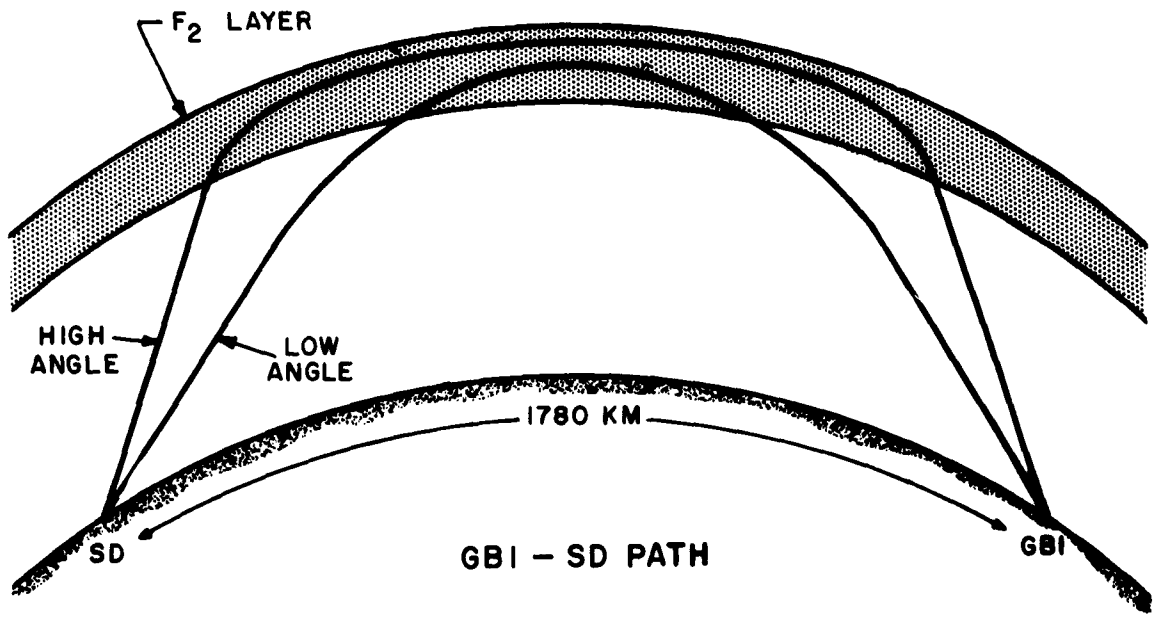

Figure 27. GBI-SDFS Path

On February 28, 1961, a set of measurements was made using the phase-coherent transmissions between GBI and SDFS. The range-time records (Figure 28a and b) show the 12-mc signal as the skip crosses the station at South Dartmouth. It should be noted that the actual time of occurrence of the ordinary skip is taken from the spectrograms discussed below. At this time, the skip distance was decreasing as a result of a large increase in the critical frequency of the F_2 layer. At a later time, on both

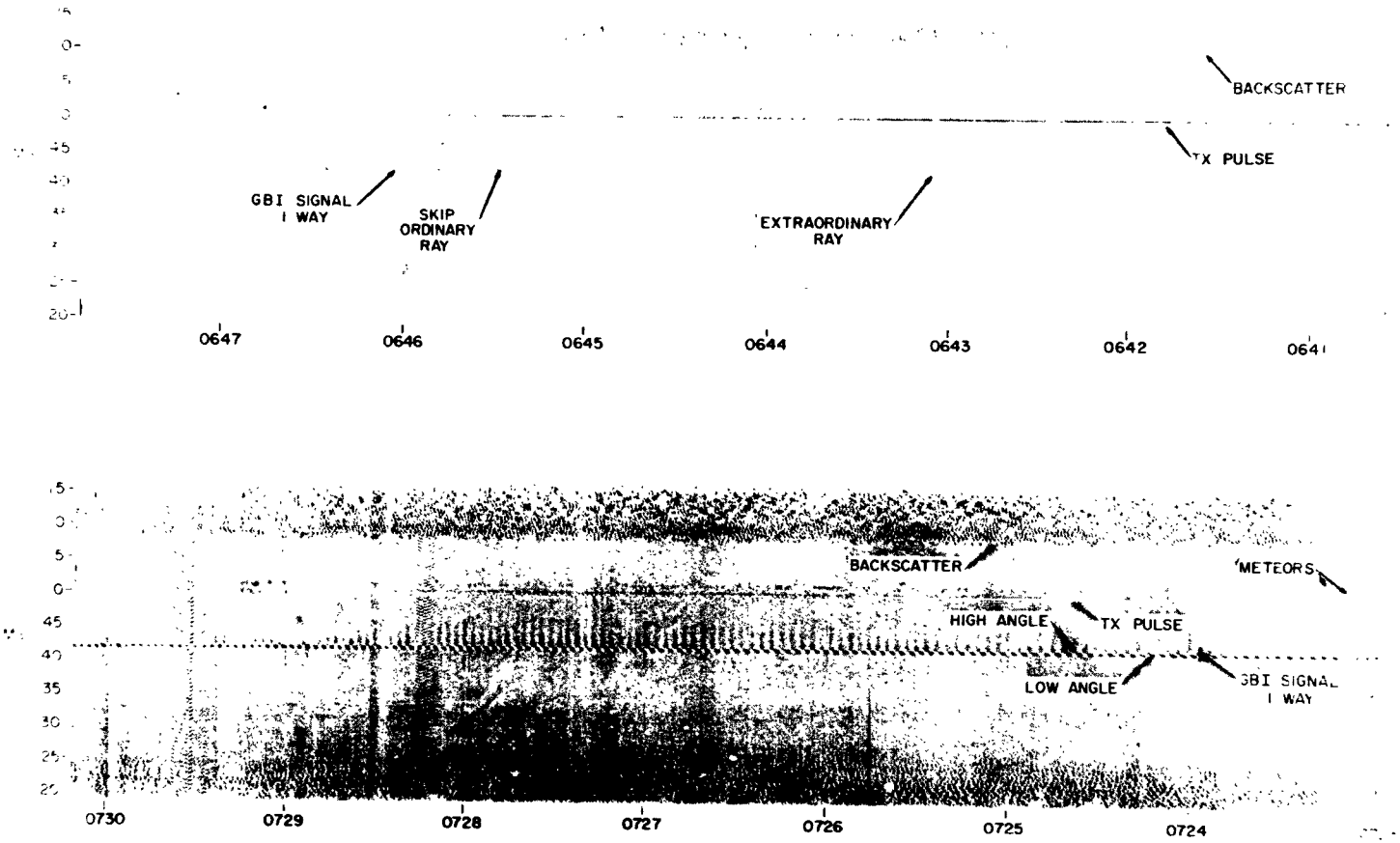

Figure 28. Range-Time Records (12 mc) for Oblique Incidence Test, February 28, 1961, 0647-0723, GBI-SDFS

operating frequencies, the range-time records show the separation of the low-angle and high-angle components.

Referring to the spectrograms in Figures 29 and 30, which give the value of Δf directly, the separation of not only the low-angle and high-angle components is shown but also the separation of the ordinary and extraordinary components. Figure 29a shows the 9-mc signal as the skip crosses the station at South Dartmouth. The component of the signal that first appears at the station is that of the extraordinary ray.

All components fade out, except that of the low-angle ordinary, which is continually tracked by the gate. This record has been offset in order to place the zero point in the middle of the record, allowing the sign of Δf to be obtained. On the spectrogram just shown, as well as the remaining spectrograms, the separation of one component from another was accomplished by following the selected mode in time with a moving gate. This method generally increases the relative amplitude of the selected component, while causing the other components to fade from the record. Figure 29b shows the high angle of the 9-mc signal, with the appearance of the O and X components at different times on the record. Figure 29c shows the ordinary and extraordinary components of the low angle on 9 mc, with Figure 29d showing only the ordinary component when the gate is moved to a greater delay time (approx. 30 μs).

Much the same sequence is seen on the 12-mc records, with Figure 30a and b showing the separation possible on the high angle between the O and X components with the gates placed approximately 50 μs apart. Figure 30c and d show the separation of the low angle on 12 mc into its respective O and X components.

Figure 30e and f show the 12-mc signal as it crosses the skip, with the high angle separating into the O and X components. An extra component of low amplitude that fades out immediately after the occurrence of the skip is also observed.

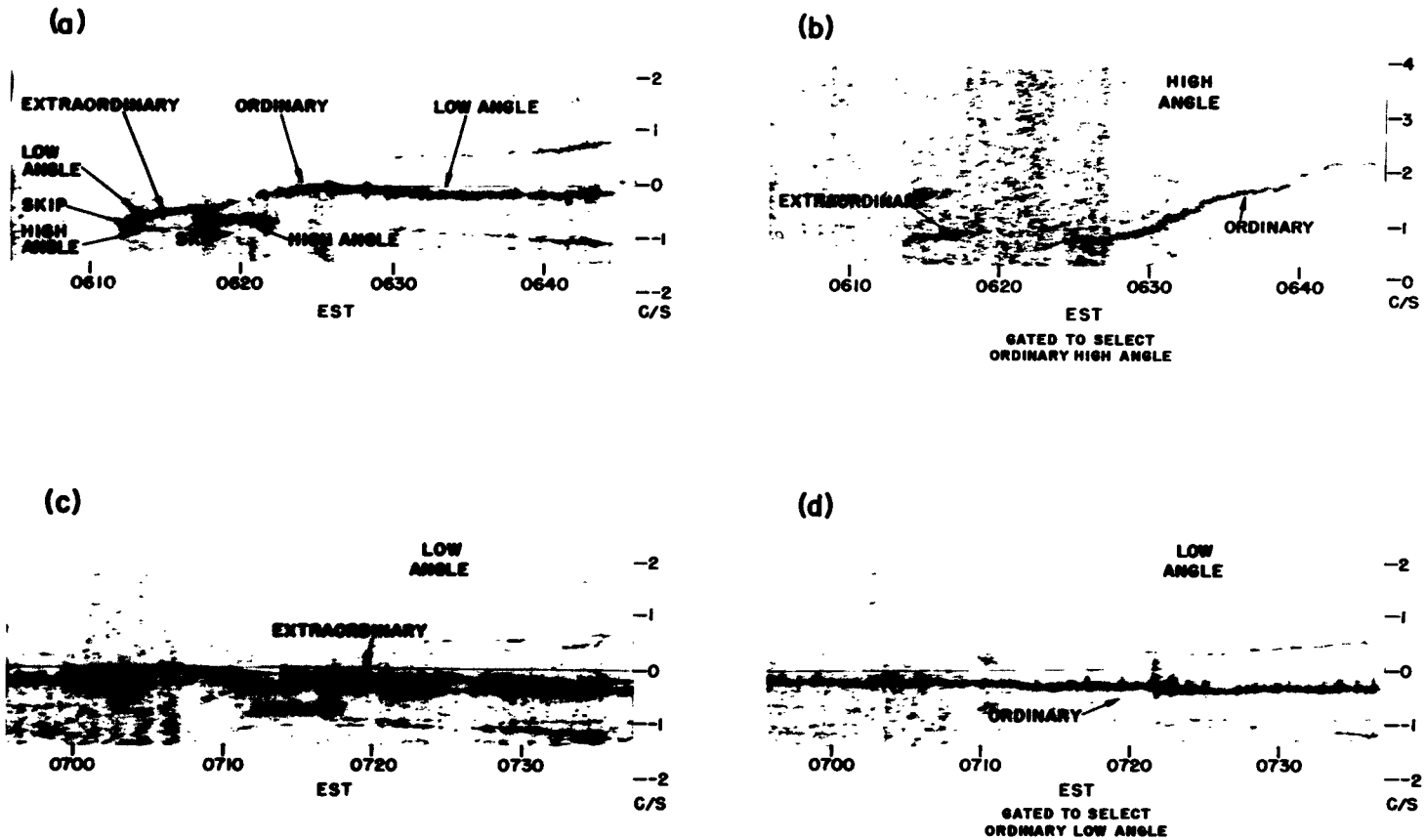

Figure 29. Spectrograms (9 mc) for Oblique Incidence Test, February 28, 1961, 0600-0800, GBI-SDFS

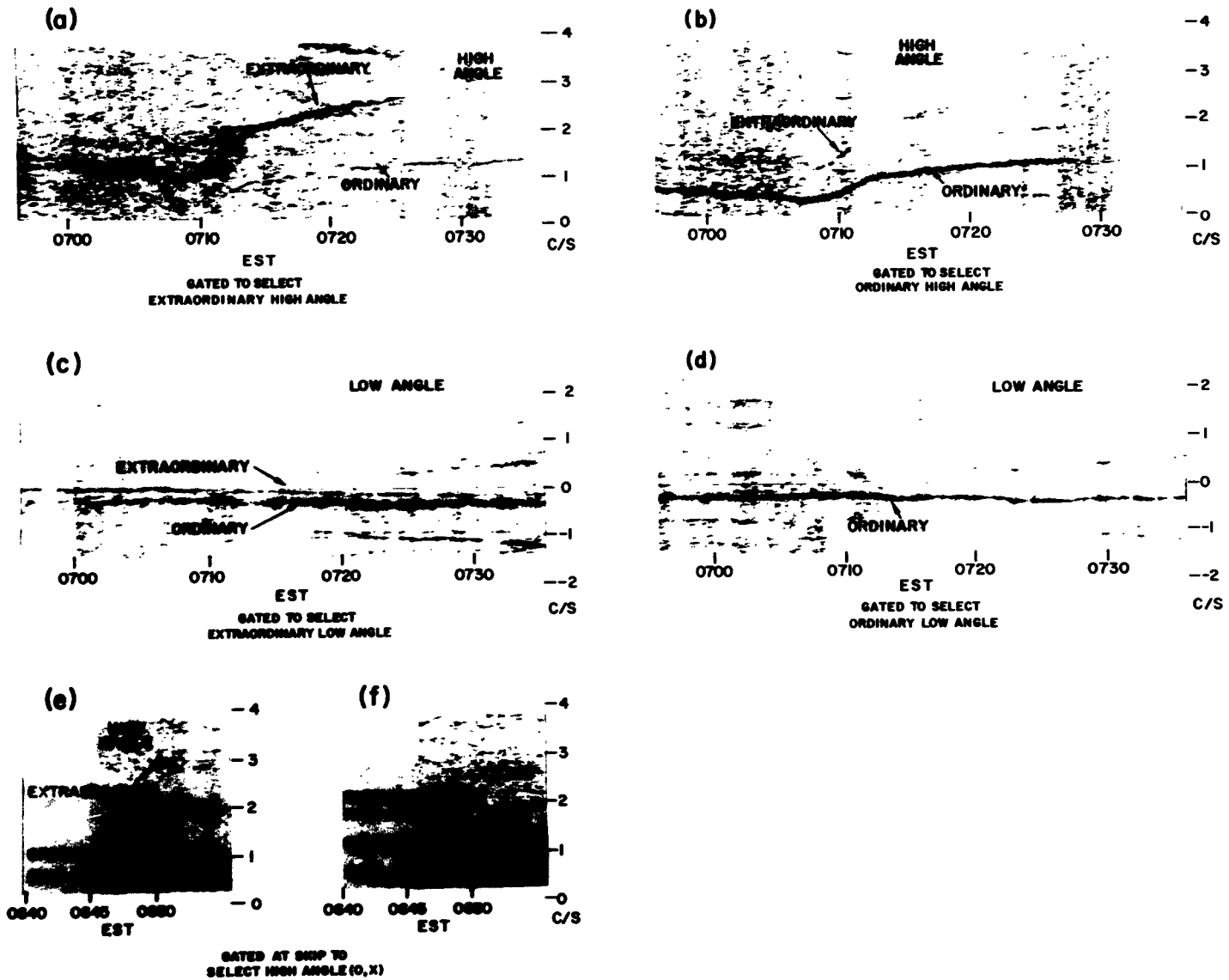

Figure 30. Spectrograms (12 mc) for Oblique Incidence Test, February 28, 1961, 0600-0800 GBI-SDFS

The spectrograms showing the various components of the 9- and 12-mc signals demonstrate the separation of the ordinary and extraordinary components of the high- and low-angle rays. Although this separation in range time of the ordinary and extraordinary components was generally quite small, on the order of 30-40 μs, the relatively large differences in frequency shift allow a distinction to be made on the spectrograms. The values of these various components scaled from the spectrograms are plotted against Eastern Standard Time and are shown in Figure 31.

In order to make a comparison between the observed values of frequency shift for the various components and the results derived from the analytical relationships, it was necessary to scale off the changes in the parameters required in the theoretical relations. This made use of a series of ionograms taken 15 minutes apart at GBI, 900 km from the center of the path, over the period 0600-0800, Figure 32. The resulting values of the true height of the F_2 layer and the respective critical frequencies were obtained for both the ordinary and extraordinary profiles by the use of a series of "best fit" parabolas with a constant semi-thickness of 100 km. It was assumed that, to a first order, the effect of the earth's magnetic field could be represented by a frequency shift of the extraordinary profile. Using the relationships shown in Figure 20 for the relative frequency, the height of the layer, and equivalent phase path, the corresponding changes in the equivalent path length were calculated, converted into the appropriate values of Δf, and the results plotted against Eastern Standard Time in Figure 33.

In the examination of the observed data in Figure 31 and the calculated results in Figure 33, it is first noticed that the curves are similar in shape with a time displacement of about 15 minutes.

This similarity of shape supports the conclusion that the frequency shift (Δf) is, in fact, a direct function of the changes that occur within the layer and is not sensitive to the model chosen. In comparison, the calculated ground distance for a given ray path is demonstrated to be sensitive to the model selected. This sensitivity results in a considerable

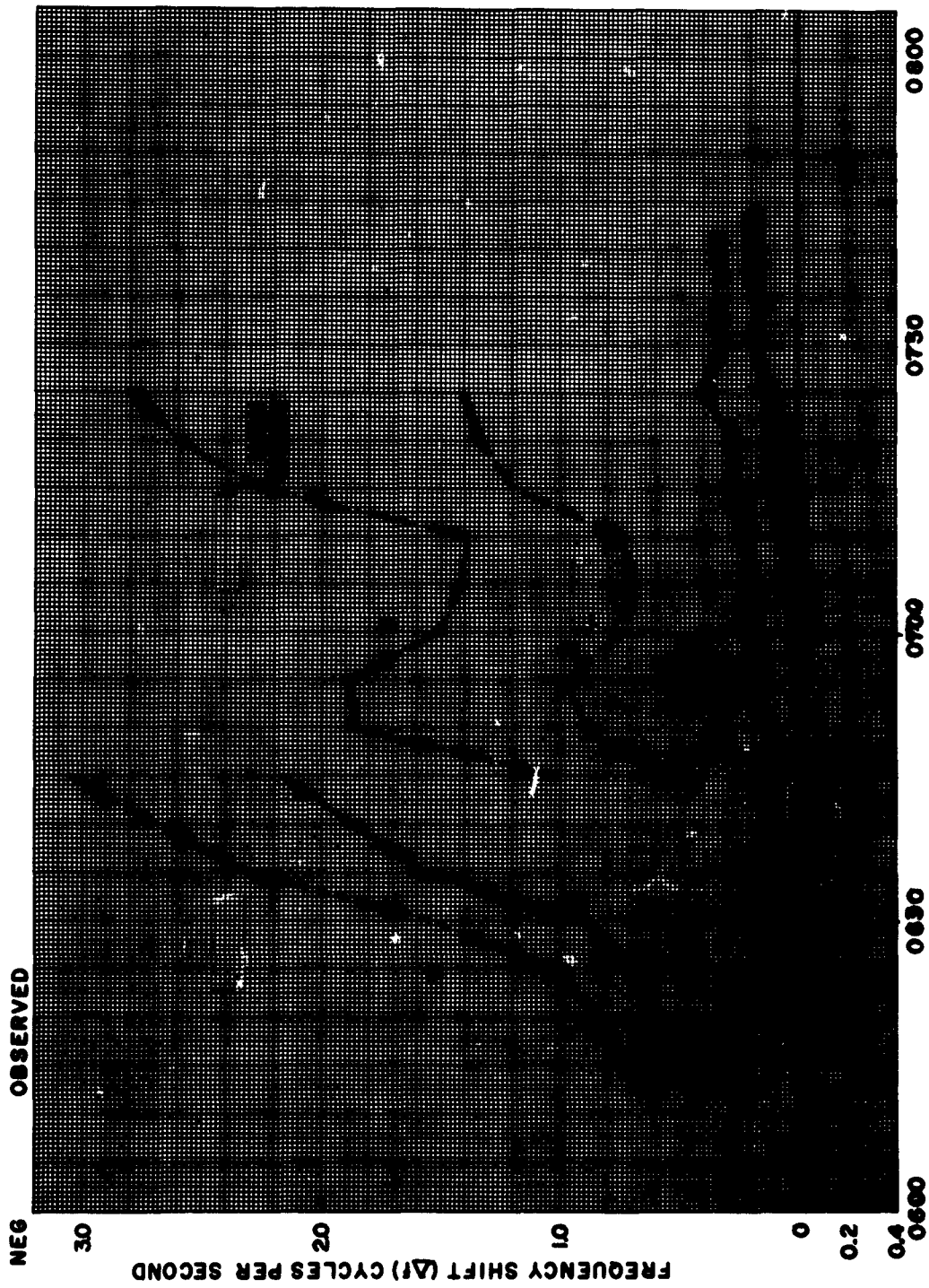

Figure 31. Frequency Shift (Δ f) vs EST (Observed)

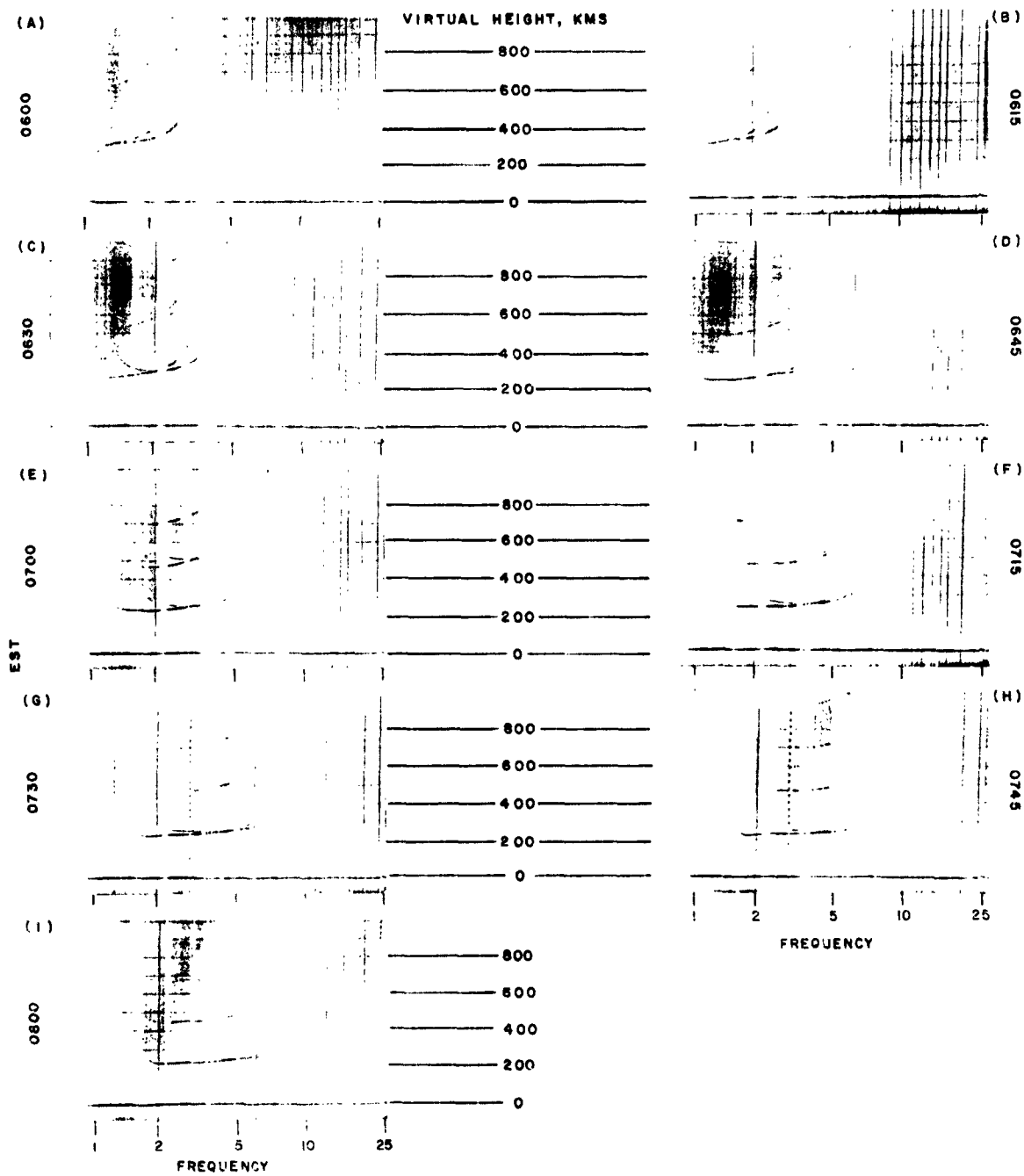

Figure 32. Sequence of Ionograms, February 28, 1961, 0600-0800, GBI

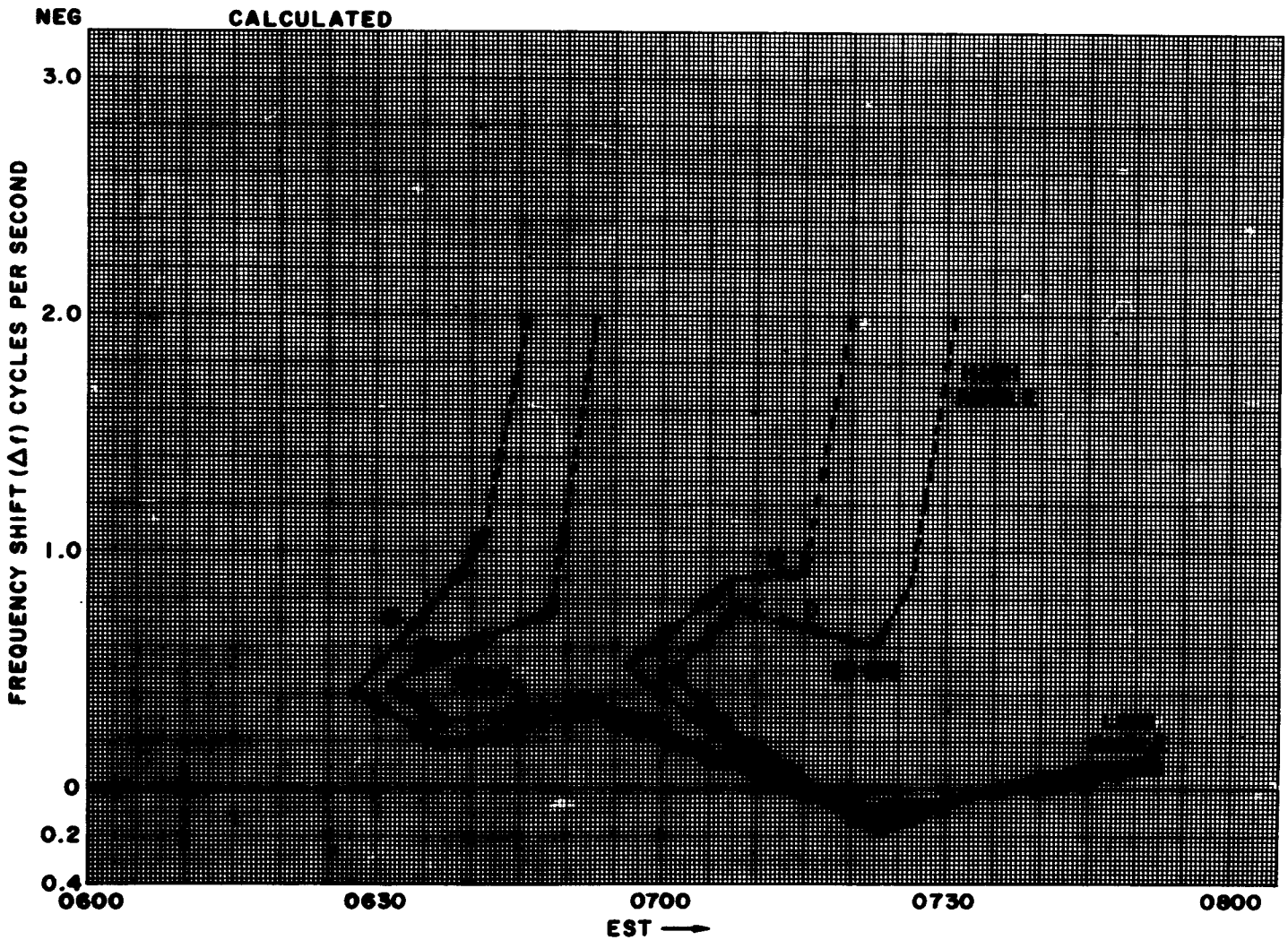

Figure 33. Frequency Shift (Δ f) vs EST (Calculated)

displacement between the time that the skip was theoretically expected to arrive and was actually observed to reach the station.

Of the possible reasons for the time displacement, we have two that are outstanding: first, the placement of the sounding station 900 km from the center of the path; second, the inability of the selected model to give exact values of the distance covered by the skip ray.

Since exact values are not necessary in the first order determination of the frequency shift, a similarity exists in the curves; a displacement in the times of occurrence of related phenomenon is, however, due to the inability of the model to give exact values of the distance of propagation.

3.4.4 Conclusion

To summarize the results of this section, the observed results obtained from both oblique and vertical incidence experiments agree reasonably well with theoretically expected values drawn from a simplified model. From the results of the theoretical section, regarding frequency shifts (Δf) resulting from normal ionospheric variations, the following conclusions can be drawn: *

Vertical Incidence: The higher the operating frequency, the higher the value of Δf.

Oblique Incidence

Low Angle: Same as vertical incidence.

High Angle: Low operating frequency — high Δf.

Ordinary (O) versus Extraordinary (X)

Low Angle: Δf O greater than Δf X

High Angle: Δf X greater than Δf O

*Change in layer height with time is assumed to have second order effect.

Backscatter: The farther from the leading edge, the greater the width of the spectrum.

Multihop (for fixed distance): The greater the number of hops, the greater the value of Δf.

At the present time, vertical incidence soundings provide a useful means of obtaining the ionization profile from measurements taken at ground level. The demonstrated sensitivity of phase measurements to ionospheric changes offers a possible addition to existing methods for determining not only the true profile but small perturbations upon the profile. In the future program, consideration will be given to determine if such an approach is feasible.

3.5 Special Effects

3.5.1 Sudden Ionospheric Disturbances

The usual way of detecting ionospheric disturbances at high frequencies is by observation of the field strength of distant transmissions. The occurrence of a short-wave fadeout (SWF) is indicative of a disturbance. A second, and perhaps more sensitive, indication of ionospheric conditions has recently been used at Raytheon. It consists of measurements of the phase or frequency changes in received signals. When an SID occurs, a perturbation in the received signal frequency, i.e., a sudden frequency shift, is observed having a very rapid onset and comparatively short duration. An interesting feature of the sudden frequency shift is that it precedes the recognizable absorption effect and signals the onset of an SWF. Data illustrating these effects were obtained during SID's which occurred on December 1, 1959 and April 5, 1961.

The ensuing data to be shown was collected using a pulse system, similar in concept to widely used ionospheric sounding equipment; the results were derived from both long-distance ground-backscatter

signals and the pulse transmissions of a distant cooperating station. The unique feature of the system is that coherent detection is used to allow examination of the phase or frequency changes in the received signals. For the long one-way path signals, this requires that all transmitter and receiver injection frequencies be derived from very stable frequency standards.

The pulse-modulation technique permits examination of separate backscatter groups or individual one-way modes of propagation. For example, one-hop and two-hop, or high-angle and low-angle, or occasionally even ordinary and extraordinary components of the received signal can be identified. This mode separation is useful in studying various aspects of forward-propagated signals, but it requires special circuitry to examine the frequency stability of the individual modes. This is done by heterodyning the incoming signal with a local reference oscillator, range-gating the desired mode, and developing a waveform, using boxcar techniques, which represents the beat frequency for the sampled range point or mode. Spectrum analysis of this waveform provides a measure of the frequency stability of that particular propagation path.

3.5.1.1 The SID of April 5, 1961

A gross picture of the behavior of the frequency of an entire group of received signals can be obtained by presenting the coherently detected signal in an intensity-modulated range-time display. A display of this type is shown in Figure 34 for ground-backscatter data obtained at South Dartmouth, Massachusetts. These data were taken simultaneously on several frequencies during an SID which occurred on April 5, 1961.

Data on 12 mc, 22 mc, and 25 mc appear from top to bottom in the illustration. Echo ranges are plotted vertically downward and time of day is plotted horizontally from left to right. On these records, light regions represent backscatter returning in phase with the local standard; dark regions represent out-of-phase backscatter. Moving in time from left to right at a constant range, the backscatter alternates in and out of phase. This

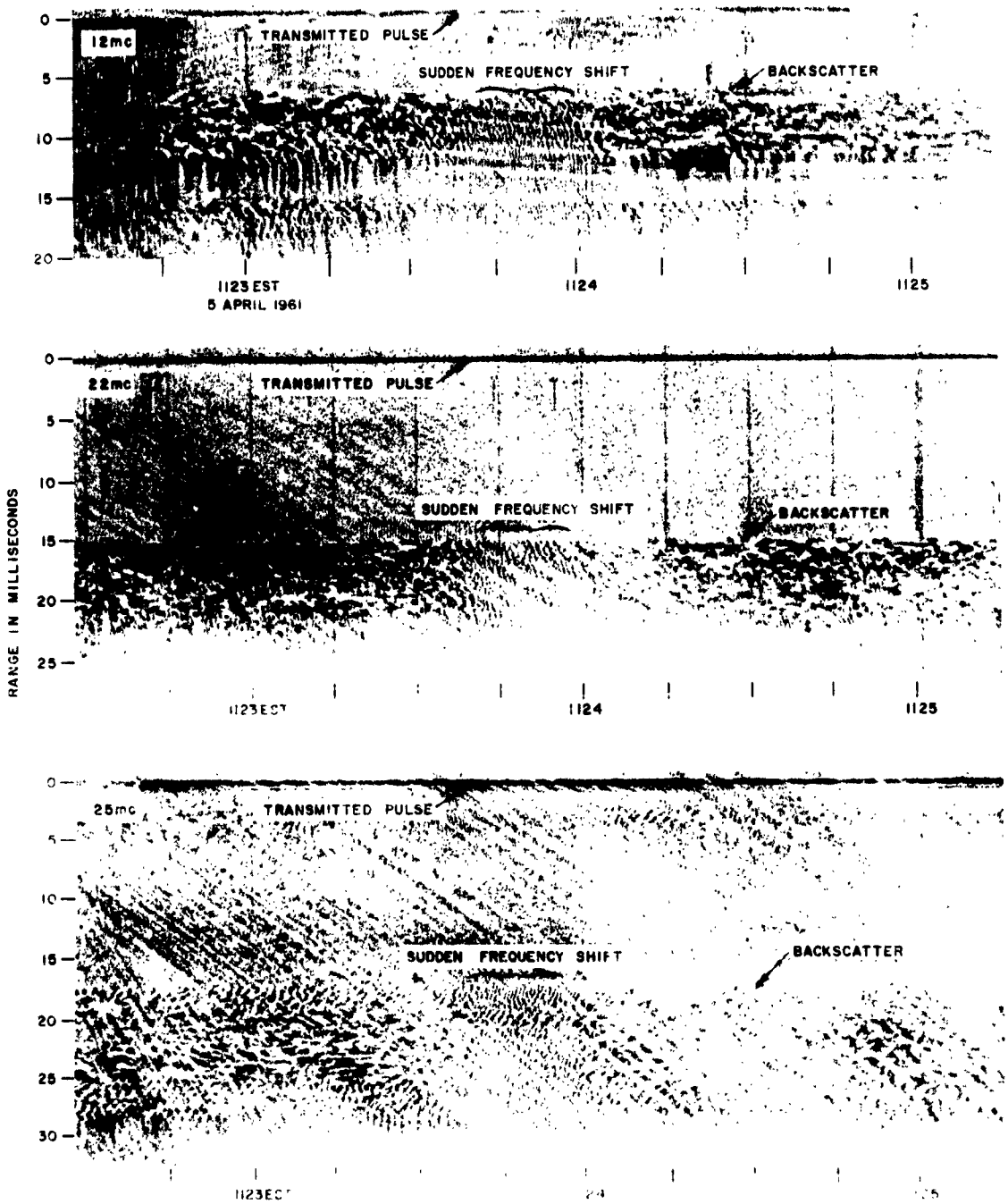

Figure 34. Range-Time Presentation of Coherently Detected Backscatter

rate of alternation is associated with the stability of the ionosphere; thus, it is affected by events such as SID's.

A sudden frequency shift occurs in the backscatter between about 1123:30 and 1124:15 EST. The onset time and duration of this disturbance are essentially the same on each frequency and at all ranges within the backscatter.

By range gating either coherently detected or envelope detected backscatter, the phase or amplitude variations with time can also be displayed by a pen-chart recorder having adequately fast response time. Data on this sort appear in Figure 35. The coherently detected data, corresponding to only a short interval at the onset of the disturbance, are shown.

An SWF follows the sudden frequency shift on each frequency. The relative amplitude of the envelope detected backscatter is shown at the bottom of Figure 35. The frequency shift begins and ends abruptly with a total duration of about 30 seconds. This is followed by a gradually deepening amplitude fade lasting several minutes. The effect is more pronounced on the lower frequencies, the signal level dropping by about 25 db on the 12-mc frequency.

A spectrum analysis of the range-gated, coherently detected data for each of the frequencies is shown in Figure 36. The sudden frequency shift is evident near the center of each record. The frequency excursion is negative, corresponding to an increasing phase path length during the disturbance.

In addition to ground backscatter signals, a single-hop forward-propation path was in operation during the ionospheric disturbance. Pulse transmissions on 22 mc from the Canal Zone were received at South Dartmouth (a distance of 3682 km). The pulse repetition rate was 20 pps. In Figure 37, a spectrum analysis is shown of phase variations occurring in the one-hop mode F-layer signal. The first few minutes of the record represent undisturbed ionospheric conditions. The phase rate of change during

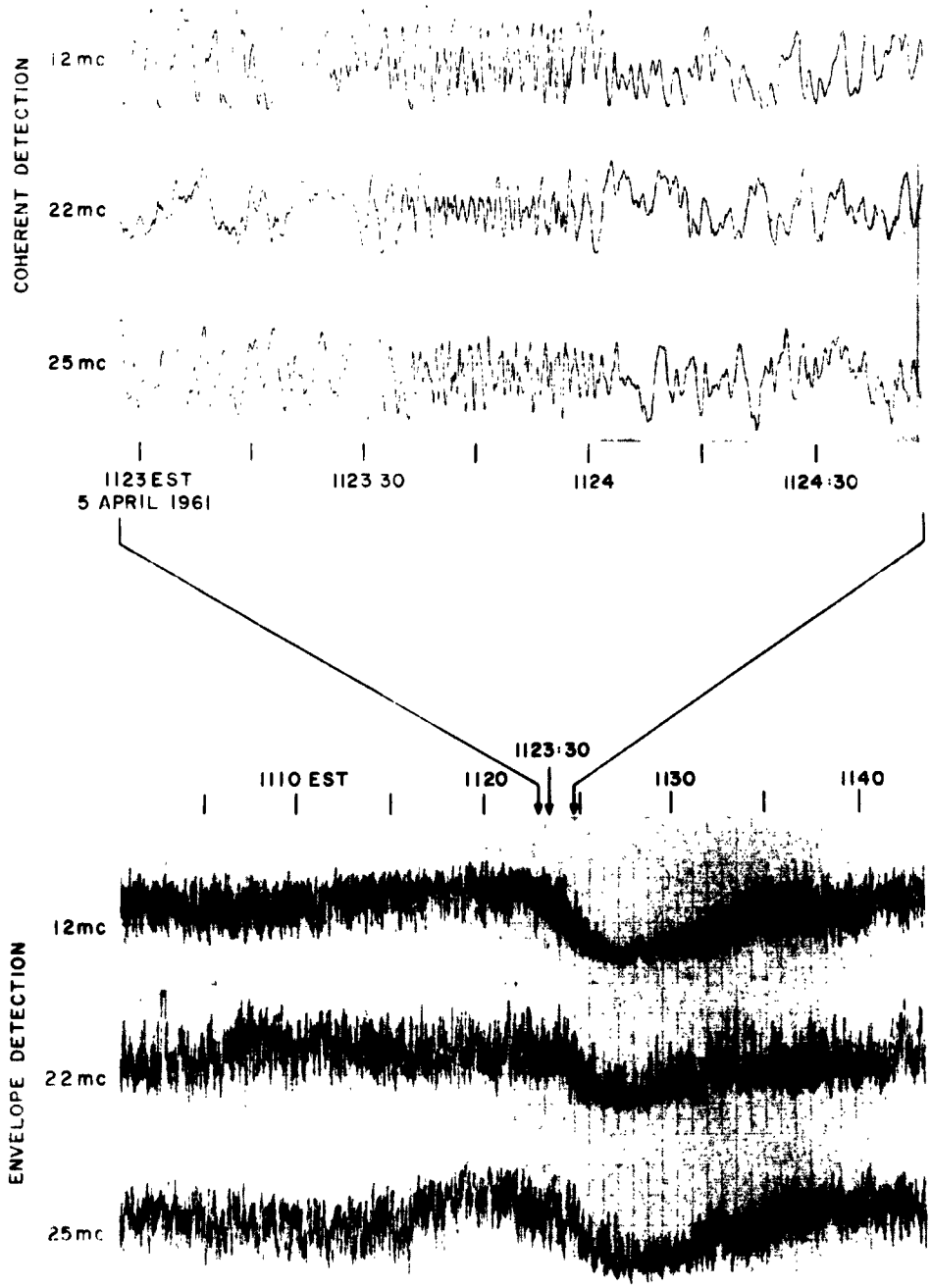

Figure 35. Frequency and Amplitude Variations in Backscatter Signals

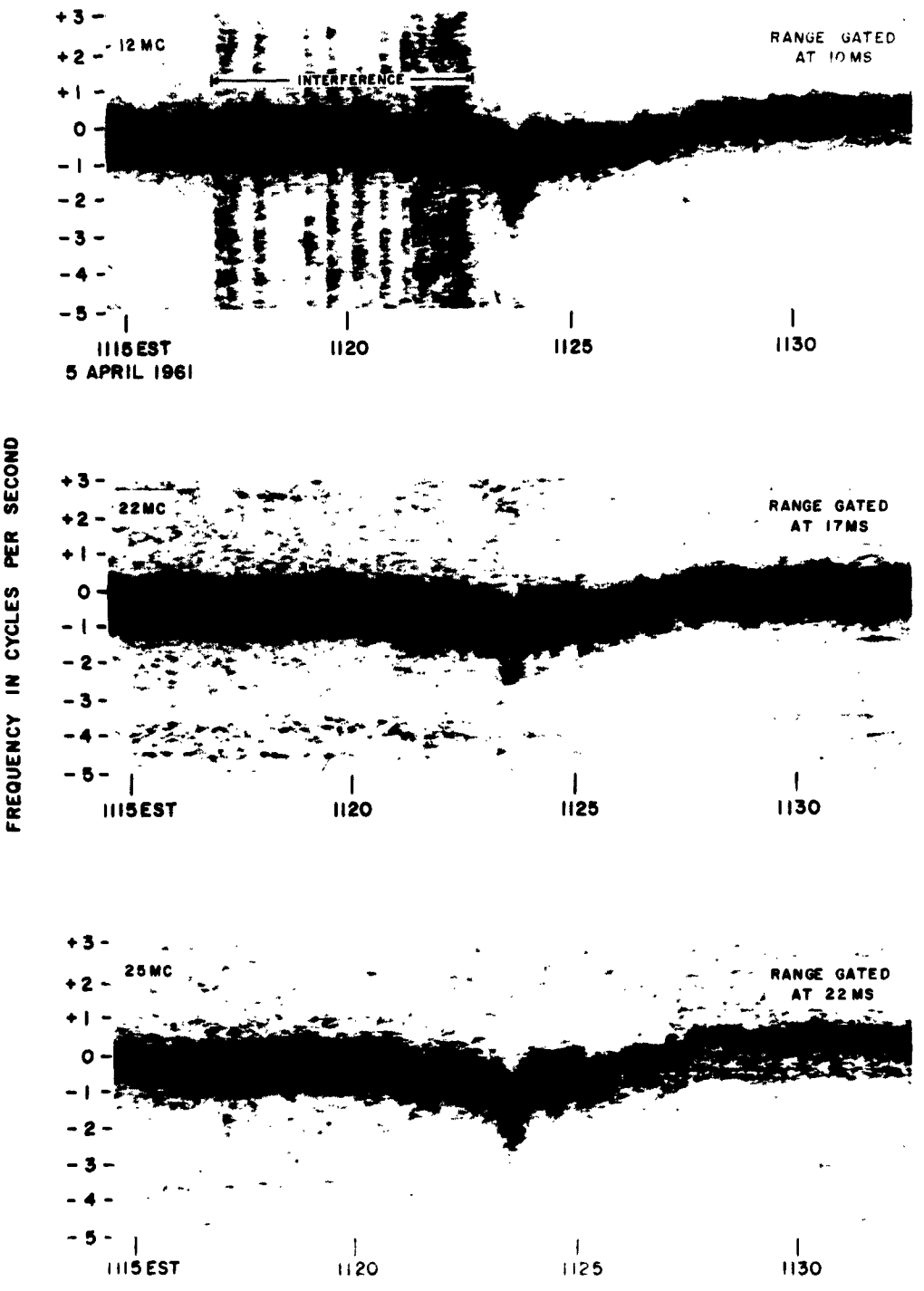

Figure 36. Spectrograms of Coherently Detected Backscatter Signals

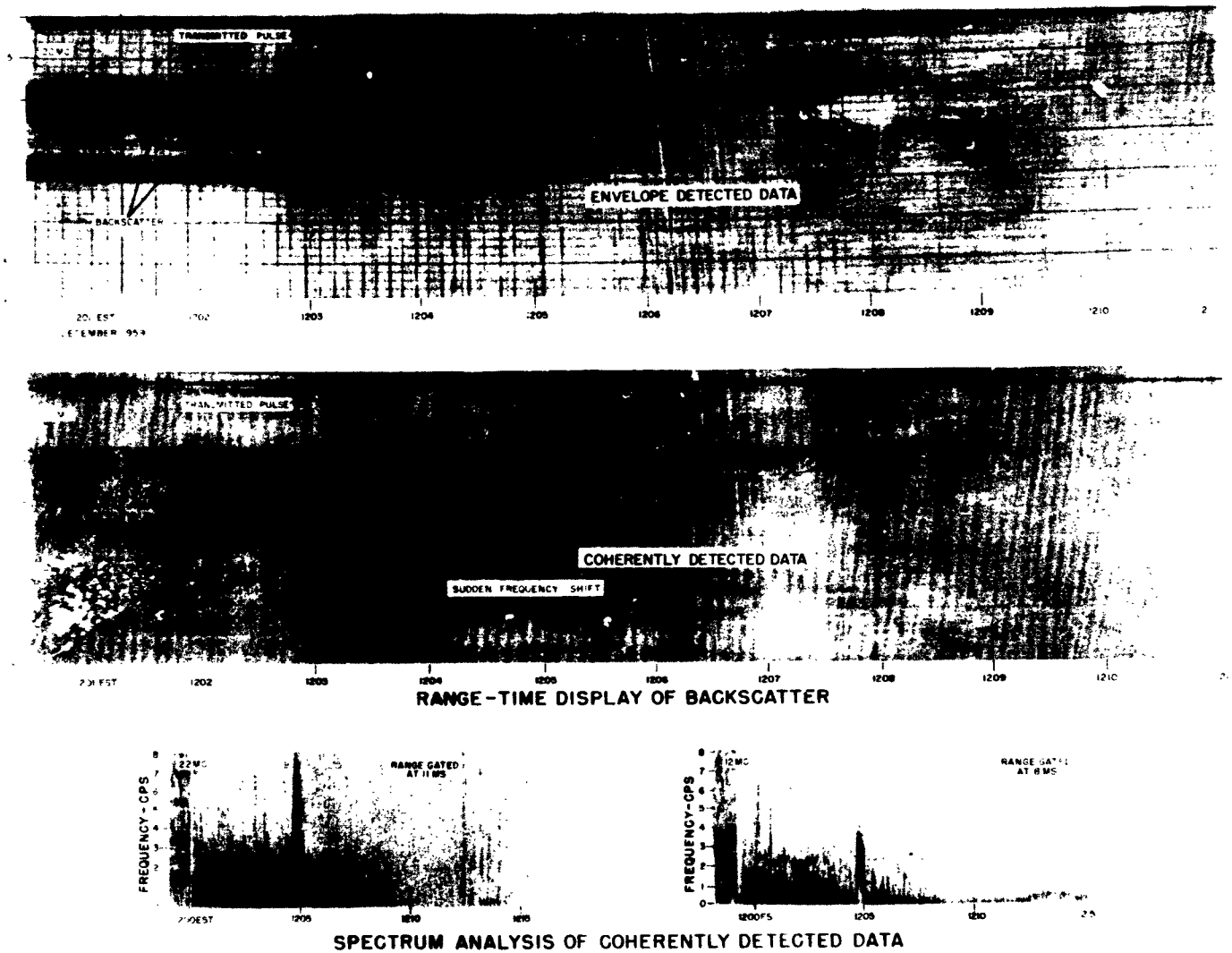

BACKSCATTER OBSERVATIONS DURING THE
IONOSPHERIC DISTURBANCE OF DECEMBER 1, 1959

Figure 37. Spectrograms and Range-Time Backscatter Displays for the SID of December 1, 1959

this period is essentially constant. At 1120:58, an abrupt frequency excursion takes place. The magnitude of the frequency shift is uncertain because of ambiguities introduced as a result of the pulse-repetition frequency and the "folding" which occurs around the center frequency. One possible description of the actual frequency behavior has been sketched in Figure 37 (bottom) to show how the spectrogram in the Figure could be related to the actual situation. (In the case shown in Figure 37, the data were processed by offsetting the reference frequency by 5 cps. Different values of offset gave correspondingly different spectrograms.)

Several characteristics of the one-way path data appear to be significant in comparison with the backscatter data. First, the magnitude of the frequency shift is much greater; second, the time of onset and termination may be much more precisely specified; third, the onset of the disturbance is recognizable about two minutes earlier than in the case of backscatter. Examination of the forward path signal apparently offers a more sensitive measure of the ionospheric effects being produced. Although the backscatter soundings were made in the same directions as the one-way path circuit and covered essentially the same area of the ionosphere, the frequency shift was not as prominent as in the one-way case. The abrupt and distinctive frequency shift which occurs in the one-way signal is apparently a precursor to an impending SWF. The data may also be applicable to more fundamental studies of solar-ionospheric relations. A presentation of frequency versus time, as shown in Figure 37, can be used (since frequency is the time derivative of phase) to obtain a measure of the changes in phase path length between the stations. This is related to the ionization along the ray path and, consequently, could prove useful in studying solar disturbances and their effect on the ionosphere.

Table 3 compares the preceding data with other reports of solar activity—as published by the Central Radio Propagation Laboratory.

Table 3

April 5, 1961

	Sudden Freq Shift		SWF		Solar Radio**
	Backscatter	Forward	Backscatter	Solar Flare*	Emission
start	1123:30	1120:58	1124	1056	1123:5
max	1123:45	indet	1127	1125	1125.5
end	1124:05	1127:50	1135	1135	1127.5

* Observed at Huancaya, importance 1, SWF observed

** Observed at Ottawa - 2800 mc

Times are Eastern Standard Time

3.5.1.2 The SID of December 1, 1959

A second example of a sudden frequency shift which precedes the amplitude fade during an SID was collected on December 1, 1959. Backscatter was collected on 12 and 22 mc at South Dartmouth during the disturbance. A comparison of envelope detected and coherently detected 22-mc backscatter appears at the top of Figure 38. The sudden frequency shift occurs at 1204:20 and lasts until about 1205. As in the disturbance of April 5, 1960, the anomaly occurs simultaneously throughout the backscatter. The amplitude begins to drop as the phase anomaly ends. The fact that the sudden frequency shift precedes the observable absorption effect is also demonstrated clearly in the spectrograms of Figure 38. Table 4 provides a comparison of these data with the solar-flare and solar-radio-emission reports of the Central Radio Propagation Laboratory.

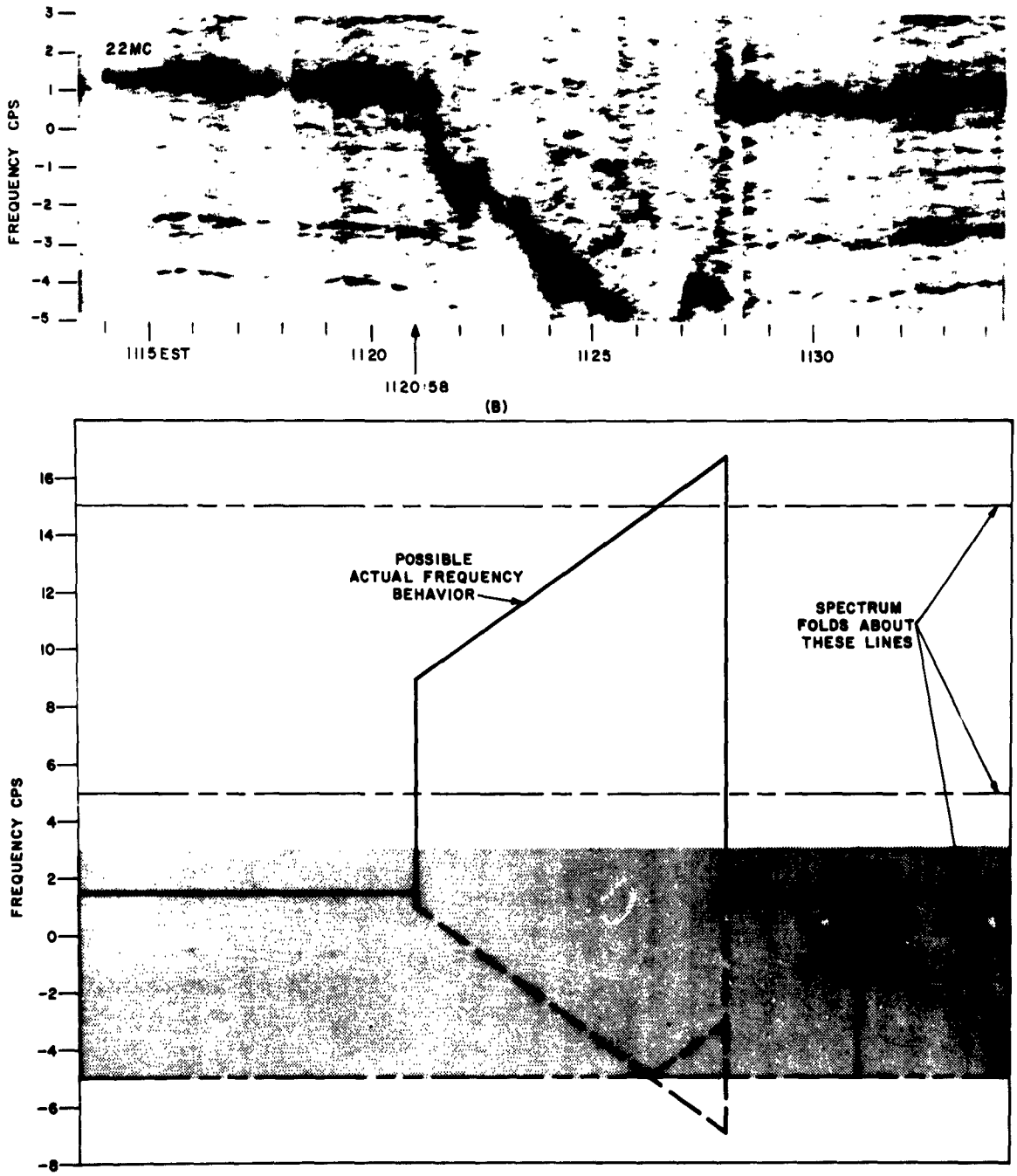

Figure 38. Spectrogram of Coherently Detected, Forward Propagated Signals

Table 4

December 1, 1959

	Sudden Freq Shift	SWF		Solar Radio
	Backscatter	Backscatter	Solar Flare*	Emission
start	1204:20	1204:30	1138	1022
max	1204:45	indet	1208	indet
end	1204:55	>1300	1446	>1552
*	Observed at Sac Peak, importance 2, SWF observed			
*	Observed at Ottawa - 2800 mc			

3.5.1.3 Concluding Remarks

The data shown indicate that measurements of frequency shifts at HF constitute a relatively sensitive method of displaying some of the ionospheric effects produced by solar disturbances. It is possible that this type of measurement could be used to describe the physical nature itself of the solar disturbances. To do this, the effect of both the ionization density and ray-path changes on the received frequency would have to be taken into consideration. Aside from its possible application to the description of solar phenomena, the identification of sudden frequency shifts might be of immediate use to long-range HF communicators as an indication that an SWF was about to occur.

3.5.2 Anomalous Phase Disturbances

Examination of backscatter and one-way propagation records have revealed two special types of phase disturbances: one is observed during the disturbed condition identified as spread F; the other is observed in conjunction with widespread disturbances at E layer heights (Es).

On February 24, 1961, range-time records of 9-mc

phase detected backscatter soundings were observed to consist of a fine-textured pattern, characteristic of highly disturbed conditions. The phase characteristics of the disturbance were similar in some respects to those of the SID disturbances. The period of the record (0715, Figure 39a) following the disturbance is representative of non-disturbed conditions usually observed at this time of day.

The disturbance in the 9-mc backscatter lasts for about 35 minutes and is seen in the first part of the range record (Figure 39a). Although heavy interference was present throughout the entire test, major changes in the delay time of the backscatter leading edge from 0649 to 0715, as well as a considerable change in the range-time position of the trailing edge of the backscatter due to amplitude fading, were observed during the test. Large phase excursions were also observed in the spectrograms of the 22-mc backscatter taken during the latter part of the disturbance (Figure 40). The phase excursions are roughly twice as large as those usually observed at this time on 22 mc (see Figure 6, section 3.3.1) and present an unusual pattern not seen under normal conditions.

A search of the GBI h'—f records (Figure 39b to e) indicates that a spread F condition prevailed from about midnight to about 0800 with definite peaks occurring at 0030, 0300, and 0600. The last major disturbance occurs during the same time interval that the phase disturbances in the backscatter records were observed.

The second type of anomalous phase disturbance was observed from 1330 to 1400 on December 21, 1960. The effect was noted on both the one-way signal for GBI and the backscatter transmission from SDFS. The disturbance was first noted on the spectrograms (Figure 41a to f) on which the phase path characteristics of the high- and low-angle paths from GBI to SDFS are shown. The effects of the disturbance on 1-hop backscatter result in a series of excursions about three times higher than the average at this time of day on 22 mc (see Figure 6, section 3.3.1). The pattern followed by the excursions is approximately the same on both the high- and low-angle rays,

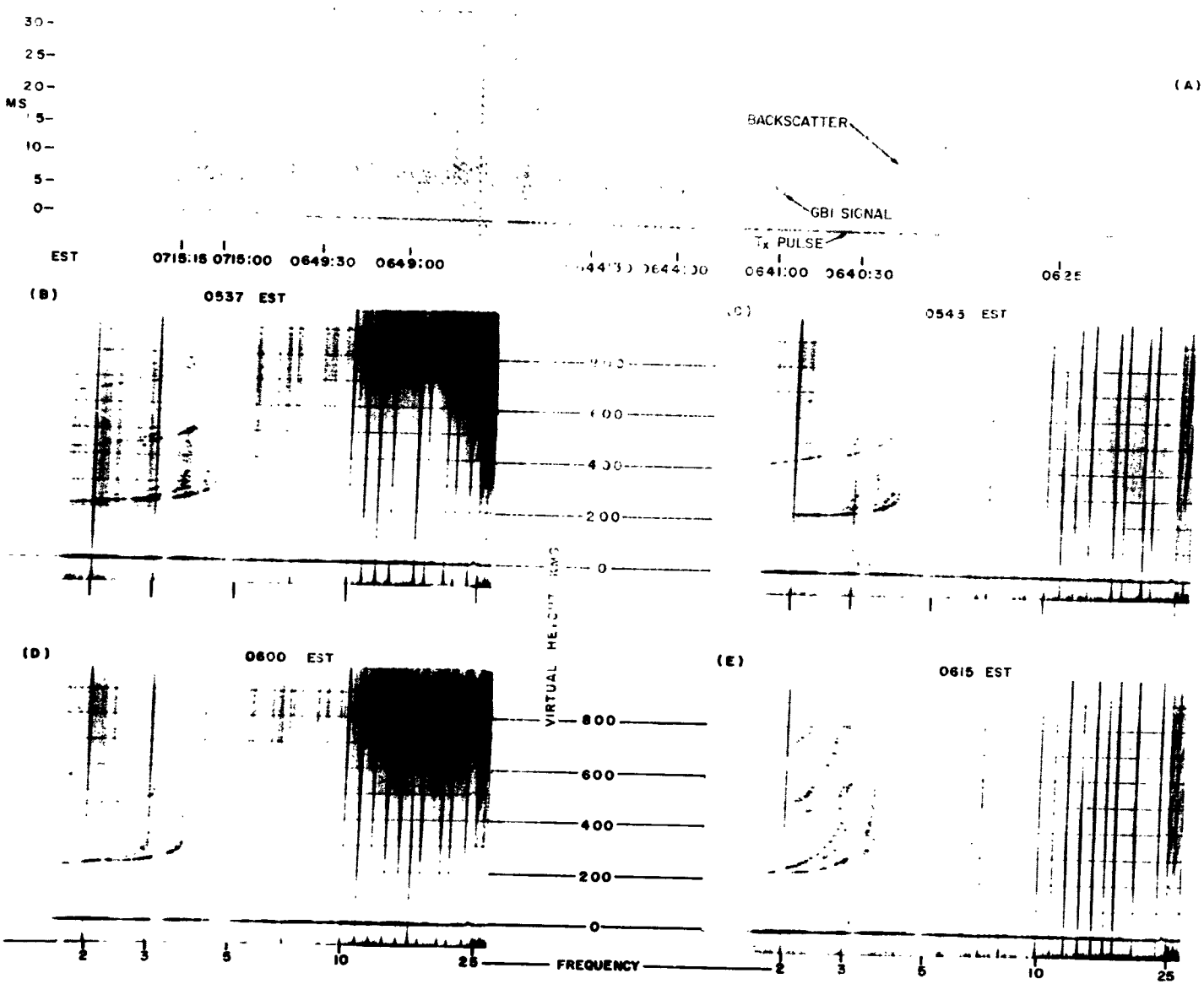

Figure 39. Ionograms and Range-Time Records for Spread F Disturbance, February 24, 1961

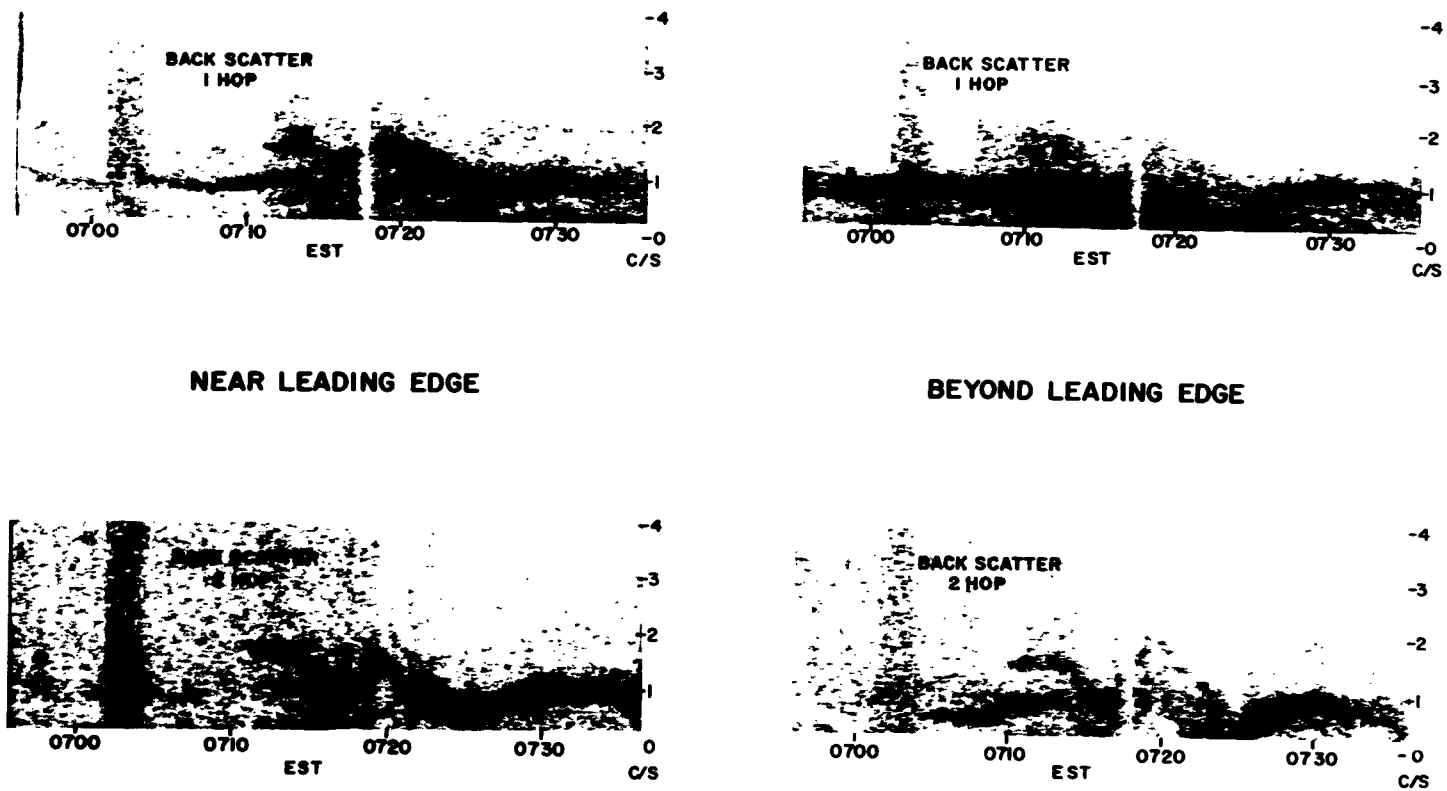

22 MC SPECTROGRAMS FOR SPREAD F DISTURBANCE
FEB 24, 1961

Figure 40. Spectrograms (22 mc) for Spread F Disturbance, February 24, 1961

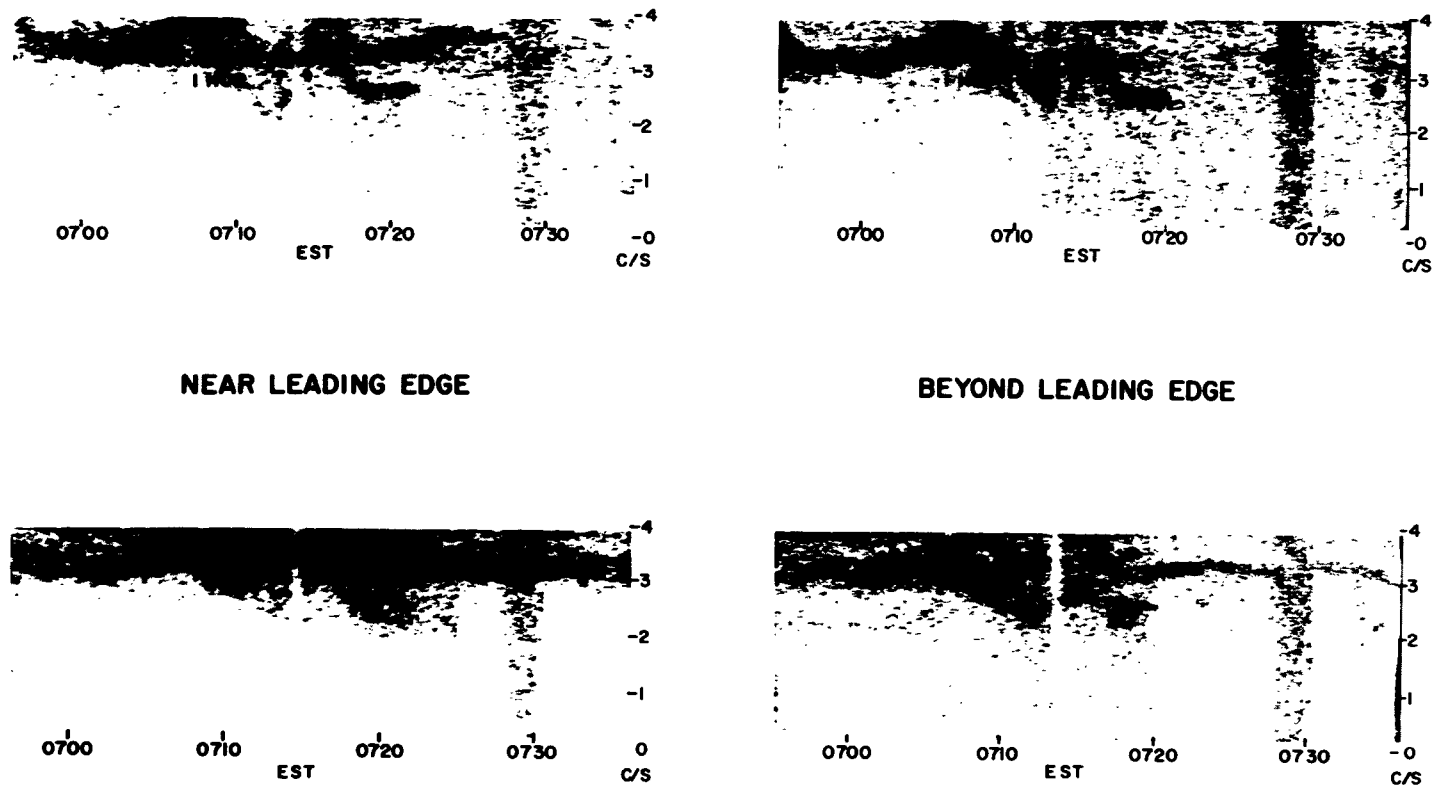

Figure 40. Spectrograms (22 mc) for Spread F Disturbance, February 24, 1961

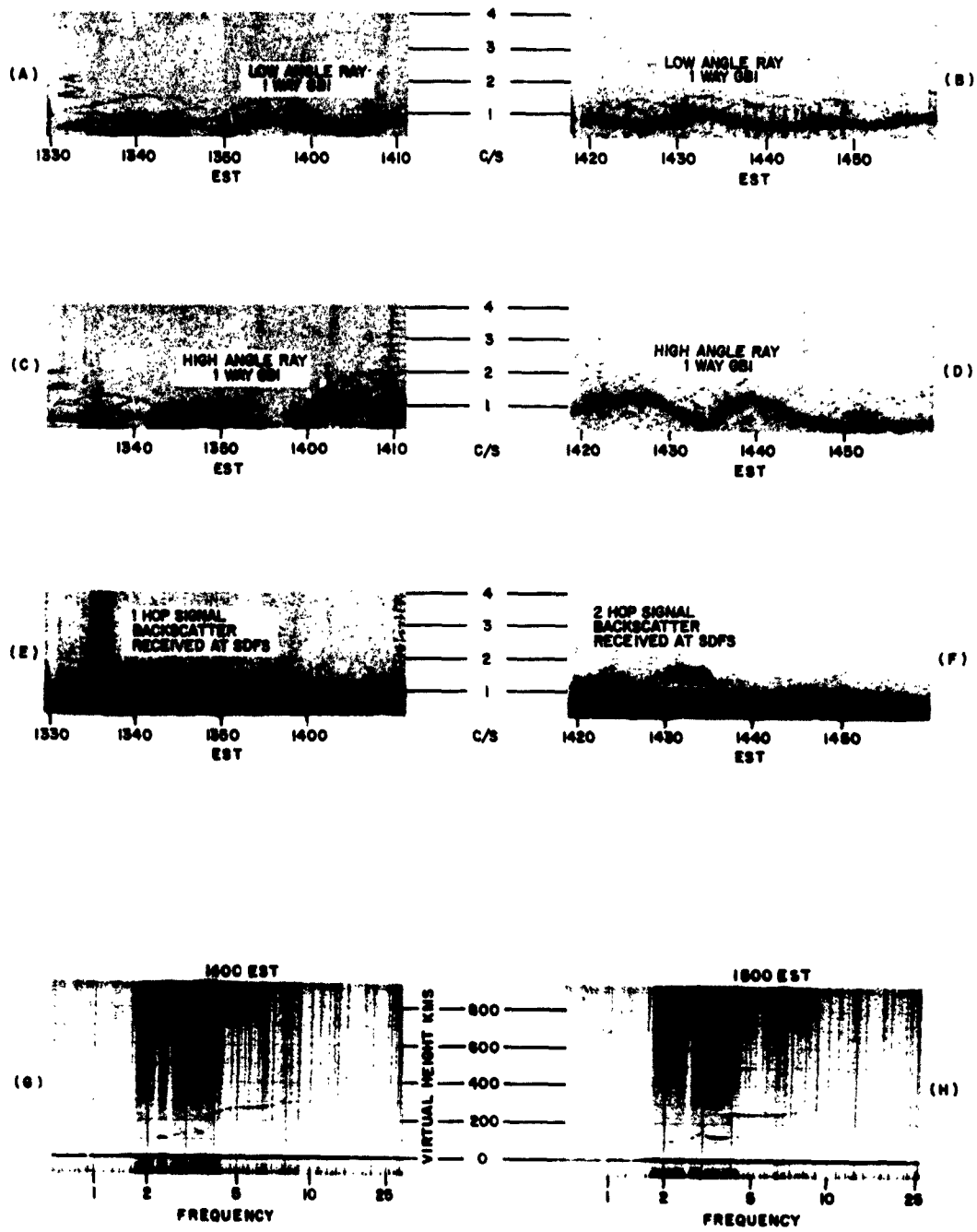

Figure 41. Ionograms and Spectrograms for E Layer Disturbance, December 12, 1960, GBI

with a 10-minute delay between the occurrence of the same effect (Figure 41a to d). Unusual changes in the spectrum of the backscatter, both one-hop and two-hop, are observed for 1330 – 1400 (Figure 41e to f). Vertical incidence h'—f records (Figure 41g to h) taken at GBI show the development of a highly intense patch of sporadic E, immediately following the observed disturbed conditions in the backscatter and on the one-way transmissions.

3.5.3 Conclusion

The type of ionospheric disturbances that have been represented here show the extremes that may be observed in the spectrum frequency, with continuous observation over long periods of time. The possible reasons for their appearance and for the characteristic patterns that are shown in the phase records remain questions to be answered in future investigations.

4. AROUND-THE-WORLD SIGNALS

At various times in the literature, there have been reports of signals identified as having propagated around the world along essentially great circle paths. In many cases, surprisingly high signal strengths were observed, thereby attaching some importance to these signals as possible alternative modes of communication in the event of disruption to long distance links using normal modes. Two theories are generally put forward to account for the existence of these signals. The first assumes a series of multihop reflections between the ionosphere and the ground; the second is more generally held and assumes that rays launched near the horizon are trapped by tilted layers in the upper ionosphere, while continually radiating downwards to earth. In some cases, the signals have been reported to circulate past the receiver four or five times, with a 5- to 10-db signal loss for the second and succeeding circuits around the world. [1]

During the course of the experiments being carried out to examine backscatter characteristics, several attempts were made to observe around-the-

---

[1] Isted, G. A. "Electromagnetic Wave Propagation," Academic Press, 1960, p. 517, International Conference Papers Edited by M. Desirant and J. Michiels.

world signals. In reviewing the work of past investigations for evidence of preferred directions, a rather general opinion seems to be that the path of the circulating signals is more or less confined to the twilight belt round the world.[2] As a starting point for the pulse-propagation tests to be described below, all azimuths were searched for evidence of this azimuthal preference. In October and November of 1960, a back-to-back arrangement of Yagi transmitting and receiving antennas was rotated through 360°, in steps of 30°. On three occasions in this period, weak signals were received on a frequency of 22 mc at delay times of about 138 ms. In each instance, the signals were above the noise level for brief periods during midmorning and were observed over about a $\pm$ 30° change in azimuth from the optimum direction of about 80° true. There was no apparent change in the signals when the transmitting and receiving directions were reversed.

In these early tests, more comprehensive and accurate observations were curtailed by insufficient signal amplitude. Three tests in late December 1960 and one in January 1961 were made with higher power (100-kw peak). The dates and times of the experiments and a comment on the signal levels observed are given below.

December 27, 1960 (no signals observed)
December 28, 1960 (weak signals - 0825-1015 EST)
December 29, 1960 (strong signals - 0905-1040 EST)
January 25, 1961 (strong signals - 0930-1247 EST)

Using a time base of 150 ms, detectable signals of low amplitude were seen on December 28 at a delay of 138.5 ms. The following day and on January 25, signal levels were relatively high for periods of an hour or more. The following description is of measurements made during the latter two days at the times indicated above.

---

[2] Ibid

On December 29, 1960, transmissions were on 22 mc, using a five-element Yagi, having a measured 32° beamwidth. A log periodic antenna with a nominal 55° beam was used for reception. Path preference was found by rotating both antennas in 10° steps (always keeping them 180° apart), as shown in the upper left of Figure 42. The voltage output of the receiving antenna was recorded for the approximate five-minute period between the stepped rotations. This is shown in the lower portion of Figure 42, where a peak signal from the direction of 65° true is indicated. The combined pattern of the receiving and transmitting antenna is shown also for comparison. Some azimuthal spreading of the signal energy seems to be indicated from the slightly broader directional characteristic of the signal.

The next step tried in the experiment consisted of keeping the transmitting antenna beamed at a fixed 70°, while rotating the receiving antenna. The receiving antenna response, shown in the right section of Figure 42, is a substantial duplication of the antenna voltage pattern with no indication of serious horizontal anomalies in the path geometry.

The conclusion drawn from this test was that the around-the-world signals have a preferred horizontal direction of arrival. However, signal energy probably arrives over a spread of a few degrees about this optimum direction, which in this test was found to be 65°. Apparently, the direction of maximum return is closely related to the zone of twilight. In Figure 43, the 65° great circle path through South Dartmouth is shown for comparison, with a trace of the constant 90° sun zenith angle at 0900 and 1000 EST in January. The close similarity of these curves is consistent with previous reports that the circulating signals tend to conform to the twilight belt around the world.

On a later test, the vertical angle of arrival of the signal (on 22 mc) was measured with the use of two identical Yagi antennas spaced above ground at heights of 60 feet (1.35 λ) and 25 feet (.56 λ). The system was oriented in azimuth to 70°. From the antenna vertical patterns, a plot was made of the ratio of the outputs as a function of vertical angle. The system was put into operation on January 25, from 1040 to 1240 EST, during which time two or

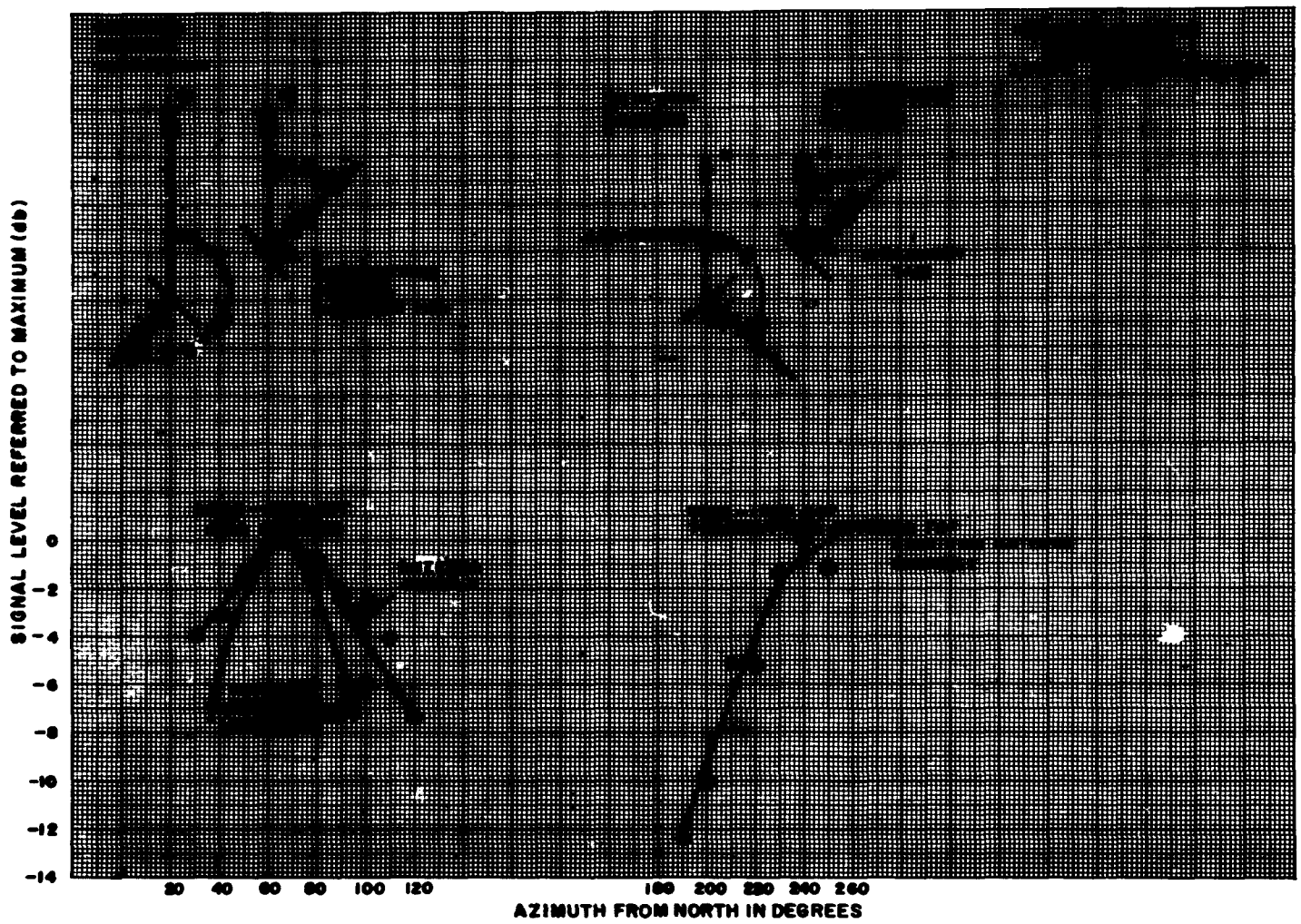

Figure 42. Horizontal Angle of Arrival Observations

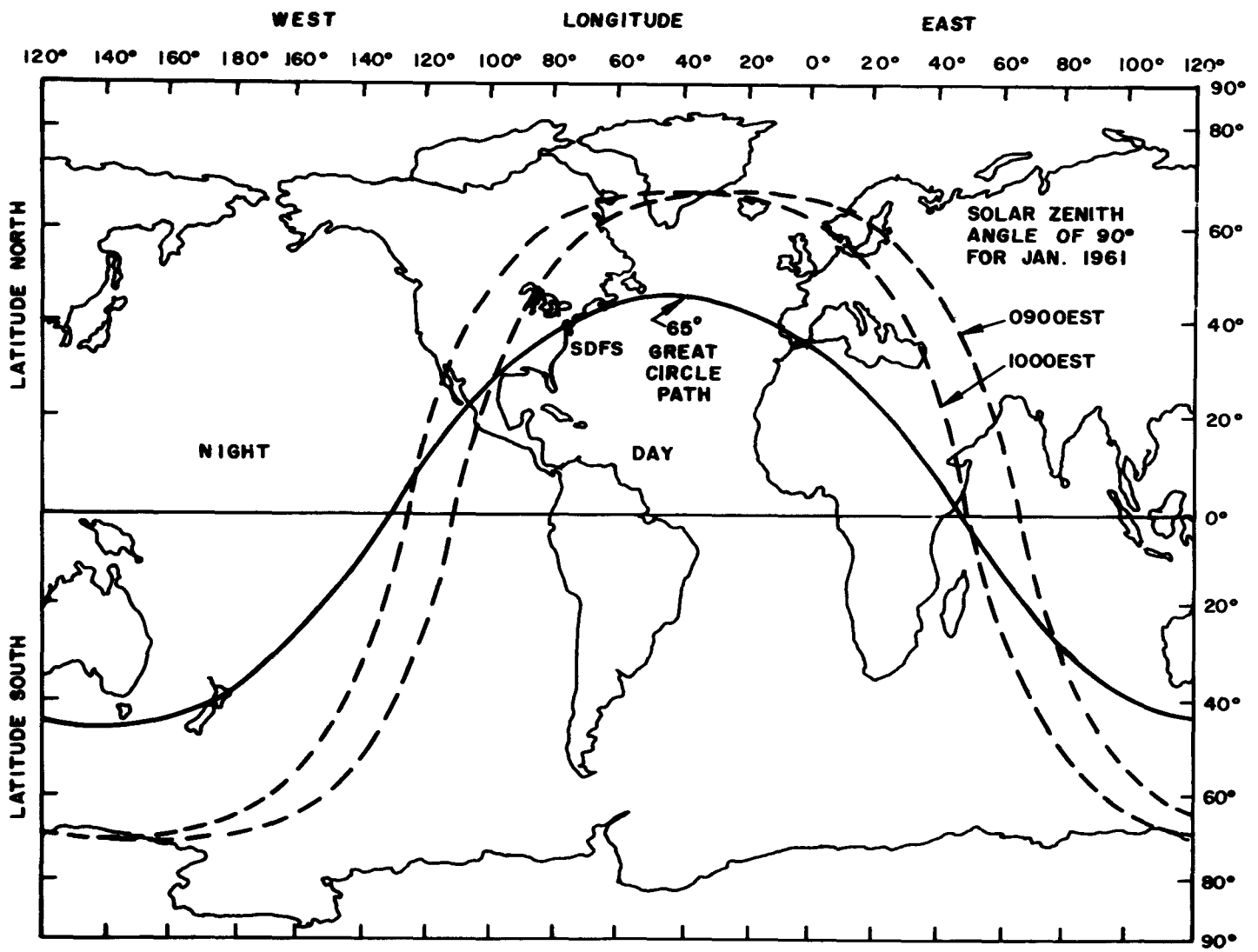

Figure 43. Twilight Zone and Great Circle Propagation Path

more components of the signal were seen at delays of 138.4 ms and 139 ms. Since the components were separated in range over most of this period, their amplitudes were individually measured and recorded. The measured elevation angles for both components shown in Figure 44 tend to disperse widely about a mean of 5°. Undoubtedly, some of the fluctuation is due to medium to strong interference noted during this period. The break in the data at 1054 EST was primarily because of this. Unfortunately, the choice of antenna spacings resulted in a 5° change in angle for a 3-db change in the signal ratio, and should therefore be modified for future work on angle measurements. Taking account of these shortcomings, the view is held that Figure 44 is probably a fair qualitative description of the range of vertical angles obtaining during the experiment and should therefore be useful in guiding more precise experiments in the future.

During the same test on January 25, two broadband antennas were used to observe the characteristics of the circulating signal as the operating frequency was changed. A sloping V-antenna, oriented at 84°, was used in reception of the signal transmitted from a log-periodic antenna, beamed at 260°. Seven frequencies were sequentially transmitted in the range 12.6 mc to 27.8 mc and detected on pretuned receivers, switched into the common receiving line. By using the receiving system as a field strength meter, a plot of the measured field strength against frequency leads directly to the amplitude-frequency characteristic of the around-the-world signal. To obtain accurate results, this would require a careful calibration of the entire receiving system, including the effect of the antenna on each frequency. While this was not done, the receiver gains were set to be approximately equal, so that receiver output in a transmission period (several minutes per frequency) can be considered as a rough measure of the amplitude-frequency characteristic. A-scope photos of the signals are shown in Figure 45. The average receiver output is plotted against frequency in Figure 46. To indicate possible effects of the antenna pattern, the position of the primary vertical lobe of the sloping V is also shown in Figure 46. The skirts of the curve near 14 to 27 mc show that propagation around the world was confined to that band during the experiment. The peak around 19 to 22 mc may be an exaggeration caused by a matching of the

Figure 44. Vertical Angle of Arrival Measurements

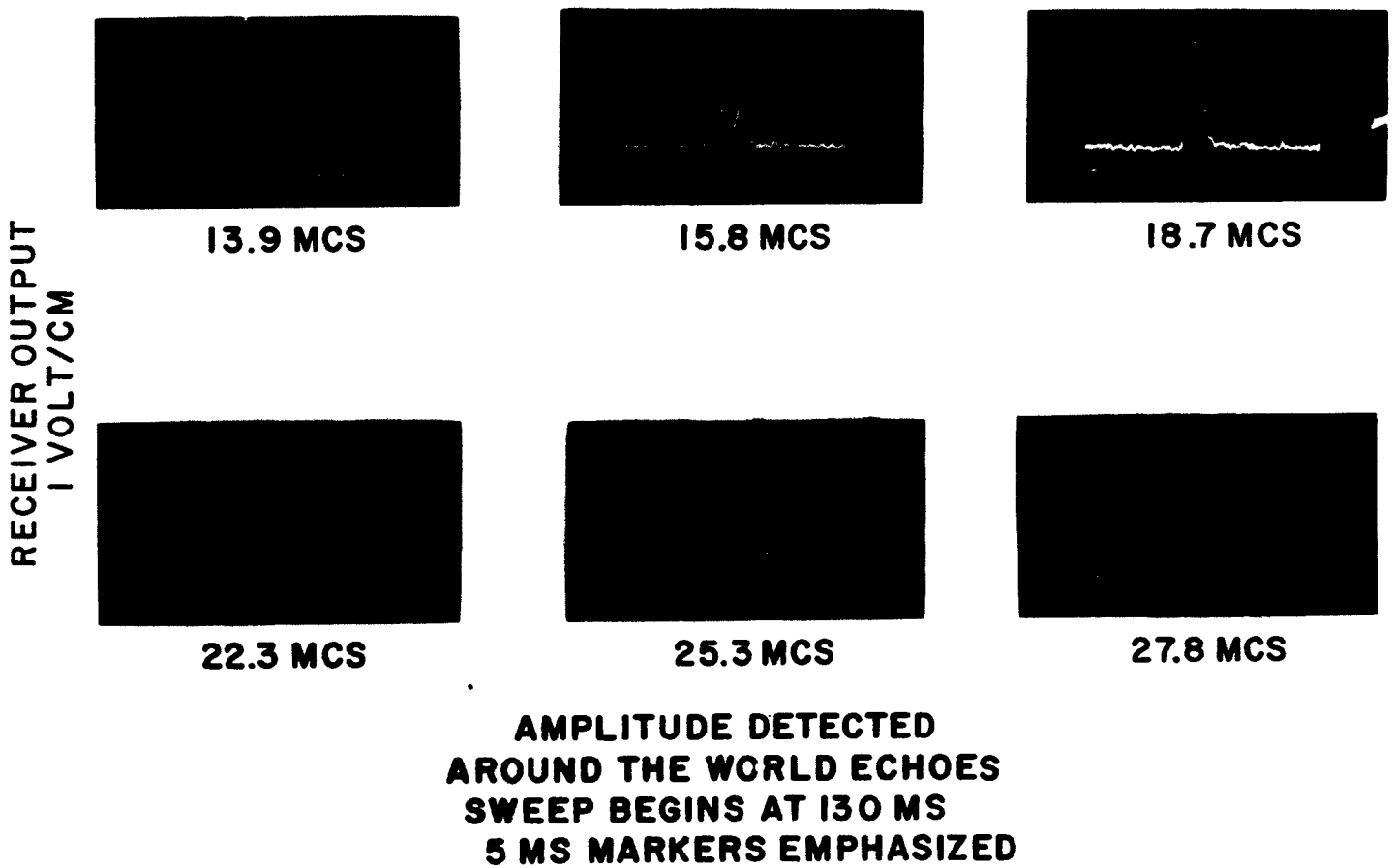

Figure 45. A-Scope Display of Around-the-World Signals

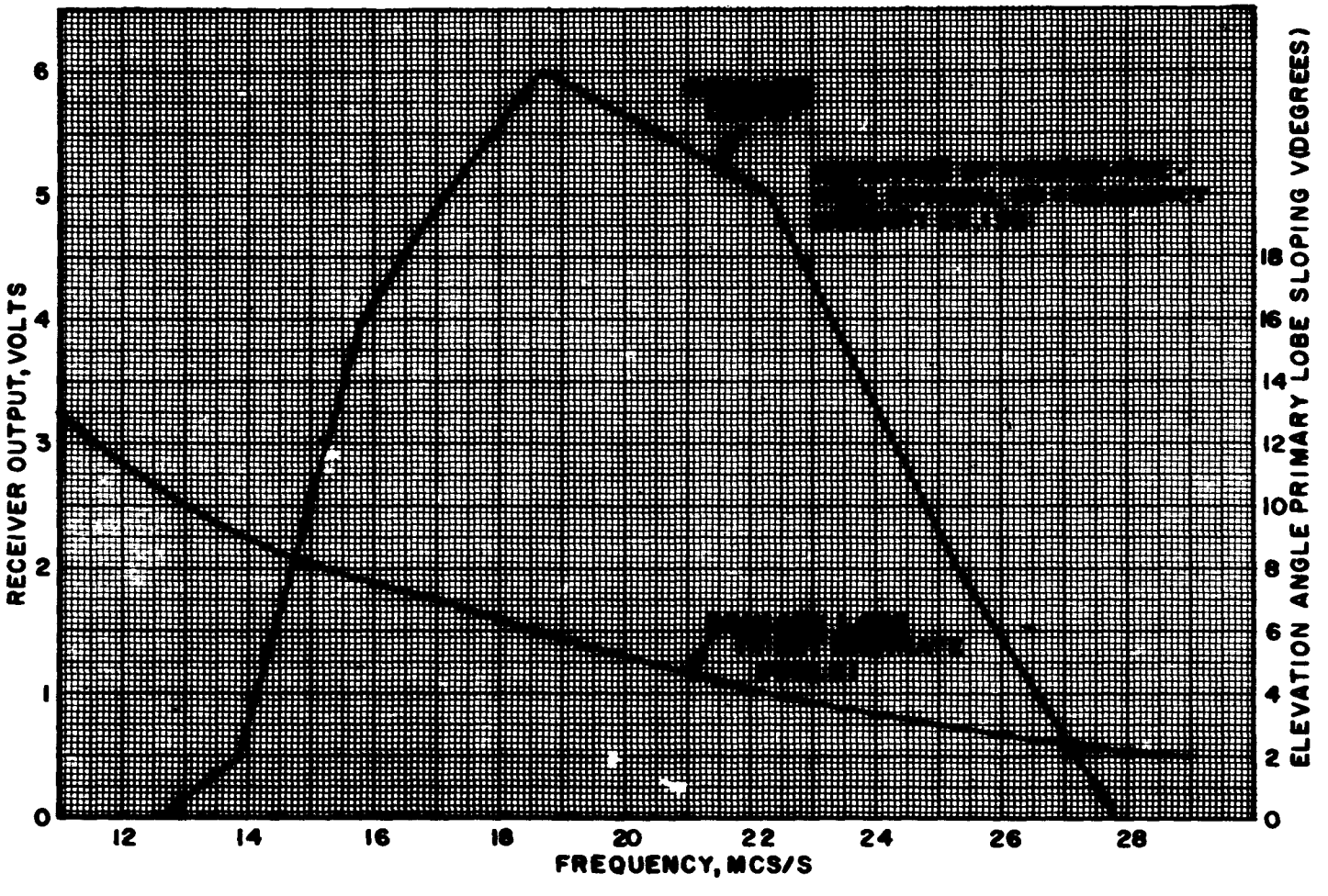

Figure 46. Amplitude-Frequency Characteristic

downcoming vertical angle with the primary lobes of the receiving antenna for these frequencies.

Using a time base of 150 ms, observed transmission times of the circulating signal were of the order of 138 ms. Transit times, as scaled off from film records of the received signals, are shown in Figure 47. On some frequencies, two or more components were observed; although as a general rule, the first arriving component was higher in amplitude. The tramsmission time is amazingly insensitive to the operating frequency, as Figure 47 shows, even though a slight change was observed on 22 mc when the transmission direction was shifted.

The body of data which has been adduced concerning the signal characteristics is not sufficient in itself to differentiate between multihop propagation and that supported by tilted layers or trapped modes.

It can be said that if the process is multihop, probably a low-angle ray is involved, because the transit time has been observed to be practically constant with frequency. This can be seen by consulting Figure 48, which represents a typical dependence of propagation time on ground distance. For rays sufficiently behind the skip distance, the dependence is essentially linear. Also, the low-angle branches for the different frequencies approach and become asymptotic. Individual high-angle branches for these frequencies tend to diverge. Thus, even though ionospheric conditions vary over the path, the linearity and frequency convergence properties of the low-angle ray result in a transit time-frequency dependence very much like the observed one.

On these grounds, the high angle in multihop can probably be ruled out, but the other processes mentioned earlier cannot be so eliminated. Similar considerations apply to the relatively low vertical angles measured and the confinement of the ray path to the twilight belt. Because of the ambiguity which still exists, a fundamental aim of future work in this area should be to devise and carry out experiments capable of distinguishing between the various modes of propagation.

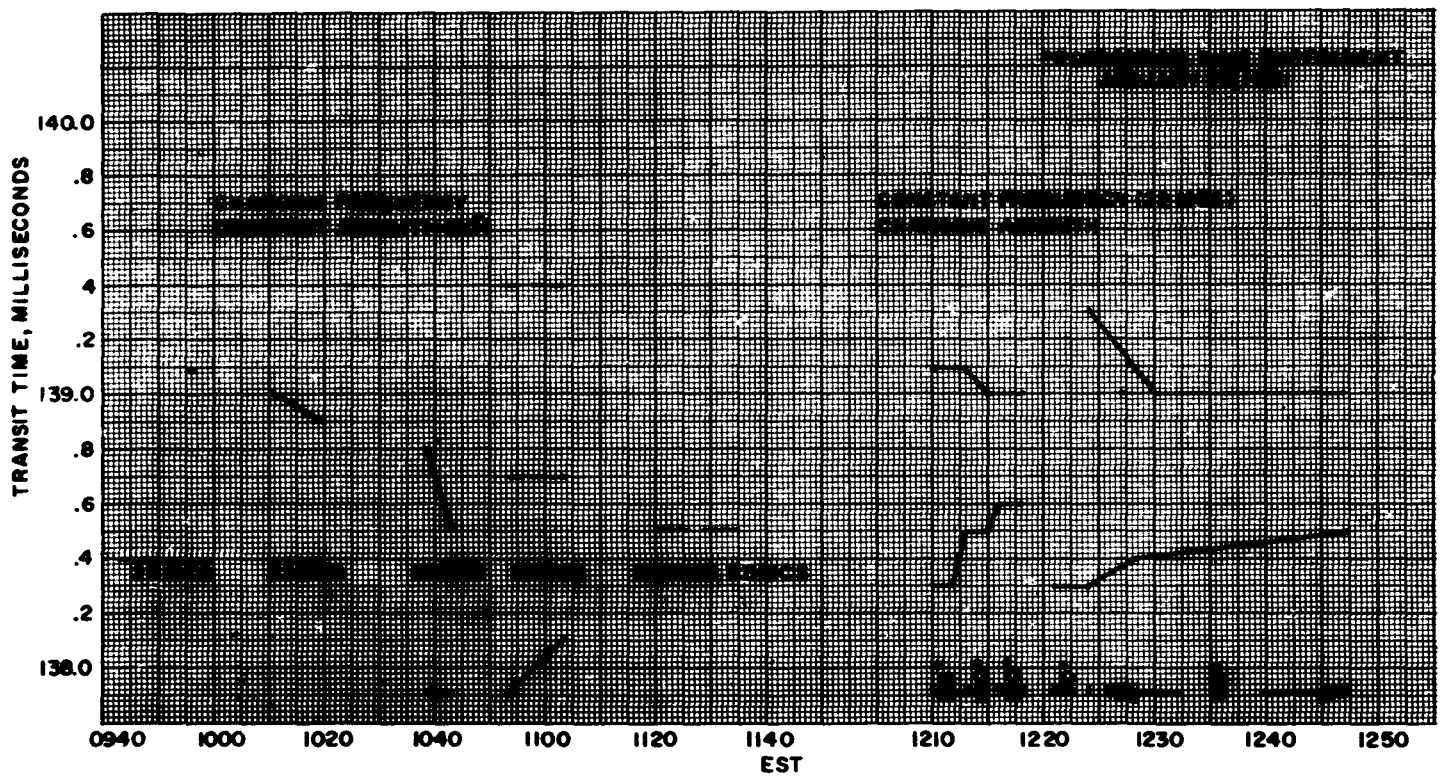

Figure 47. Transmission Time-Frequency Characteristic

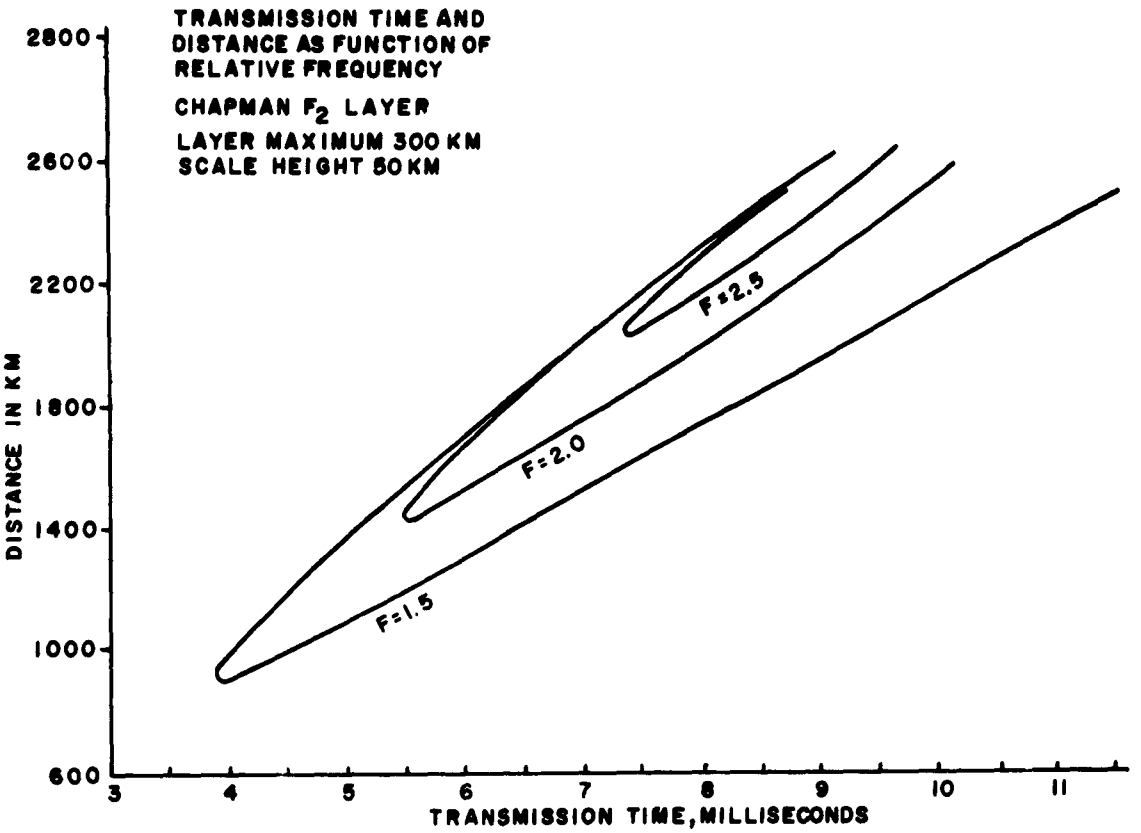

Figure 48. Graph of One-Hop Distances and Transmission Times

The experiments may be summarized as follows. The observed circulating signals tend to follow the twilight belt around the world. The best times of observation in Winter 1960-61 were midmorning. The most favorable direction was 65°. Transmission on several frequencies resulted in detectable signals over the 14- to 27-mc band. The times of arrival of the first modes detected seemed to vary very little with frequency. A measurement of the vertical angle of arrival on 22 mc, subject to some qualification, placed the elevation angle in a range of 5° to 10°.

5. AUTOMATIC PUNCHED PAPER TAPE DATA COLLECTION AND PROCESSING

5.1 Introduction

A factor often neglected in the planning of routine propagation experiments is the costly, time consuming, and subjective reduction of raw data from strip chart recordings into a more compact and useful form. The

considerable savings possible for many programs contemplating routine collection of data prompted a study of systems, with the object of reducing the cost, time, and subjectivity limitations of the usual methods of data handling. Such a system would have as its goal the ability to automatically sample propagation data during an experiment, storing the information in a suitable format so that calibration and analysis could be performed on digital computers commonly available to research establishments. It was decided to incorporate punched paper tape as the means for storage of the automatically sampled data.

Upon investigation, it was found that there were three computers available which would be acceptable for the processing of the data to be collected on the punched paper tape. These were the LGP-30 Computer, made by Royal McBee Corporation, and two IBM Computers, the 650 and the 704. The advantages offered by the LGP-30, although roughly 1/15 as fast as the IBM 650, are the relatively low cost of operation and the ability to accept a paper tape insert. The advantage of the IBM 650 and 704 was chiefly the high rate of data processing that could be achieved, balanced against a high initial cost and the necessity of a tape to card conversion. The conclusion arrived at was to develop a tape format compatible with both data processing systems.

5.2 System Considerations

The design of the overall system divided itself into three separate parts:

1. Designing of the necessary instrumentation (Black Box Design).

2. Choosing the desired system capabilities and defining the tape format.

3. Writing a sample program by which the data would be processed on the selected digital computer.

The first question to be answered in the process of designing an automatic data collection system is, "What can be conveniently required of the system using readily available off-the-shelf equipment?" Investigation of this problem has shown that there are two major pieces of equipment available, a digital voltmeter and a paper punch. The components used in the present system are the Hewlett-Packard DC Digital Voltmeter and the paper tape punch built by Precision Specialties. The integration of the voltmeter and paper punch into the design of the system results in a method of data recording which substitutes a punched paper tape for the usual strip chart recording. The use of this type of equipment has also placed certain limitations upon the type of data that may be processed and the rate at which it may be sampled. The voltmeter allows a varying DC voltage to be sampled while the paper punch determines the maximum sampling rate, which in this application is 2/sec. The data once placed on the paper tape can be processed either by computers directly accepting punched tape or by a tape-to-card conversion.

The second question to be asked is, "What type of problems do we want to handle with the completed system?" A number of suggestions were made including decimal average, mean variance, auto and cross correlations, and cumulative probability functions. It was decided to design a system which would allow the data to be fed and stored in the memory bank of the computer, making it available for any type of processing desired.

The next problem is to determine the type of data to be placed on the tape and the various types of coding that would be necessary in order to make the information on the punched tape acceptable to the computer. The sampled data is placed upon the paper tape in binary form, along with a calibration curve for the equipment. In order to separate the data, spacer and stop codes are used. Other codes identifying the rates of sampling, the number of calibration levels and real-time markers are used as deemed necessary. The resulting format is applicable to both the LGP-30 and IBM systems.

5.3 Data Sampling and Storage System

5.3.1 General Discussion

The above discussion serves as an introduction to the basic problems encountered in the designing of any automatic data collection system. The definition of the limitations and boundaries of the system lead to a general discussion of the instrumentation of the system. The basic elements of the system which eventually evolve are shown in Figure 49. The received signal (or data) is fed directly into a receiver, which is part of the system diagram used above.

The output of the receiver is periodically sampled by a digital voltmeter upon receipt of a command signal from the timer unit. The voltmeter output then activates a paper punch mechanism so that data is stored in the form of a series of punched holes in a roll of paper tape. Auxiliary components provide automatic printing of data identification codes and manual insertion of calibration, sampling rate and real-time information at the beginning and end of test runs.

5.3.2 Instrumentation Details

The components included in the present system are:

1. Manual Tape Punch Control
   (Keyboard and Relay Diode Matrix)

2. Hewlett-Packard 606A Signal Generator with
   Voltage Attenuation System

3. SP 600 Receiver (Hammurland)

4. Hewlett-Packard 405A Automatic Digital
   Voltmeter

5. Esterline-Angus Chart Recorder with DC
   Amplifier

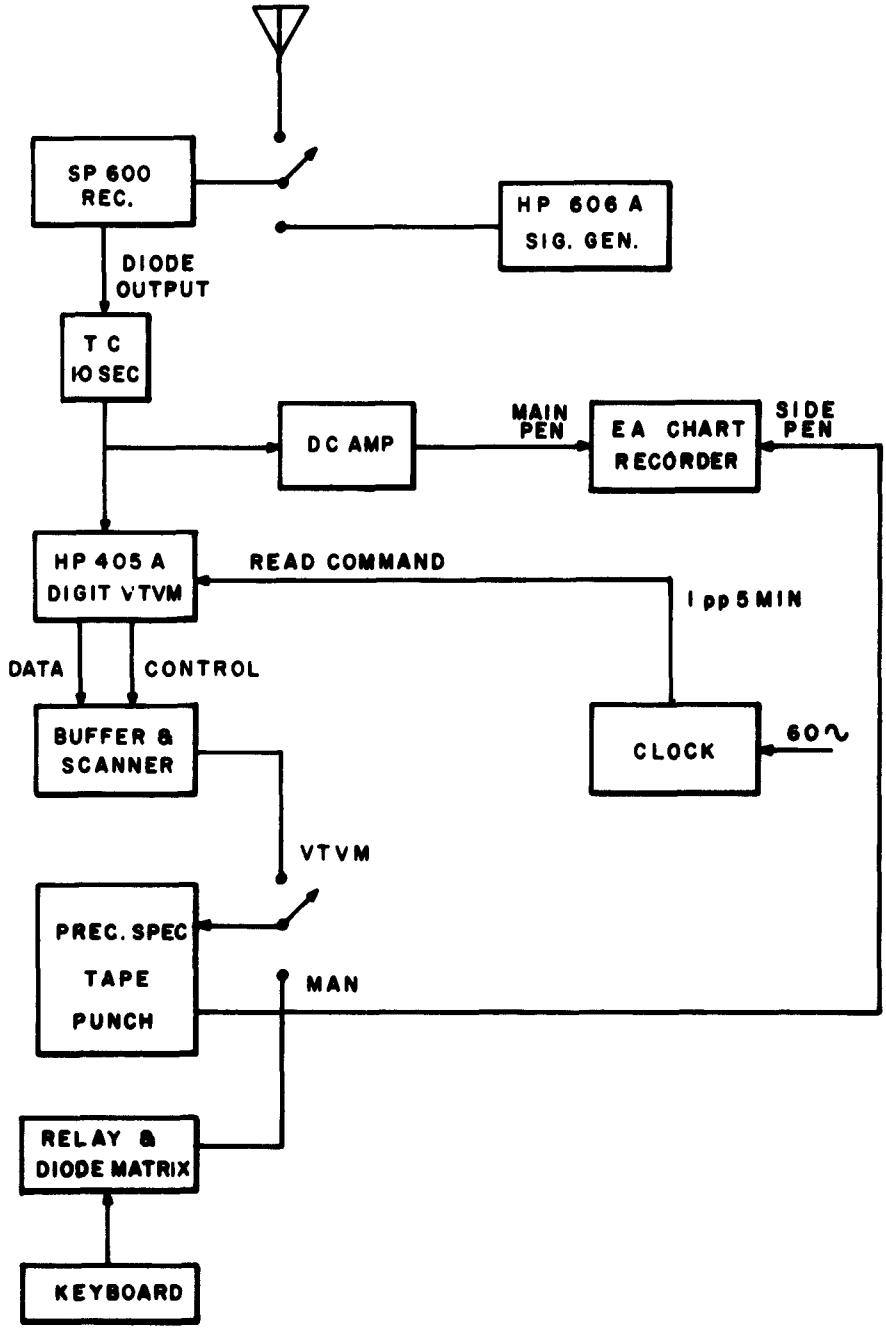

Figure 49. Tape Punch System, Block Diagram

6. Clock

7. Buffer and Scanner

8. Precision Specialities Tape Punch

The components necessary to construct were:

1. Manual Tape Punch Control (Keyboard-Matrix)

2. Clock

3. Buffer and Scanner

The manual tape punch control (keyboard and relay diode matrix) allows the operator to place on the punched tape the codes identifying rate of sampling, the 0 db reference level, the calibration levels, and the spacer (time) codes.

The signal generator is set at a value corresponding to the selected 0 db reference; the possible values are from 10^{-2}v to 10^{-7}v, in steps of 20 db. The attenuation of the voltage from the signal generator will start at the level of the selected 0 db reference and will be stepped down in 5-db units. There will be 11 steps. The computer will assume a 12th step with a voltmeter reading of 000.

The receiver is selected for a non-logarithmic response curve to obtain the smallest possible error in the conversion voltage output of the digital voltmeter to the voltage input to the receiver. The input to the digital voltmeter has the range of .999 v to .001 v.

The clock generates a series of pulses, ranging from 2 pps to 4 pph. This pulse is generated from a 60-cycle source and is fed directly into the digital voltmeter.

The EA chart can be used to give the operator a visual running record of the information being punched on the paper tape.

The buffer-scanner converts the output from the digital voltmeter into the binary coded decimal and activates the tape punch, placing the data on tape in the correct order.

The tape punch has inputs from both the manual control and the buffer-scanner and has an output on a 1-inch tape acceptable to both the LGP-30 high-speed reader and the IBM-650 tape-to-card converter. A roll of punched tape can hold approximately 12,000 pieces of data.

This system is automatic. Once running, it may be left unattended for any length of time desired, with the only limitation being the stability of the receiver and the length of a roll of tape.

5.4 Tape Format

5.4.1 General Discussion

The form in which the data may be placed upon the punched paper tape and the necessary codes for computer compatibility determine the format of the punched paper tape. Of the 15 possible numerical designations, 10 are used for storage of the sampled data and 5 for identification purposes.

The symbols found on the tape will include:

1. Data-in coded binary
2. Calibration levels
3. 0 db reference

4. Spacing record-true time record

5. Rate of sampling

6. Identification codes for each of the above

5.4.2 Detailed Discussion

The tape format consists of information in binary coded decimal form. The number 352 would be represented thus:

(3)	(5)	(2)
0011	0101	0010

This type of coding may be transferred directly to punched cards from the punched tape or converted by the LGP-30 into straight binary by subroutine. Besides the collected data, the information found to be necessary on the punched tape is:

1. Rate of sampling

2. Calibration levels

3. Spacer codes

The maximum sampling rate of about 2 samples per second is set by the digital voltmeter and paper punch. Internal controls are provided to vary the rate of sampling from 2 samples per second to 4 samples per hour.

The calibration levels are necessary for establishing the relation between the voltage input to the receiver and the voltage output of the digital voltmeter. Assuming the relation to be logarithmic, it is determined that with 12 calibration points a linear interpolation can be used with an

error no greater than .25 db under all conditions.

The spacer codes are necessary for division of the data into required groups; they allow accurate determination of the number of samples taken over a given time interval. The spacer codes will be manually placed on the punched tape before and after each test run. They will include in code form the day of the year and the minutes of the day in binary coded decimal. At the fastest sampling rate, two per second, it is necessary to use a spacer code once per day.

The information placed on the tape, besides the data, is known as control data. The control data is denoted by the use of a coded value described below. The values eligible for use are those not possible to be interpreted as numerical data, hence, the values "eleven" through "fifteen" are represented in straight binary. Their assignments and meanings are as follows:

Code 15 - Rate of sampling

Code 14 - 0 db reference

Code 13 - Spacing record

Code 12 - Calibration level

No code - Data

5.4.2.1 Code 15

The next record will contain a number in the range 1 to 12 (represented in straight binary), denoting the rate at which the data will be sampled during the experiment. The correspondence between the number and the actual sampling frequencies will be established at the beginning of the experiment (Table 5).

Table 5

Binary Representation	Rate of Sampling
1	2 per second
2	1 per second
3	30 per minute
4	12 per minute
5	4 per minute
6	2 per minute
7	1 per minute
8	30 per hour
9	15 per hour
10	12 per hour
11	6 per hour
12	4 per hour

It is required that the heading of the computer printout contain the sampling rate in its coded form.

5.4.2.2 Code 14

The next record will contain the coded equivalent (in straight binary) of the 0 db reference for the calibration of the receiver. The item will be coded into the range from 1 to 6, where the value of the item will correspond to the reference power level. It will be required that the computer printout contain the reference in its coded form.

5.4.2.3 Code 13

The next record will contain the day of the

year (1 to 366) and the minute of the day at the time the test was started. A code 13, with the spacer code containing the appropriate time records, will be placed at the end of each test and after any divisions found necessary in a test. At the end of the initial set of control records, code 13 will be the only control data to be repeated during the rest of the experiment; and the next record, following the spacer code itself, shall be the first data record observed. The initial time shall also be printed as a part of the heading on the printout. Provision is made in the program routine to skip down the tape to a specified spacer code before starting the processing of data.

5.4.2.4 Code 12

The next record on the tape will contain the number corresponding to a calibration point for the receiver and the rest of the system. The number will be the reading of the digital voltmeter, corresponding to a previously selected attenuator setting falling within the 60-db range below the reference level. This information will be in BCD (binary coded decimal). There will be 11 of these numbers at the start of the experiment, each number being preceded by a 12 code.

All data records will be in the form of three digit numbers, with each digit in BCD. This format of the data tape is compatible with both the LGP 30 and IBM 650. Figure 50 is a sample of the punched tape showing the sequence of operations discussed above.

5.5 Program Requirements

The foregoing paragraphs have completed a discussion of the recording of the control data and the storing of sampled data on the paper tape. The next and final step is the processing of the stored data in accordance with a prescribed routine by digital computers. Therefore, a program is necessary whose function is to accept and read in the data at high speed, convert the input into straight binary, calibrate the data with reference to the selected calibration table, and store the calibrated samples in the memory bank of the computer.

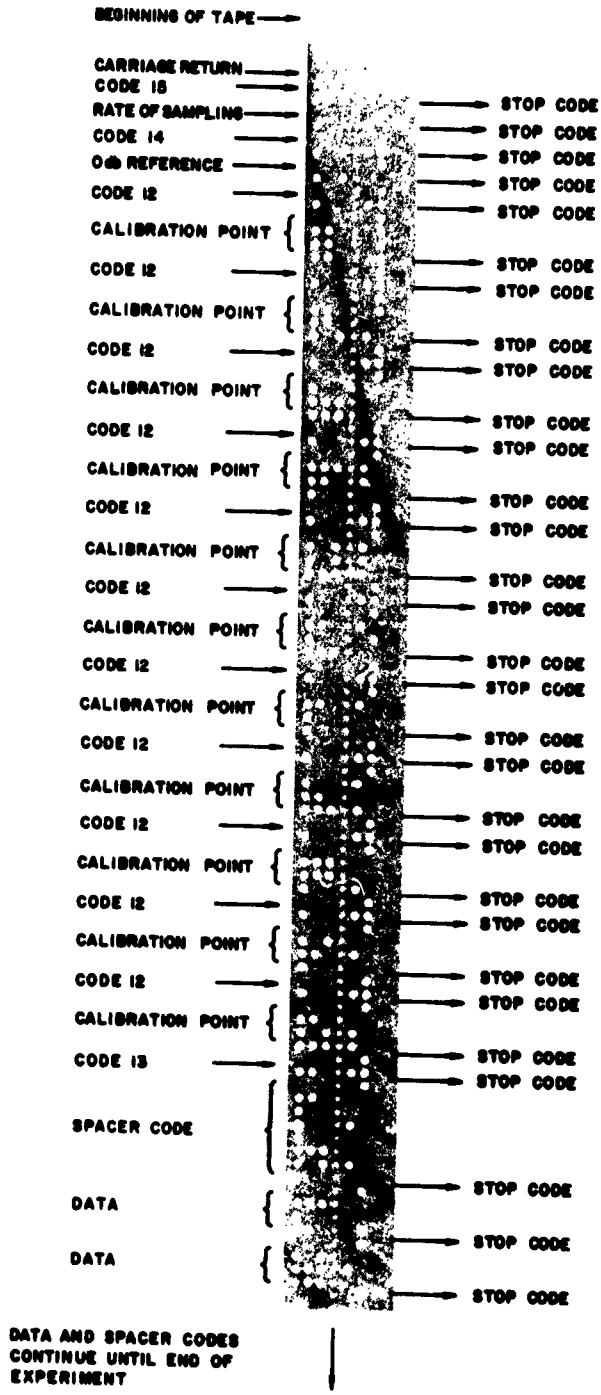

Figure 50. Data Tape Format

The final item of the program is a subroutine, which will process the stored samples in the desired manner and print out the results. Figure 51 shows a simplified form of the flow chart of the completed program, including processing subroutine, which was developed from the preceding specifications.

5.5.1 Sample Tests

To check the format and program, a simulated test was devised, containing 288 pieces of data and the necessary codes and calibration levels. The test was to determine hourly averages from signal levels sampled at 15-minute intervals over a 3-day period. The program was required to select and average the samples falling within the same hour throughout the 3-day period and print out the results. The 24 results checked against hand calculations proved to be accurate. A similar test was conducted over a period of 24 hours on the tape punch and sampling system, in order to determine the stability of the final system. A sampling rate of 12 per hour was used and the received signal level from Radio Station WWV was monitored. No errors were detected in the signal levels read out on the punched tape. A plot of the results read from EA charts and those from the paper tape are shown in Figure 52. The differences are due to the reading errors of the information taken from the EA charts.

5.6 Conclusion

The completed system achieves, in both performance and flexibility, the goal of a low-cost, accurate, data processing system directly applicable to field use. The system may be placed in a remote sector of the field and set up to sample data over a period of weeks (or months) without supervision. The data, when collected, will be on punched tape and can be machine processed to give such things as averages, distributions, fading characteristics, correlation functions, and so forth.

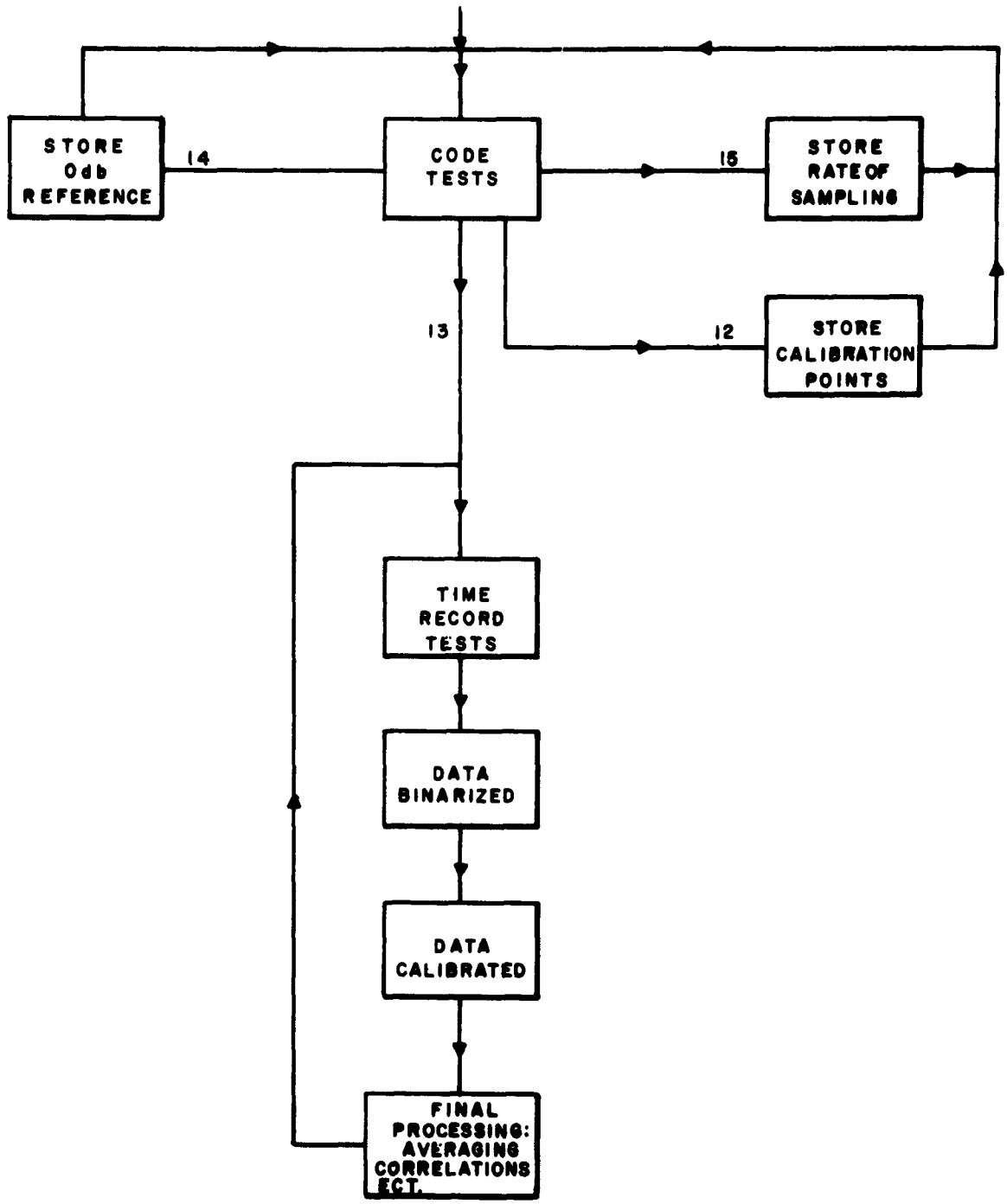

Figure 51. Program Flow Chart

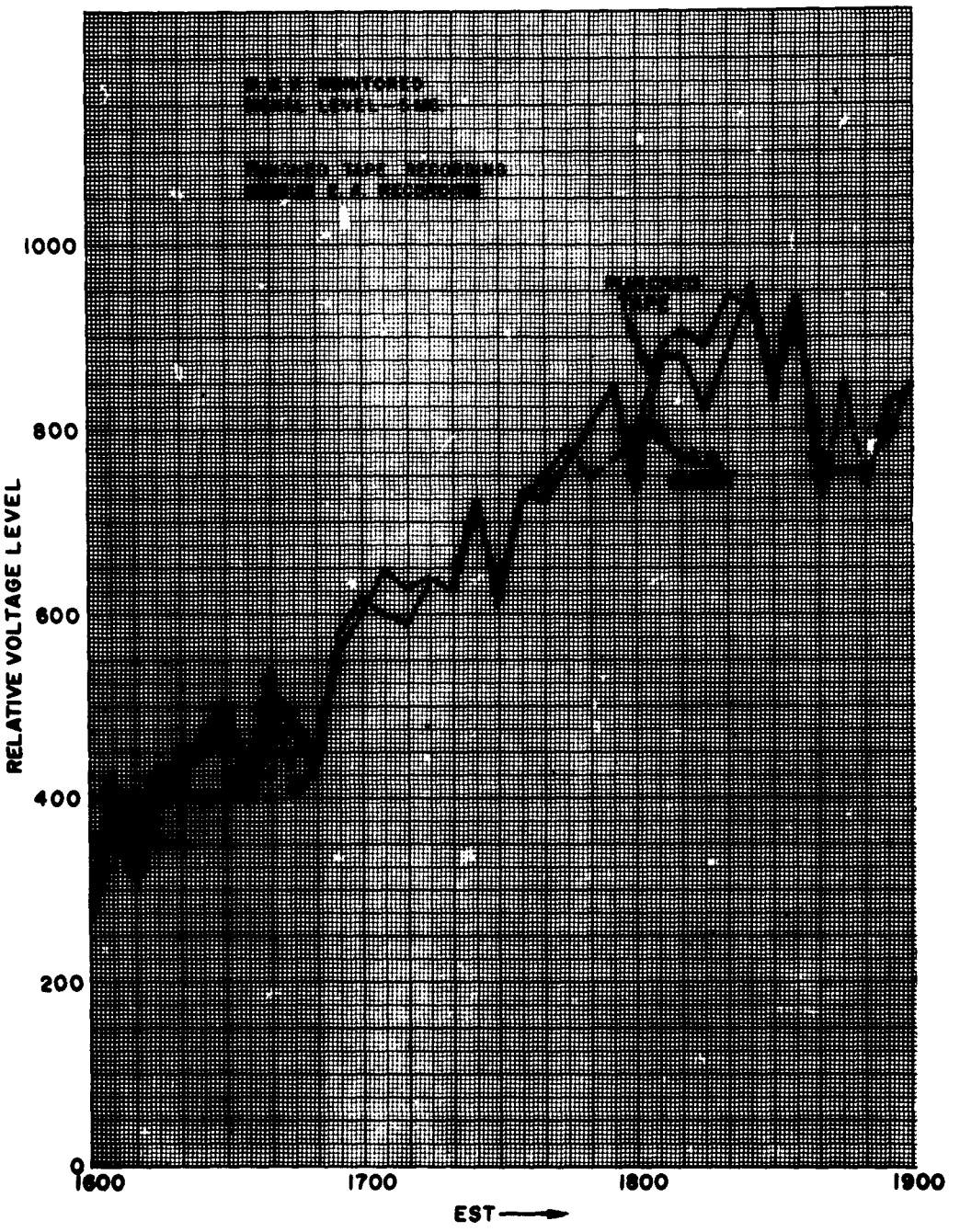

Figure 52. Punched Tape Recording vs EA Recording

6. SPORADIC E

6.1 Project Purpose

Two main sources furnish most of our knowledge of sporadic E today. By far, the more prolific source is represented by the many vertical sounders now in wide distribution around the world. A second, but less comprehensive source, is derived from monitoring of HF and VHF transmissions at oblique incidence. In fairly recent times, the growth in the number and availability in vertical soundings has led to many investigations of the spatial and temporal distribution of ionospheric irregularities by examining the correlation between sounding data at two or more spaced locations. In consequence, our present knowledge of the details of sporadic E ionization is to a large extent based on such usage of vertical incidence data.

Because of certain limitations, there has always existed some question as to the reliability and usefulness of sporadic E data acquired by these techniques. To avoid some of the drawbacks of this method, it has been proposed to study sporadic E by observations from one site using the backscatter technique. An essential feature of this plan involved substituting a radio interferometer for the Yagi or for long wire antennas more commonly used in backscatter work. The object in substituting the interferometer was to take advantage of their characteristic multilobed pattern for the tracking of a moving discrete patch of dense ionization. In this application, tracking was accomplished by observing the amplitude fluctuations, as successive lobes illuminated the patch moving across the beam. Thus, the mean direction of motion of the patch was determined at the observation times. By observing the range times of the leading and trailing edge of the backscatter, the distance away from the transmitter of the patch center and an estimate of its effective size could also be obtained.

To implement this technique, an interferometer on 22 mc was constructed at SDFS and operated from September 1960 to March 1961. Concurrently, auxiliary systems were also designed and operated to furnish supplementary data with which to compare the interferometer results. The results of the various experiments are considered in detail in the following paragraphs.

6.2 Preliminary Study

Sporadic E literature has been freely consulted for data to be used in designing the interferometer and for planning its use in backscatter experiments. Some of the data bearing directly on these problems are summarized briefly below.

6.2.3 Vertical Structure

6.2.3.1 Thickness

Studies of ionograms frequently show little or no retardation, especially at night. Estimates vary from 1 to 5 km for several types.[3,4] Recent rocket experiments tend to indicate a thickness of 1 to 2 km.[5]

6.2.3.2 Height

Height of sporadic E is generally accepted to be 100 to 110 km. In the temporate zone, there is very little variation of height with the solar zenith angle.

6.2.4 Horizontal Structure

6.2.4.1 Size

Estimates are highly variable and reflect

---

[3] Smith, E.K., NBS Report 5564-1958.

[4] Ellyett, C. and Watts, J.M., Journal Research NBS, Vol. 630, No. 2 Sept. - Oct. 1959, p.117.

[5] Jackson, J.E. & Seddon, J.C., "Ionosphere Electron Density Measurements with Navy Aerobee - Hi Rocket, Journal Geo. Research, 63, 197 (1958).

differences in observing methods, power levels, and observation frequencies, especially when the shape of the patch in question has gradually tapering edges, or is imbedded in a blobby background. In the present literature, references can be found to sizes as small as 1 km or as large as 1000 km.[6,7]

6.2.4.2 Motion

The apparent drift of E_s may be due to an actual drift of ionization, or by a formation-recombination change. Quite a few references to drift velocities around 50-70 m/s, random in direction, can be found. Stanford University sources found about the same average velocity from PPI data on backscatter return, but indicated a definite westerly trend in drift direction.[8]

6.2.5 Distribution

Studies of temporate zone E_s indicate strong diurnal and seasonal trends. Seasonally, there is a definite summer maximun in June, July, and August and a less prominent one in December and January. Diurnally, the maximums of occurrence in summer are at 1000, 1700, and 2300 hours. In the winter, the maximums are at 1200, 1500, and 2300 hours. Most observers find negligible geographic variation across the temporate zone of North America.

6.3 Interferometer Design

---

6 Findlay, J. W., "Moving Clouds of Ionization in Region E of the Ionosphere" Jour. At. Terr. Phy., 1952, Vol. 3, p. 73

7 Gerson, N. C. "Sporadic E Propagation," Jour. At. Terr. Phy., 1955, Vol. 6, p. 113

8 Peterson, A. M., "Ionospheric Backscatter," Annals of the IGY, Pergamon Press, 1957, Vol. III, pt. IV, 369

The properties of sporadic E just referred to were applied to developing the interferometer for the proposed experiments. The eventual configuration was also influenced by a restriction on the choice of operating frequency to one of five available in the 6- to 30-mc band. A choice of 22 mc was made, using previous experience with sporadic E experiments to guide the eventual selection.

The spacing of the elements was chosen on the principle that the system has maximum resolution when the azimuthal angular spread of the patch matches, or is a few degrees smaller than a single lobe width. It was apparent, however, that the lobe structure of a single interferometer could not match all expected patch sizes. Thus, both a narrow beam and a wide beam interferometer eventually resulted, by combining the outputs of three spaced elements. To determine the beamwidths actually desired, a study was made of patch sizes and distances to detectable patches expected on 22 mc. From PPI data collected under a previous contract, it was determined that the majority fell in a range of 100-300 km in diameter. To find the expected distances, CRPL series D predictions were consulted for the period of operation. Using thin layer computations, the range of distances expected to the patch center was found to be from 500 to 1000 km. The maximum and minimum angular spreads corresponding to these values are 34° and 6°, respectively. The element spacings were actually chosen to result in 10° and 30° beamwidths at the half-power points.

Elements of the interferometers consist of three 3-element Yagi antennas. The spacing of the towers supporting the antennas are such that the end antenna is common to both interferometers (Figure 53). The antennas are on a true east-west line, in view of the expected westerly trend of patch drift, and are each rotatable, so that the system as a whole could be beamed north or south. The supporting towers are 60 feet high. At 22 mc, the resulting vertical pattern has half-power points at 5° and 18°, which, with the reflecting height at 100 km, correspond to reflection distances of 300-750 km.

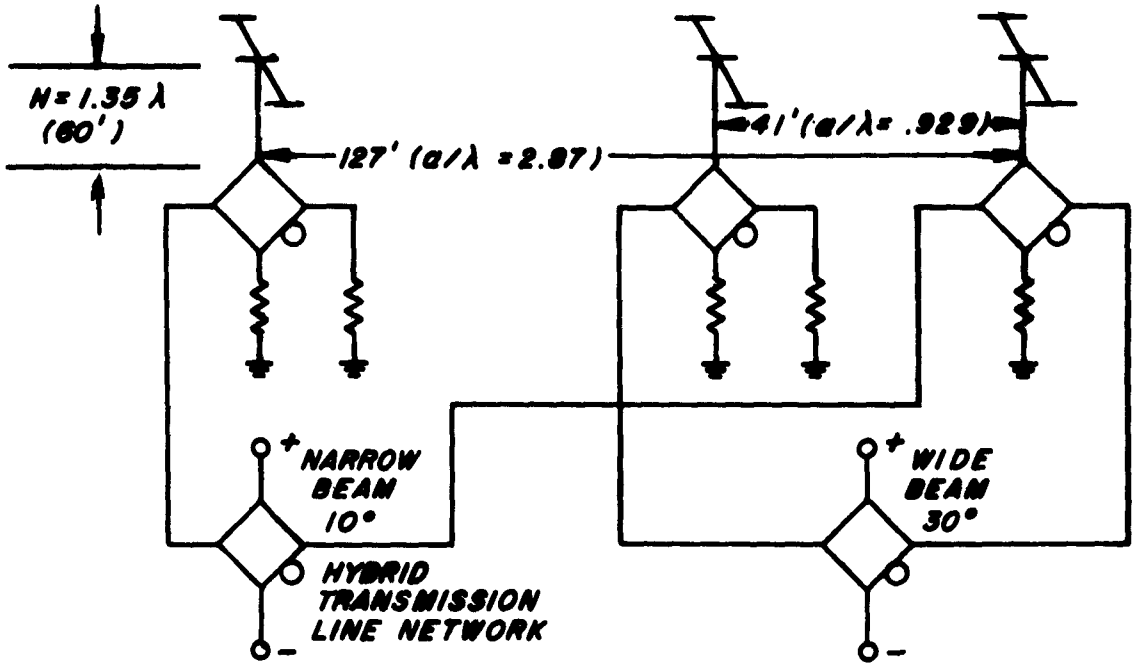

Figure 53. Interferometer Element Configuration

6.4 Receiving, Transmitting, and Recording System

In Figure 53, it is shown how the three antennas were combined to give the effect of four independent horizontal patterns. By careful adjustment of transmission line hybrid networks, the outputs of the end antenna and either of the other two antennas were combined to give sum and difference outputs. The outer pair, because of its greater spacing, constituted the narrow beam interferometer. Similarly, the closer spacing of the inter pair resulted in the wide beam. Patterns resulting from any one pair are shifted relative to each other by a beamwidth (Figure 54).

To complement the observations from the interferometer system, a five-element rotatable Yagi antenna was added. This antenna was automatically put into rotation every 5 minutes during operating periods, requiring 1 minute to complete a rotation. Operating periods coincided with operation of the interferometer, except for two months of preliminary observations while the interferometer was being built.

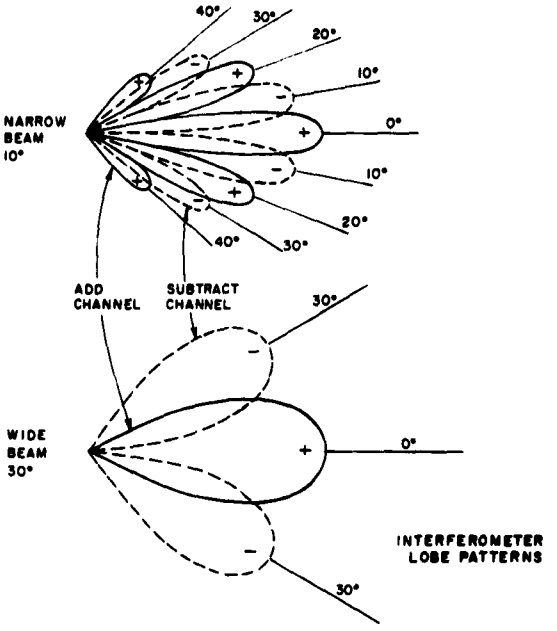

Figure 54. Interferometer Lobe Patterns

A conventional pulse transmission system was used in the program. Two-hundred microsecond pulses were transmitted 20 times a second at a peak power level of about 100 kw. The transmitting antenna was the rotatable five-element Yagi; while in its rest position, it was usually 180°.

Received signals were detected with four Hammarlund SP600 receivers connected to each of the interferometer outputs. A similar receiver was used for reception from the rotating antenna. On a few occasions, phase variations in the signal were recorded by connecting a coherently detecting receiver in parallel with an SP600. Receiver outputs were recorded on magnetic tape, using techniques identical with those discussed before. Two entirely conventional methods of processing data are generally used. A gating system identical to that shown previously in Figure 2 was used to observe the envelope detected signal at range times of interest. For a permanent record of the signal history, the four outputs were recorded on Esterline-Angus Strip

Chart Recorders. Signals received over the rotating antenna were detected and recorded on film as a PPI display.

6.5 Data Results

Construction of the interferometer was started in June 1960 and completed by the end of August. In September and October, a few preliminary tests were made primarily for the purpose of making adjustments and evaluating system performance. When these checks were completed and normal operation assured, the interferometer was operated to collect data on a more or less regular schedule from October 1960 to January 1961. A total of 53 hours of recordings was accumulated.

Analysis of the recordings produced results which were far below expectations. A careful search of the 53 hours of recorded data revealed only a few cases of a recognizable signal of sporadic E origin. In only one of these instances was a useful signal level actually maintained for the time required to draw conclusions about its motion. In general, neither occurrence rates nor signal amplitudes from sporadic E reflections on 22 mc during the recording period were sufficient for the purposes of the data collection program. Therefore, no useful results can be reported concerning the evaluation of the interferometer technique, as of this time.

Since the experiments were made with reasonably high power levels and antenna gains, the meager data obtained was probably the result of operating at too high a frequency for the ionization levels then occurring. Such a frequency (22 mc) might have been adequate during the months of peak sporadic E activity (May to August), but it is now apparent that considerably lower frequencies are mandatory for the autumn and winter lull periods. In the light of this experience, it is strongly recommended that future applications of this or related techniques incorporate more versatility in frequency selection, in order to combat unexpected frequency dependences.

Continued reliance on operating the interferometer system held

little promise for substantial results until Summer 1961, at the earliest. Greater emphasis, therefore, was given to PPI recordings on photographic film, since, owing to the inherent signal integration of this process, the collection of useful data was less dependent upon a good signal-to-noise ratio. A total of 110 hours of such recordings was taken on 22 mc, with 12 antenna rotations in each hour. Sporadic E was observed about 10% of the time, and 38 distinguishable cases were identified and examined. Sixteen cases of the total occurred in June 1960, the remaining observations taking place from October 1960 to January 1961. June measurements were generally marked by higher amplitude levels. PPI film records of this period show the sporadic E backscatter appearing as an intense patch on the photograph, with sharply defined boundaries. These records were analyzed for estimates of the size of the sporadic E region. The later observations were less clearly defined on the film records and were not analyzed for size data. These records were examined for the direction to the patch center from South Dartmouth. In some cases, the records of an individual patch showed a substantial change in size between the time of appearance and eventual fadeout. In these instances, the analysis included several representative samples over the observation period. Directions seldom varied, however, so individual patches are represented by a single sample in the analysis.

From PPI recordings, the size of a sporadic E patch may be estimated in two ways, as indicated in Figure 55. The first method assumes that the forward and backward reflections are specular-like and occur at a 100-km height. The ground distance to the nearest and farthest reflection points is calculated from the leading and trailing edges of backscatter scaled from the PPI records. The difference between these distances is a radial measure of patch size.

It is recognized that the size of the sporadic E patch, as measured this way, is influenced by ionization density of the path (especially at the near edge) and by system sensitivity, as well as the coverage of the antenna, on the far edge. Nevertheless, the result is thought to be useful. Alternatively, the horizontal size can be estimated from the azimuthal extent of the patch as

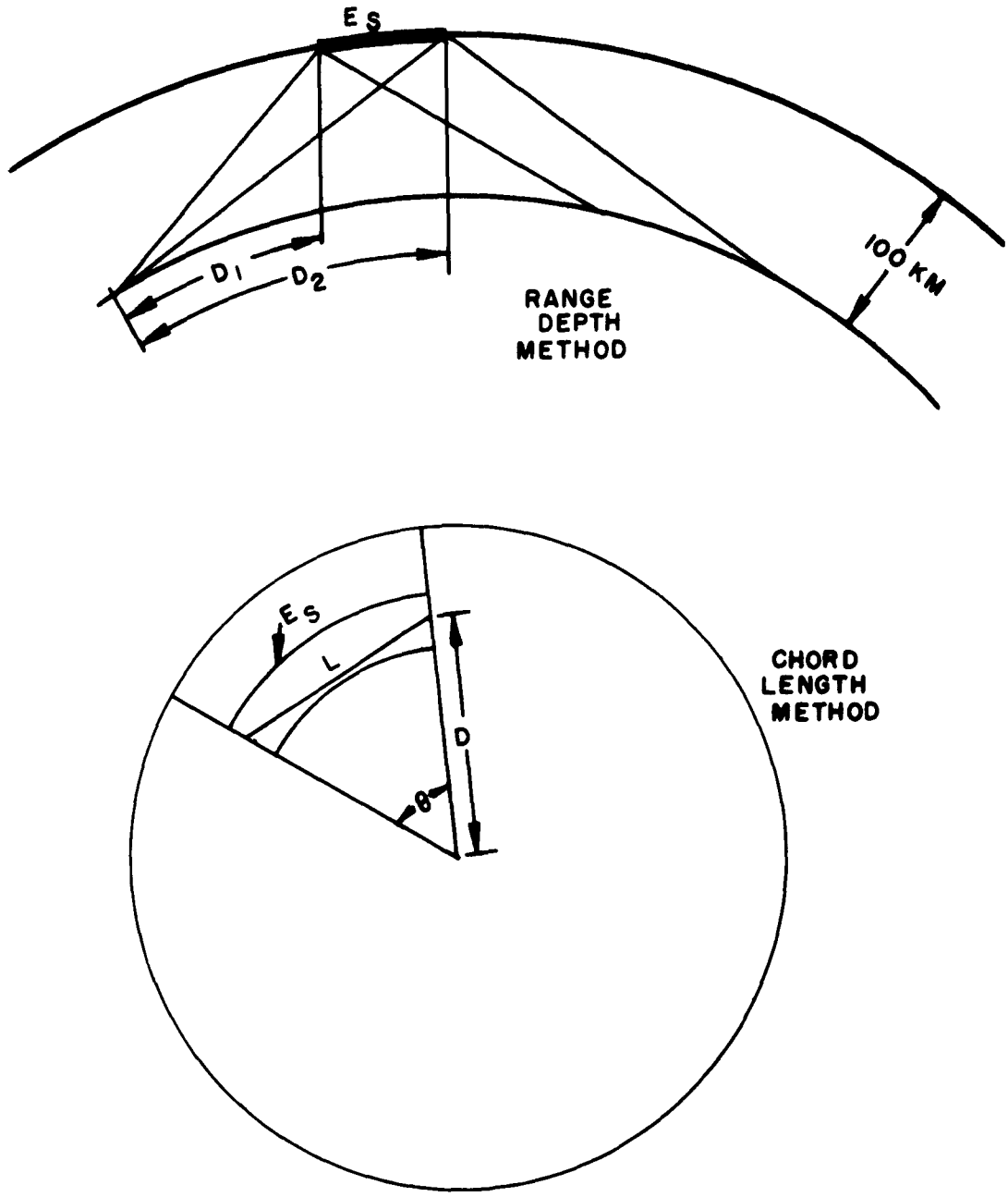

Figure 55. Illustration of Patch Size Computations

seen on the PPI. Although the accuracy of this method is limited by the azimuthal resolution or beam width of the antenna, we have adopted the simple expedient of subtracting a nominal 60° beamwidth from the PPI patch to obtain the effective patch dimensions.

Both types of estimates are shown in Figure 56. A spread of values of 75-372 km (averaging to 211 km) was found by the range depth method. The chord method yielded a range of 0 km (corresponding to a visible subtended angle of 60° or less) to nearly 300 km. The average for these measurements was 121 km. At least a part of the difference of 90 km probably results from signal levels falling to a point near the threshold sensitivity of the film. Under these conditions, a subtraction of 60° is excessive, and the calculated central angle of the patch found by this method becomes too small. For these reasons, it is concluded that the average of 211 km found by the range depth method is more representative as a measure of the patch size on 22 mc.

In looking for directional preference in the 22 cases in October to January, the direction to the patch center was scaled off to the nearest 45° sector. The distribution given in Figure 57d shows trends favoring due north and south. Because of the limited data included in the distribution, the analysis was extended to include older records not previously examined for directional trends. These were of transmissions on 9, 12 and 22 mc in 1953 and 1954. In general, the distributions for 9 and 22 mc (Figure 57a and c) show a strong bias towards due south. On 12 mc (Figure 57b), a slight peak is noted towards south, but this is followed by a more prominent peak for northerly directions. On the basis of these widely separated samples, there is considerable evidence to support the inference that observations of sporadic E and, hence, the possibility of communications with this mode, should be measurably better along a north-south path, in preference to an east-west path, in Eastern United States.

In summary of the results of the sporadic E studies, the failure of the interferometer technique to achieve anticipated results was caused by insufficient signal levels in comparison with that required for useful measurements. The most feasible solution in view of the power levels employed

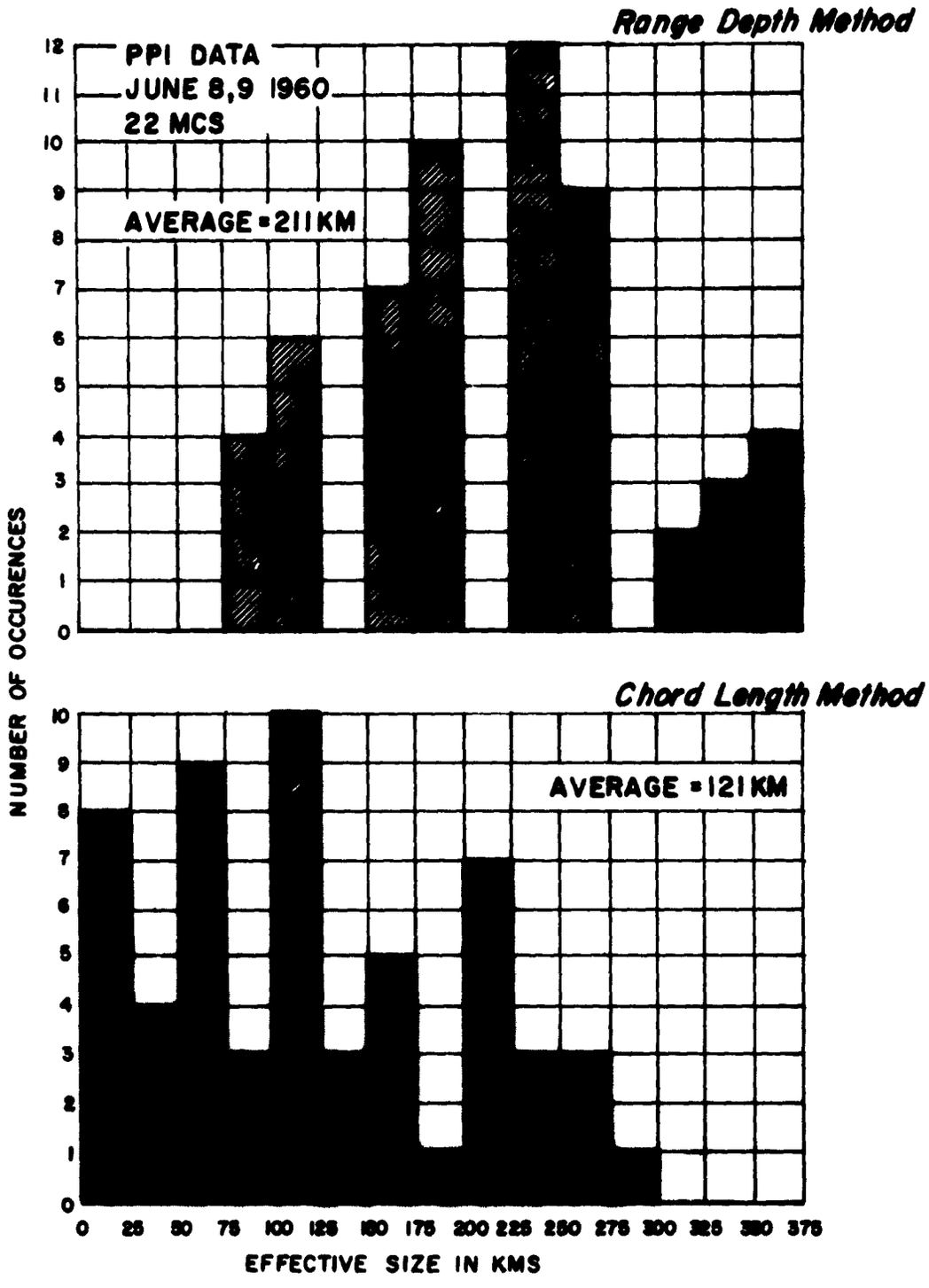

Figure 56. Distribution of Estimated Sizes

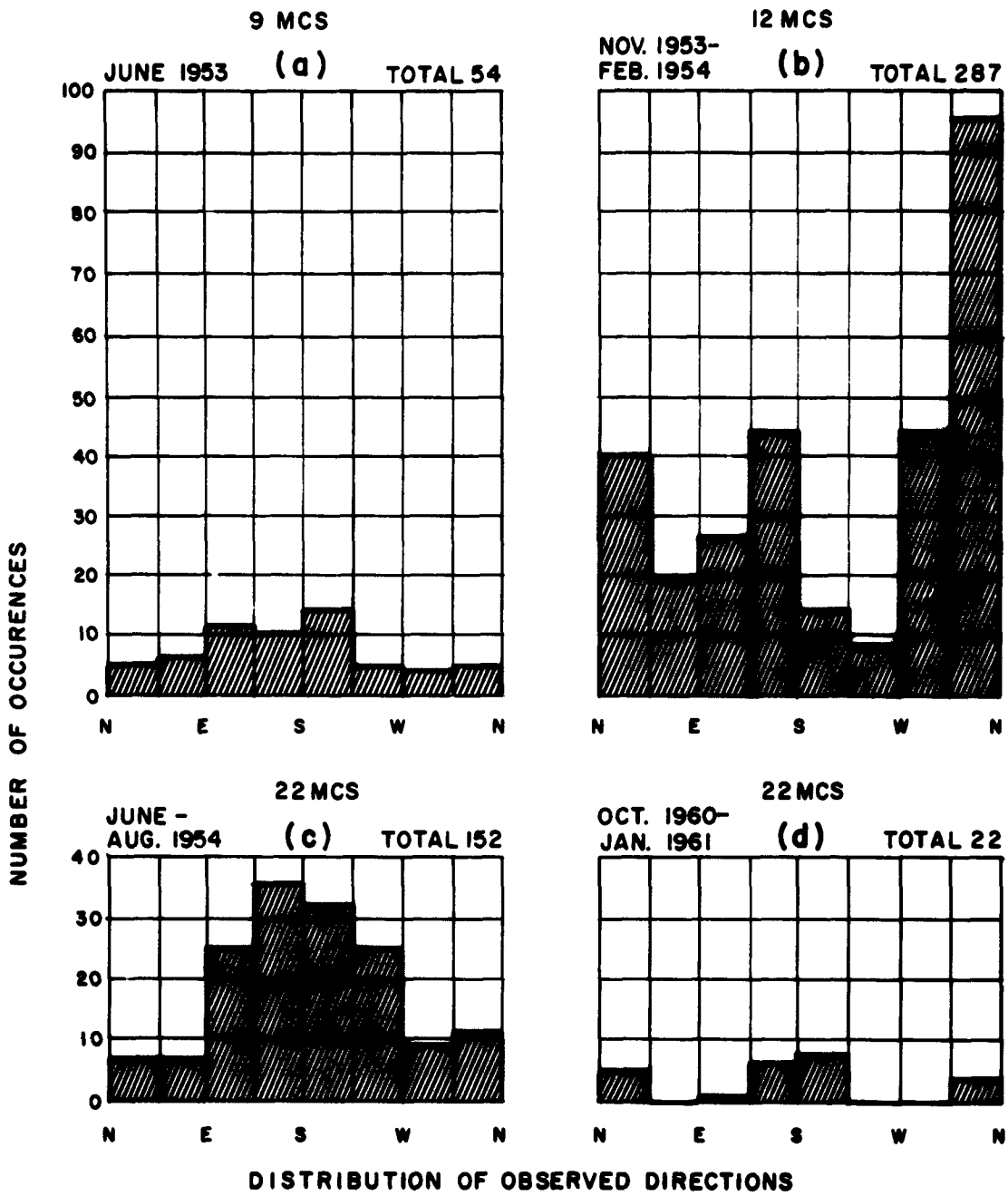

Figure 57. Distribution of Observed Directions

is the use of a lower operating frequency, relatively free of interference at the receiving site.

Sixteen observations of sporadic E from PPI records of 22-mc transmissions have led to an estimate of the average size of the ionizing region of approximately 220 km. From PPI records, it is also concluded that observations of sporadic E from South Dartmouth are maximum due south. A secondary maximum towards north is usually, but not always, present.

7. SUMMARY AND CONCLUSIONS

Spectrum analysis of 22-mc ground backscatter has shown distinct and recognizable differences in the phase characteristics of quiet and disturbed ionospheres. In a typical quiet ionosphere, the deviation of the band center is highest in the morning, when backscatter forms and decreases in range. Values of 1.2 cycles are typical. The deviation steadily decreases until a minimum of 0.4 to 0.7 cycle is attained at noon, increasing again in the late afternoon when the backscatter begins to move out in range. The U shape of the diurnal change correlates well with the rate of change of the skip distance. Disturbed conditions are marked by considerably higher frequency deviations in the spectrum. In the case of SID's, their onset may be noted by an abrupt shift of 2 to 4 cycles, preceding absorption effects by approximately a minute. A few experiments were made to determine whether terrain conditions affect the spectral composition of backscatter. The tests were inconclusive when no adequate means of separating ionospheric from ground components were found.

The phase stability of forward paths was studied by detecting the received signals coherently. Calculations were also made from a plane-earth plane-ionosphere model to enable a computation of expected frequency shifts from data extracted from vertical incidence ionograms. Some agreements were obtained in four cases involving reflections at vertical incidence and in one application to an oblique path between South Dartmouth and Grand Bahama Island.

Observations of around-the-world signals in January 1961 appear to substantiate previous conclusions that the path was essentially confined to the zone of twilight. A horizontal direction of 65° true from South Dartmouth was found. The vertical angle was estimated to be in the vicinity of 5° during one test on 22 mc. The mode of propagation supported frequencies from 14 to 27 mc. Practically no change in the transit time of the first arriving signal was noticed as the frequency was swept through this band.

Design, construction, and tests on the punched paper tape system have been completed. The system samples and encodes the output of a receiver up to a rate of 2 samples per second. The encoded sample is then punched on a paper tape. A code format was chosen which permits the completed tape to be processed and analyzed on either a Royal McBee LGP-30 or an IBM 650. A 24-hour stability test gave completely satisfactory results. A program to simulate a propagation experiment was developed and used to check the process from sampling input to machine computation; this had excellent results.

Sporadic E experiments with the 22-mc interferometer were handicapped by low sporadic E activity. The experience gained with this technique indicates better results should be obtainable using lower frequencies. PPI data on several frequencies show that sporadic E is observed most frequently in a direction south from South Dartmouth. A secondary maximum was frequently observed in the north. Rough estimates of the "size" of sporadic E clouds were made from PPI displays of backscatter. Average values of 121 to 211 km were found by these methods.

8. RECOMMENDATIONS

The sampling of ionospherically reflected signals by coherent detection has established several interesting results which offer possibilities for advancing the communications art in the future. The use of HF backscatter to detect onset of a disruption to communications is one area which promises a useful application. Also, reasonably good agreements were found between observed and calculated frequency shifts on forward paths, offering some hope

of eventually inverting the process to determine the state of the ionosphere by observing the shifts in a spectrum of transmission frequencies. It is recommended that these investigations be advanced beyond their present status. A future expansion of these topics should plan experiments drawn from present knowledge, which will furnish detailed data on the effects of normal and highly disturbed ionospheric changes on backscatter and forward propagated paths. These plans would also include a development of techniques enabling the diagnostic use of frequency shift observations in a routine manner.

While knowledge about the characteristics of around-the-world signals is increasing gradually, the nature of the mode of propagation itself is still in doubt. It is recommended that experiments be designed with the capability of distinguishing between the multihop and tilted layer theories.

GENERAL INFORMATION

Contributions to the work reported herein have been made by the following:

Donald A. Hedlund, Department Manager
James F. Roche, Staff Engineer
Leonard C. Edwards, Section Manager
Harry Hoogasian, Project Engineer
} Planning and Supervision

David W. Blood
Daniel B. Odom
George D. Thome
} Data Analysis

J. Daniel Moylan } Instrumentation

Joseph J. Molla
Gerald L. Hall
John S. Underwood
} Field Operation and Data Collection

LIST A

Code	Organization	No. of Copies
AF 5	AFMTC (AFMTC Tech Library - MU-135) Patrick AFB, Fla.	1
AF 18	AUL Maxwell AFB, Ala.	1
AF 43	ASD (ASAPRL) Wright-Patterson AFB, Ohio	1
AF 124	RADC (RAYLD) Griffiss AFB, New York Attn: Documents Library	1
AF 139	AF Missile Development Center (MDGRT) Holloman AFB, New Mexico	1
AF 244	AFOSR (SRY) Wash 25, D. C.	1
AF 318	ARL (Technical Library) Building 450 Wright-Patterson AFB, Ohio	1
AF 319	AFSC (SCAXC) Andrews AFB Wash 25, D. C.	1
Ar 5	Commanding General USASRDL Ft. Monmouth, N. J. Attn: Tech. Doc. Ctr. SIGRA/SL-ADT	1
Ar 9	Department of the Army Office of the Chief Signal Officer Wash 25, D. C. SIGRD-4a-2	1
Ar 50	Commanding Officer Attn: ORDTL-012 Diamond Ordnance Fuze Laboratories Wash 25, D. C.	1
Ar 67	Army Rocket & Guided Missile Agency Redstone Arsenal, Ala. Attn: ORDXR-OTL, Technical Library	1

G2	ASTIA Arlington Hall Station Arlington 12, Virginia	10
G 68	National Aeronautics & Space Agency 1520 H Street, N. W. Wash 25, D. C. Attn: Library	1
G 109	Director Langley Research Center National Aeronautics and Space Administration Langley Field, Virginia	1
M 6	AFCRL, Office of Aerospace Research (CRRELT) L. G. Hanscom Field, Bedford, Mass.	10
N 1	Director, Avionics Division (AV) Bureau of Aeronautics Department of the Navy Wash 25, D. C.	2
N 29	Director (Code 2027) U. S. Naval Research Laboratory Wash 25, D. C.	2
I 292	Director, USAF Project RAND via: AF Liaison Office The Rand Corporation 1700 Main Street, Santa Monica, Cal.	1
AF 127	Boston Sub Office Patent Prosecution Branch (Hq. AMC) Murphy General Hospital, Building 133 424 Trapelo Road, Waltham 54, Mass.	1
AF 253	EOARDC Shell Building 47 Rue Cantersteen Brussels, Belgium	1
Ar 107	U. S. Army Aviation Human Research Unit U. S. Continental Army Command P. O. Box 438, Fort Rucker, Ala. Attn: Maj. Arne H. Eliasson	1
G 8	Library Boulder Laboratories National Bureau of Standards Boulder, Colorado	2

M 63	Institute of the Aeronautical Sciences 2 East 64th Street New York 21, New York Attn: Librarian	1
N 73	Office of Naval Research Branch Office, London Navy 100, Box 39 F. P. O. New York, N. Y.	10
U 32	Massachusetts Institute of Technology Research Laboratory of Electronics Building 26, Room 327, Cambridge 39, Mass. Attn: John H. Hewitt	1
I 239	Smyth Research Associates 3555 Aero Court, Research Park San Diego 11, California	1
I 956	AVCO Corporation Research and Advanced Development Division 201 Lowell Street Wilmington, Mass. Attn: Dr. R. Penndorf	1
	Send all remaining copies to: Hq. AFCRL OAR (CRRK, H. J. Marsh) L. G. Hanscom Field, Bedford, Mass.	5

LIST J

AF 2	ADC (ADLAN-G) Ent AFB, Colorado Springs, Colo.	1
AF 19	AWS (AWSSS/TIPD) Scott AFB, Illinois	1
AF 29	APGC (PGTRI, Tech Lib) Eglin AFB, Fla.	1
AF 30	AF Missile Development Center (MDWO) Holloman AFB, New Mexico	1

AF 34	SAC Offutt AFB, Nebraska	1
AF 35	TAC Langley AFB, Virginia	1
AF 133	WADD (WCOSI) Wright-Patterson AFB, Ohio	1
AF 159	ARDC (RDSFIL, Hq. Technical Library Branch) Andrews AFB, Wash 25, D. C.	1
AF 222	AF Institute of Technology Library (MCLI-ITLIB) Building 125, Area B Wright-Patterson AFB, Ohio	1
AF 300	AFRD AFOSR (RREE-H, Mr. Samuel Milner) Wash 25, D. C.	1
Ar 10	Massachusetts Institute of Technology Signal Corps Liaison Officer Cambridge 39, Mass. Attn: Mr. Alvin D. Bedrosian, Room 26-131	1
Ar 25	Commanding Officer U. S. Army Signal Research & Development Lab. Attn: Technical Documents Center Fort Monmouth, New Jersey	1
Ar 49	Commanding Officer U. S. Army Signal Engineering Laboratories Attn: SIGFM/EL-AT Fort Monmouth, New Jersey	1
G 33	Documents Expediting Project Library of Congress Wash 25, D. C.	1
G 41	Federal Aviation Agency Bureau of Research & Development Wash 25, D. C.	1
G 48	Exchange and Gift Division Library of Congress Wash 25, D. C.	1
G 84	Federal Aviation Agency Civil Air Surgeon Library Wash 25, D. C.	1

N 4	Chief, Bureau of Ships Department of the Navy Wash 25, D. C. Attn: Code 320	1
N 9	Chief, Bureau of Ordnance Department of the Navy Wash 25, D. C. Attn: Code Ad-3	1
N 13	Chief of Naval Operations Department of the Navy Wash 25, D. C. Attn: Op-413-B21	1
N 16	U. S. Naval Air Missile Test Center Point Mugu, Cal. Attn: Code 366	1
N 85	Commanding Officer and Director U. S. Navy Electronics Laboratory (Library) San Diego 52, California	1
N 23	U. S. Naval Ordnance Laboratory White Oak, Silver Spring 19, Maryland Attn: The Library	1
N 26	U. S. Naval Ordnance Test Station China Lake, Cal. Attn: Code 753	1
N 27	Librarian U. S. Naval Postgraduate School Monterey, Cal.	1
N 35	Commanding Officer and Director U. S. Navy Underwater Sound Laboratory Fort Trumbull, New London, Connecticut	1
N 37	Office of Naval Research Department of the Navy Wash 25, D. C. Attn: Code 427	1
N 48	Commanding Officer U. S. Naval Air Development Center Johnsville, Pennsylvania Attn: NADC Library	1
I 130	Parke Mathematical Labs., Inc. Bedford Road Carlisle, Mass. Attn: Dr. Nathan Grier Parke, III	1

I 187	Electromagnetic Research Corporation 5001 College Avenue College Park, Maryland Attn: Mr. Martin Katzin	1
I 371	Battelle Memorial Institute 505 King Avenue Columbus, Ohio Attn: Dr. Iver Igelsrud Chief, Information Management Division	1
U 37	University of Michigan Engineering Research Institute Willow Run Airport Ypsilanti, Michigan Attn: Librarian	1
U 59	Library Georgia Technology Research Institute Engineering Experiment Station 722 Cherry Street, N. W. Atlanta, Georgia Attn: Mrs. J.H. Crosland, Librarian	1
U 61	Brown University Division of Engineering Providence, Rhode Island Attn: Dr. C. M. Angulo	1
U 102	Harvard University Technical Reports Collection Gordon McKay Library 303A Pierce Hall, Oxford Street Cambridge 38, Mass.	1
U 279	Documents Division Florida State University Library Tallahassee, Florida	1
	Defence Research Member Canadian Joint Staff 2450 Massachusetts Avenue, N. W. Wash 8, D. C.	1